APPLICATION OF GEOPHYSICAL TECHNIQUES FOR GROUNDWATER INVESTIGATION IN LAKE NAIVASHA AREA, KENYA

Yulian Gressando
(Republic of Indonesia)

April, 1999

INTERNATIONAL INSTITUTE FOR AEROSPACE SURVEY AND EARTH SCIENCES

APPLICATION OF GEOPHYSICAL TECHNIQUES FOR GROUNDWATER INVESTIGATION IN LAKE NAIVASHA AREA, KENYA

Yulian Gressando
(Republic of Indonesia)

Thesis submitted as a partial fulfillment of the requirements for the degree of Master of Science in Environmental System Analysis and Monitoring - Water Resources International Institute for Aerospace Survey and Earth Sciences (ITC) – Enschede The Netherlands

Degree Assessment Board

Prof. Dr. Ir. J.C. Van Dam (Chairman)	Delft University
Prof. Dr. A.M.J. Meijerink (Head WRS Department)	ITC, Enschede
Supervisor : Dr. Ambro Gieske	ITC, Enschede
Co-supervisor : Drs. Robert Becht	ITC, Enschede

21st April, 1999

Acknowledgements

The study was possible as a result of the opportunity offered by International Institute for Aerospace Survey and Earth Sciences (ITC) which nominated me to attend the ITC ESM.2 course and allowed me to join the Kenya Project in the Naivasha Area, Republic of Kenya, Africa.

I wish to extend my gratitude to all those who assisted me in pursuing and finally this study. I am deeply indebted to all ITC staff members especially those of the Environmental System Analysis and Monitoring Division, who devoted their time and energy in training me as an environmental scientist. My deepest appreciation and thanks are dedicated to the following:

- *My supervisor, Dr. Ambro Gieske who supervised my work with devotion and strict criticism.*
- *My co-supervisor, Drs. Robert Becht who guided, advised and assisted me from the field work until the completed thesis.*
- *Prof. Dr. A.M.J. Meijerink (Head of the Division), for his useful critical comments and encouragement.*
- *Dr. Ir. C. M. M. Mannaerts, who permitted me to join the MSc Course in ESM.2-WRS Division.*
- *Dr. Sally Barritt, for her assistance in providing the magnetic data of the study area.*
- *Drs.D. Kovacs, for his assistance in all aspects of geophysicsl and structural geology.*
- *All other staff members of the ESM.2 course 1998/1999*

To all the ITC community at large whose names I am not able to include here, but who assisted in one way or another, I am deeply grateful.

I owe a lot to the various Kenyan authorities and people who offered help during the fieldwork. My thanks go to the Kenya Wildlife Service (KWS) and Water Resources Assessment Project (WRAP) in Nakuru District for providing the necessary field facilities and literature on the study area.

I would like to express my gratitude to my colleagues who supported me during the course, Tetra Januariadi and his family, Zuhdi and Sunuprapto. I also would like to express my deep gratitude to my course mates, Anthony Nduah, Robert, Behar, Toni, Ahmad Sala, Fathi, Ashfaque, Salazar, Zeng Shu, Mekkonen and Mbui for their contributions and company.

Lastly my affectionate thanks go to:
My parents, brothers, sister and relatives, your prayers and blessings have made it possible for me. Also I thank my close friend, Novita Sunarya, for her support during this study. Lastly, my dear friends Wisnu, Dessy, Tiwi, Adinda, and all others who already supported me for this study. "Thank you very much!"

Abstract

The area of investigation is situated geographically between 210000 – 220000 m and 9930000 – 9906000 m (UTM grid system). Administratively, it is within the Naivasha Area, Nakuru District, and Republic of Kenya.

The survey's purpose is twofold:

- *To characterize electrical resistivities of subsurface strata in the area to try to relate the geophysical response to groundwater depth.*
- *To study the geophysical response of faults in the study area.*

In order to reach this objective, a geophysical survey was carried out in the selected area including the following activities:

- *Measurement and analysis of 25 vertical electrical soundings (VES).*
- *Measurement and analysis of 5 horizontal electrical profiles (CST).*
- *Preparation and study of two geophysical well logs in recently drilled boreholes in the area.*
- *Study of regional magnetic data (made available by ITC, Delft).*

For the resistivity work an ABEM Terrameter 300C was used, while for the geophysical well logging an ABEM Terrameter SAS LOG 200 was employed. Both instruments belonged to the Water Resources Assessment Project in Kenya (WRAP) which is a co-operation project between the Netherlands and Kenyan Governments. After a preparation period at ITC (Enschede) the fieldwork took place in Kenya in October 1998. During this period a crew of 4 persons (WRAP Project) with a 4x4 vehicle was made available by WRAP.

In Chapters 1 to 5, the study area is introduced and a discussion is given of the geophysical methods used. The analysis and results are presented in Chapter 6. Conclusions and recommendations may be found in Chapter 7.

List of Contents

List of Figures

Figures

Figure

List of Tables

Tables

Chapter 1
Research Statement

1.1. Background

The Kenya Rift Valley is part of a worldwide system of sublinear belts of active seismicity, volcanicity and heat flux defining the edges of lithosphere plates. The tectonics of the rift valley system is characterized by incipient plate margin construction, where oceanic crust is created at spreading centres. It continues northwards through the Afar region where it forms a 'triple junction' with the Red Sea and Gulf of Aden spreading axes where new crust is being generated (Figure 1.1.).

However, in this particular study area (Fig. 1.1) separation is not complete although geophysical evidence strongly suggests that the lithosphere is anomalously thin representing the incipient nature of the breakup process (Wendland and Morgan, 1982).

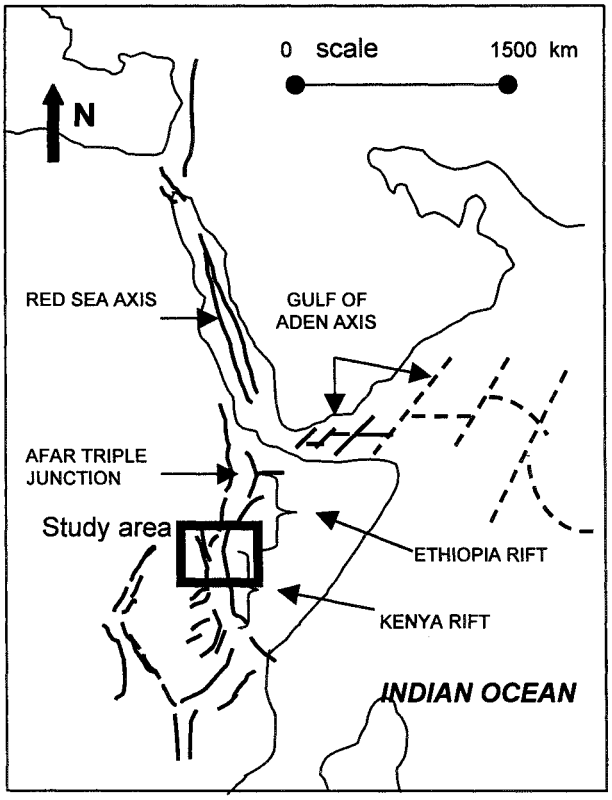

Figure 1.1. Relation of the Kenya/Ethiopia Rift to the Red Sea and Gulf of Aden spreading axes.

The Naivasha Area is part of the Kenya Rift Valley. The aquifers in the fault system have been subject of many groundwater investigations. This is due to the fact that in many parts of the Naivasha Area, the depth to the groundwater table is highly variable. The relation between the tectonics of the area and aquifer formation is poorly understood.

On the other hands, the rift valley is well known as an ancient habitat of mankind (Leakey, 1931). It has been especially attractive for early settlement because of the freshwater availability and surrounding lush vegetation. In the Naivasha Area, the large estates have gradually been subdivided into small farms by land-buying since 1963. Dairying continues side-by-side with irrigated temperate arable cropping, vegetable horticulture and flower growing on the more fertile volcanic soils, where water for irrigation is available.

Recent population increases due to birth and migration has altered the land use patterns in the catchments. For example, the population of the catchment has increased from 600,000 people in 1979 to 1,011,000 in 1989 (Stuttard et al., 1995) showing a rise of 411,000 or 69% over ten years.

The impact of the rapid population changes and the diversification of the agriculture sectors have increased the demand on water resources in the area. However, the limitations the fresh water supply, either from surface run-off, lake water or groundwater, form a challenge for further study in order to maintain water availability for future generations.

1.2. Problem Formulation

Water has traditionally been regarded as an inexhaustible gift of nature. The population growth accompanied by agricultural development and increasing world industrialization is straining water resources. There will be a critical shortage of water of suitable quality to sustain future growth unless water management is substantially improved.

The management or exploitation phase of the development of surface water and groundwater resources is the main phase, which addresses resource development, comparison of policies and strategies, and assessment of the regional surface and groundwater exploitation.

To satisfy the demand, accurate and sufficient data are required. Boreholes are the sources which provide accurate information about the subsurface water supplies. Since drilling is very costly, a limited number of test holes are drilled in some

selected locations of the study area as control points. In this case the test holes were drilled near the lake.

Geophysical work (electrical resistivity surveying) has been carried out in the area to support the ongoing hydrogeological investigations. The relationship was studied between the electrical parameters especially the product of the resistivity of the aquifer and its thickness. Results were compared with those of previous geophysical investigations. From the relation of all the data obtained, conclusions were drawn for the area with respect to the influence of faulting on aquifer structure and to the relation between resistivity and water table depth.

1.3. Objective

1.3.1.General Objectives

The general objective pursued by this research in the study area is to characterize the geophysical response of the rocks below the surface in order to provide information about 'the behavior' of the groundwater table and the aquifer in relation to lithology and the presence of the faults.

1.3.2. Derived Objectives

To achieve the objective, the following derived objectives have to be reached:

- to determine the depth to the groundwater in the study area
- to delineate the faults, in order to study the behavior of the aquifer due to these faulting
- to predict the groundwater flow direction outwards the lake

To reach these objectives, the following questions need to be answered:

- which types of lithologies are present in the study area
- how can the aquifer be represented by its geophysical response
- which parameters determine the presence of groundwater table below the surface
- is there any relationship between the presence of the fault and the aquifer in the study area

1.4. Conceptual Framework

The research involves two types of studies:

- Pre-fieldwork study of the area based on aerial photograph interpretation and other studies, i.e. groundwater investigation, physical property of the subsurface rock from resistivity and geomagnetic data.
- Analytical studies of fieldwork data.

The approach used in the present study is shown as a flow chart in Figure 1.2.

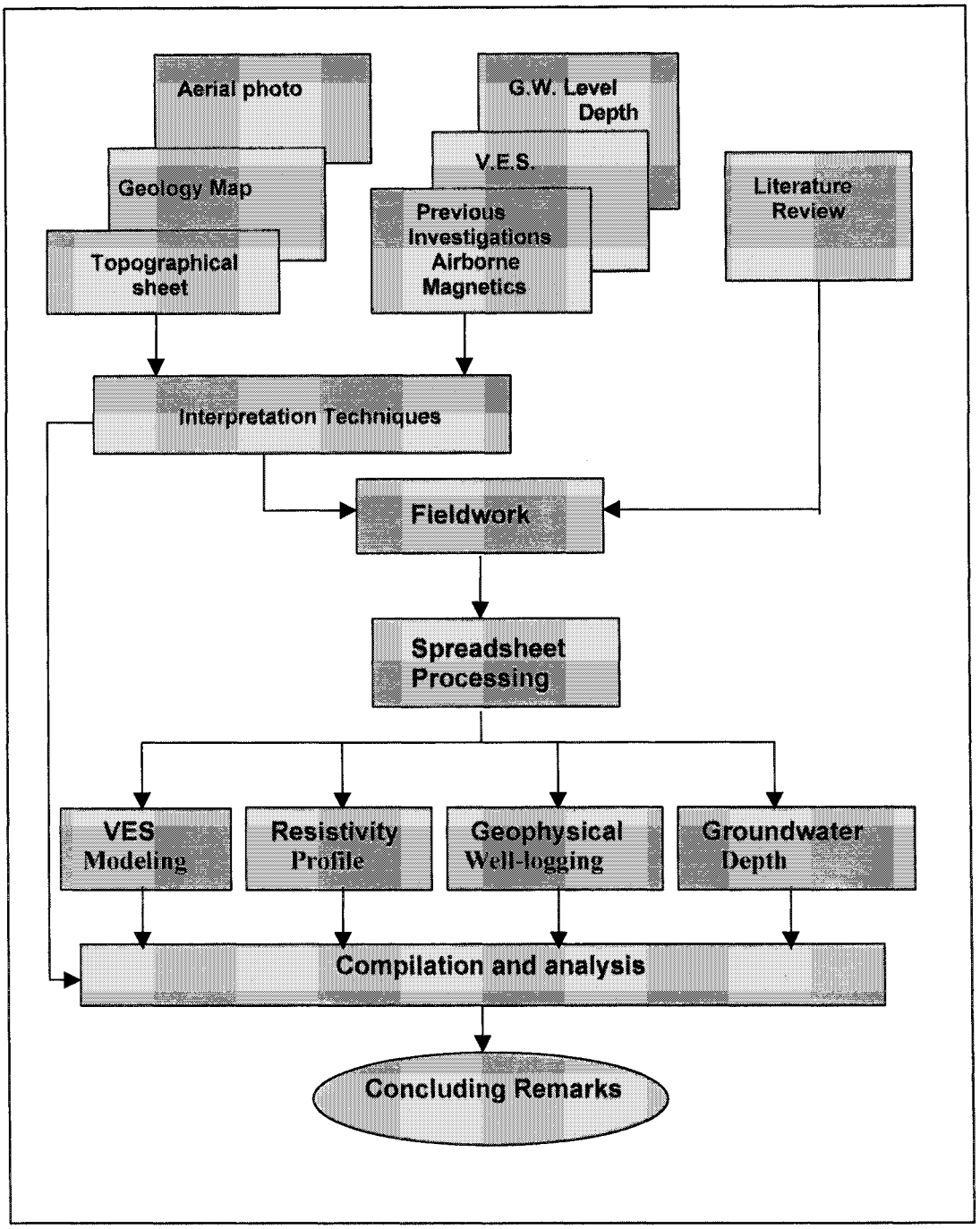

Fig. 1.2 Flow chart of the geophysical work in the present study.

Chapter 2

Study Area and Coordinate System

2.1. Study Area

2.1.1. General Information

The Naivasha area is situated between longitude 36° 00' - 36° 30' E, and between latitudes 0° 30' S and 1° 00' S (Topographic Map Sheet No. 43 S.W., 1974). Most of the area - which is approximately 1200 square miles or 3110 km^2 in areal extent – is within the Rift Valley Province, and administered by the Provincial Commissioner at Nakuru. The greater part of the area is farmed, agriculture and stockfarming being carried out side by side.

Wheat forms the greater part of the agriculture crops, farmed in the high altitude area, particularly on the Kinangop plateau (eastern part of the study area) and Mau escarpment (western part of the study area). Cattle farms are largely confined to the Rift floor and the Masai Reserve, i.e. in that part of Narok District where the indigenous people lead a semi-nomadic life with their cattle. The growing of vegetables was traditionally carried out along the shore of Lake Naivasha. This was restricted greatly in the beginning of 1956, in order to deny food to *Mau Mau* terrorists that frequented the papyrus swamps around the lake at that time. Since then the level of the lake has been rising and many acres of land have been swamped. Recently a large number of commercial farms has been established around the lake with irrigated agriculture and horticulture (flower farms).

2.1.2. Site Selection

In order to produce the best result in this geophysical study related to groundwater investigation and considering the limited time available for fieldwork, the area of study was selected before going to the field. It is situated geographically between 36° 23' 40.7'' - 36° 29' 03.5'' E and 00° 37' 57.8'' – 00° 50' 58.9'' S or 210000 – 220000 m and 9930000 – 9906000 m (UTM grid system, zone 37). Administratively, it is inside the Naivasha Area, Nakuru District, Republic of Kenya. This area is laid in the Kenyan Rift Valley, 70 km north-west of Nairobi (the capital city of Kenya). See figure 2.1.

This selection was made based on the presence of the geological features in the study area, supported by the previous available data, and the objectives of the research.

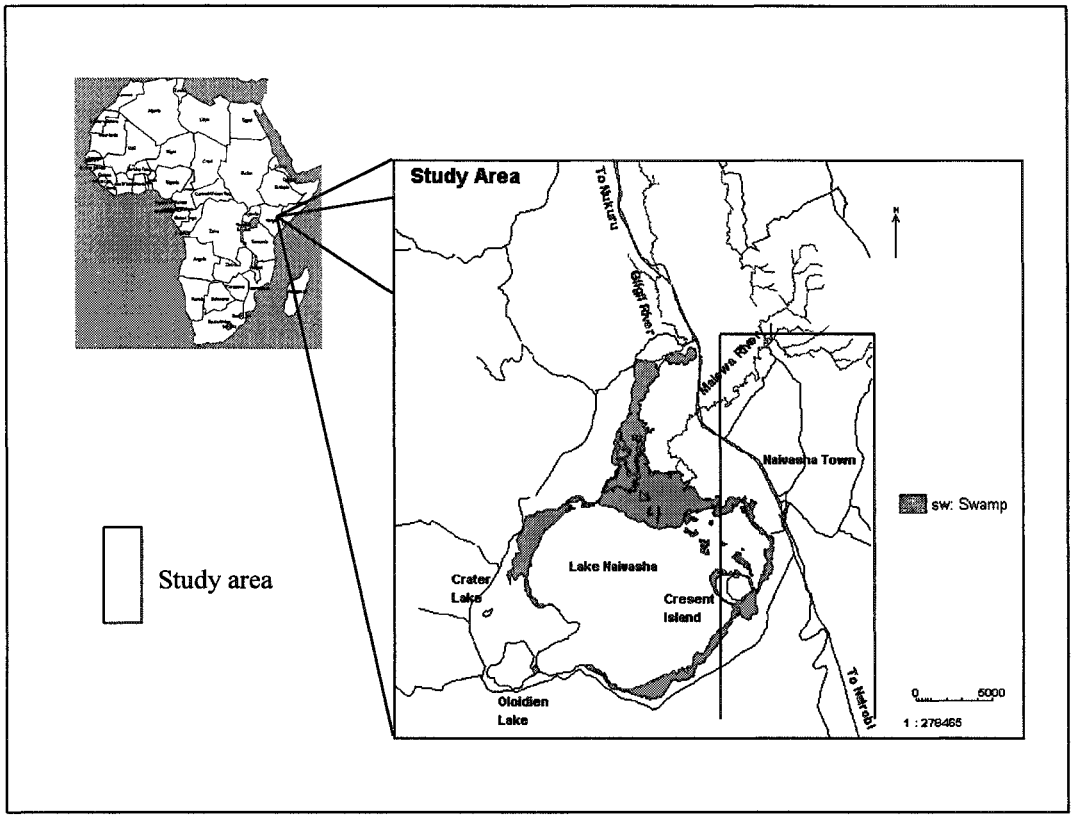

Figure 2.1. The study area

2.1.3. Accessibility

The study area is located along the East African Railway, which closely follows the main road from Nairobi in the south to Nakuru in the north. The railway itself was constructed in the early years of the present century and opened in 1901, originally also passed through the northern part of the area skirting around the southern edge of the 'Badlands' lava flows from Gilgil to Elmenteita, but was re-aligned in 1952.

Numerous roads exist in the area, serving the farming community. Their condition varies greatly according to the seasons, particularly as far as the rains are concerned. Some of the roads are likely to deteriorate rapidly with the onset of bad weather. Even in the forested western part of the lake (outside of the study area), tracks are generally in poor condition and rarely suitable for travel other than 'Toyota Landrover' or any other similar vehicles. Several roads have been made for security reasons, e.g. the road from Nairage Ngare along the Nasampolai ridge, to link up with the track from Narok to Sakutiek and Mau Narok. This road

traverses the ground and forest of the Mau Escarpment from Nairage to Mau Narok (Thompson *et al.*, 1958).

2.1.4. Terrain Condition

To most people who live in or have seen the Naivasha area, its physiography and scenery are impressive and beautiful. The rift valley morphology provides an interesting view of nature. Even more, the various volcanic masses and scarps formed both by faulting and erosion, create a topography of impressive proportions when compared with the undulating peneplains east of the Rift Valley.

The Kinangop plateau appears in the northeastern part of the area, where it lies between the southern mountains of the Aberdare range and the rift floor. It is a broad flat plain ranging in height from about 2,379 m to little over 2,440 m in altitude above sea level. West and southwest of Kinangop plateau, the rocks that form the plateau have been down-faulted in a series of steps. The majority of the faults are short and can be seen to end in one direction or another. Several of the fault-line scarps suggest slightly curved faults, with the downthrown blocks on the convex side.

Where rivers have incised themselves on the western edge of the plateau, deep valleys have been formed in the soft rocks that form the Kinangop. The Malewa River from the northern edge of the area flows in a graben at the foot of the Kinangop plateau.

The Rift floor forms part of the Gregory Rift Valley, and is diverse in its structure and topography. Numerous volcanic cones and craters, scarps and lakes, stud its otherwise monotonous terrain. A notable feature is, for example, Longonot in the southern part of the area.

The Rift floor is largely covered with sediments that accumulated in lakes during the Gamblian stage of the Pleistocene period. They contain a large proportion of volcanic materials, and a few diatomaceous beds are known to occur. Despite their extensive distribution, the Gamblian lake beds are not thick.

The slopes of the cones of acid rocks such as rhyolites and comendites are unusually steep on account of the viscous nature of the lavas at the time of their eruption. The rocks found on the Rift floor vary from undersaturated tephrites to highly acid rocks, such as rhyolites and sodic rhyolites.

The geomorphology of the area is illustrated in Figure 2.2.

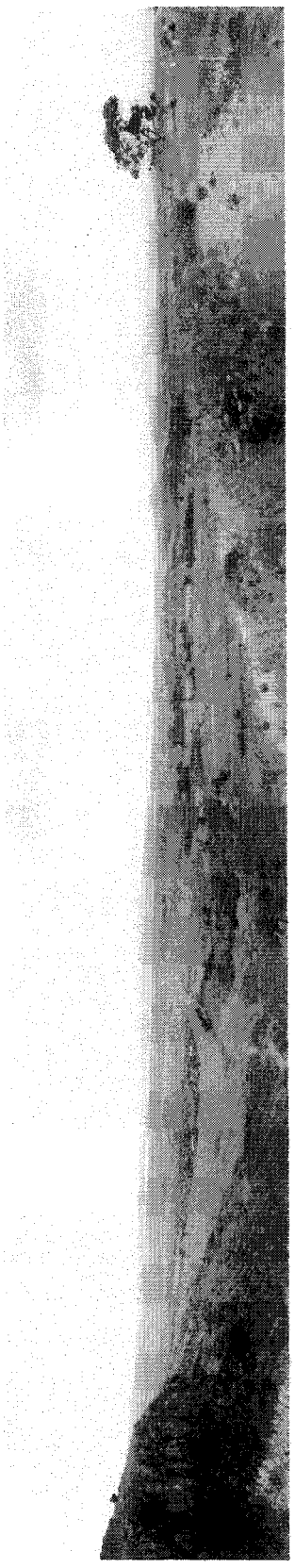

Fig. 2.2 Lake Naivasha which is situated in the Rift Floor of the Kenya Rift Valley is seen as a plain terrain, while the ridge in the left side of the picture is part of the Kinangop Plateau.

2.2. Coordinate System

Primary geophysical and geotechnical data are normally collected by instruments that record digitally. These data are usually observations taken at points or laboratory measurements on samples. Geographic locations of sample sites are, in many cases, established by hand from identifiable ground features shown on topographic base maps. Location on base maps may be digitized on a digitizing table or measured directly in the field by Global Positioning System (GPS) instruments using satellites. GPS undoubtedly become very widespread for primary collection of spatial coordinates as the accuracy and portability of these instruments improve and their costs decrease.

The location of points on the earth's surface is defined using either geographical (sometimes called global) coordinates, or planar coordinates according to specific projections. It is possible to store and manipulate all spatial data in geographical coordinates (latitudes and longitudes). However, all spatial data are visualized on paper or film with planar coordinates. Thus they require a planar map projection for storing spatial coordinates, in order to avoid the repeated transformation from geographic to projection coordinates each time the data are viewed.

In order to define projection mathematically, a geometrical model of the earth is used to generate a projection. Projection can be classified into planar (also known as azimuthal), conic and cylindrical type depending on the shape of the developable surface.

One of the most widely-used system of cartesian coordinates is the Universal Transverse Mercator (UTM) system, established in 1936 by the International Union of Geodesy and Geophysics, and adopted by many national and international mapping organizations. The UTM grid utilized the transverse Mercator projection, which results from wrapping the cylinder around the poles instead of around the equator, as for the ordinary Mercator projection.

The globe is subdivided into sixty UTM zones, numbered from west to east, starting with zone 1 at 180^0W. Each zone is thus six degrees of longitude wide, and extends from 84^0N to 80^0S. The origin of each zone is the intersection of the central meridian at the equator. Displacements in the x and y directions are called UTM eastings and UTM northings, respectively. Conventionally the origin of each zone is offset to the west, and assigned an easting of 500,000 m, so that, within that zone, eastings are always positive. The northing of the equator in the Northern Hemisphere is zero meter, but in the southern hemisphere it is arbitrarily assigned a value of 10,000,000 meter, in order to avoid negative northings. To minimize geometric distortion across each zone, the scale at central meridian is

reduced by a scale factor equal to 0,9996. This produces two parallel lines of zero distortion approximately 180 km either side of the central meridian.

As its name suggests, UTM coordinates have been widely and consistently applied. A UTM spatial reference requires three numbers, the easting, northing and either the zone number or central meridian.

Chapter 3

Literature Review

Geophysical surveys can be useful in the study of most subsurface geologic problems. Geophysics can also contribute to many investigations that are concerned primarily with surface geology. However, geophysical surveys are not always the most effective method of obtaining the information needed. For example, in some areas auger or drill holes may be a more effective way to obtain near-surface information than geophysical work. But in some investigations a combination of drilling and geophysical measurements may provide the optimum cost-benefit ratio.

A clear definition of the geologic or hydrologic problem and objectives of an investigation is important in determining whether exploration geophysics should be used and also in designing the geophysical survey. The lack of a clear definition of the problem can result in ineffective use of geophysical methods. In this study, several geophysical methods were chosen based on the above considerations. The methodology itself will be discussed in chapter five.

3.1 Direct Current (DC) Resistivity Method

The electrical properties of most rocks in the upper part of the earth's crust are dependent primarily upon the amount of water, the salinity and the distribution of the water in the rock (Zohdy et al., 1980). Saturated rocks have lower resistivities than unsaturated and dry rocks. The higher the porosity of the saturated rock, the lower its resistivity, and the higher the salinity of saturating fluids, the lower the resistivity will be. The presence of clay and conductive minerals reduces the resistivity of the rock as well.

Two properties are of primary concern in the application of electrical methods, they are: (1) the ability of the rocks to conduct an electric current, and (2) the polarization which occurs when an electrical current is passed through them -- it is called induced polarization. The electrical conductivity of earth materials can be studied by measuring the electrical potential distribution produced at the earth surface by an electric current that is passed through the earth.

3.1.1 Definition and Units

It is well known that the resistance R -- in ohms -- of a wire is directly proportional to its length L and is inversely proportional to its cross-sectional area A, that is:

$$R \approx \frac{L}{A}$$

or

$$R = \rho \frac{L}{A} \qquad (1)$$

Where ρ -- the constant of proportionality – is known as the electrical resistivity or electrical specific resistance, a characteristic of the material that is independent of its shape or size. According to Ohm's Law, the resistance is given by:

$$R = \frac{\delta V}{I} \qquad (2)$$

Where δV is the potential difference across the resistance and I is the electric current through the resistance.

Substituting equation 1 in equation 2 and rearranging, we get:

$$\rho = \frac{A \,.\, \delta V}{L \,.\, I} \qquad (3)$$

Equation 3 may be used to determine the resistivity ρ of homogeneous and isotropic materials in the form of regular geometric shapes, such as cylinders, parallelopipeds and cubes. In a semi-infinite material the resistivity at every point must be defined. If the cross-sectional area and length of an element within the semi-infinite material are shrunk to infinitesimal size then the resistivity ρ may be defined as:

$$\rho = \frac{\lim_{L \to 0} (\delta V / L)}{\lim_{A \to 0} (I/A)}$$

or

$$\rho = \frac{E_L}{J} \qquad (4)$$

where E_L is the electric field and J is the current density. To generalize, we write:

$$\rho = \frac{E}{J} \qquad (5)$$

The resistivity of a material is defined as being numerically equal to the resistance of a specimen of the material of unit dimensions. The unit of resistivity in the mks (meter-kilogram-second) system is the ohm-meter. In other systems, it may be expressed in ohm-centimeter, ohm-foot, or other similar units.

3.1.2 Rock Resistivity

The resistivity ρ of rocks and minerals displays a wide range (see Table 3.1).

Table. 3.1 Specific resistivity of various rocks and minerals (Springer, 1995).

No.	Rock type/Material	Specific Resistivity (Ωm)
1	Clay, marl, rich	3 – 30
2	Clay, marl meagre	10 – 40
3	Clay, sandy, silt	25 – 150
4	Sand, with clay	50 – 300
5	Sand, gravel in ground water	200 – 400
6	Sand, gravel, dry	800 – 5000
7	Rubble, dry	1000 – 3000
8	Limestone, gypsum	500 – 3500
9	Sandstone	300 – 3000
10	Salt beds and salt domes	> 10000
11	Granite	2000 – 10000
12	Gneis	400 – 6000

In most rocks, electricity is conducted electrolitically by the interstitial fluid, and resistivity is controlled more by porosity, water content and water quality rather than by the resistivities of rock matrix. Clay minerals, however, are capable of conducting electricity electronically, and the flow of current in a clay layer is both electronic and electrolytic. Resistivity values for unconsolidated sediments commonly range from less then 1 ohm-m -- for certain clays or sands saturated with saline water – to several thousand ohm-m for dry basalt flows, dry sand and gravel. The resistivity of sand and gravel saturated with fresh water ranges from about 15 to 600 ohm-m.

3.1.3 Principles of the Resistivity Method

In making resistivity surveys a switched direct current or very low frequency current, normally less then 1 Hz, is introduced into the ground via two electrodes. The potential difference is measured between a second pair of electrodes. If the four electrodes are arranged in any of several possible patterns, the current and potential measurements may be used to calculate resistivity.

The electric potential V at any point P caused by a point electrode emitting an electric current I in an infinite homogeneous and isotropic medium of resistivity ρ is given by

$$V = \frac{\rho I}{4\pi R} \qquad (6)$$

where $R = \sqrt{x^2 + y^2 + z^2}$

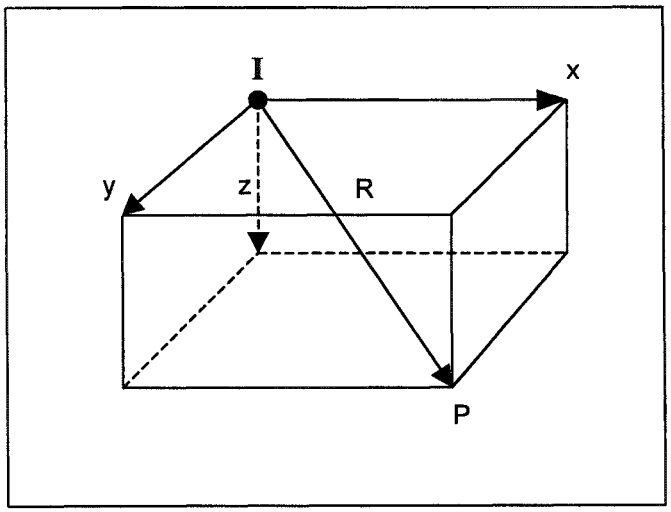

Figure 3.1. Diagram showing the relationship between a point source of current I (at origin of coordinates) in an isotropic medium of resistivity ρ and point the potential V at any point P. See Eqn 6 above.

For a semi-infinite medium, which is the simplest earth model and with both current and potential point-electrodes placed at the earth surface (z=0), equation 6 reduces to

$$V = \frac{\rho I}{2\pi\sqrt{x^2 + y^2}} = \frac{\rho I}{2\pi \overline{AM}} \qquad (7)$$

where $\overline{AM}$ is the distance on the earth surface between the positive current electrode A and the potential electrode M (Figure 3.2.).

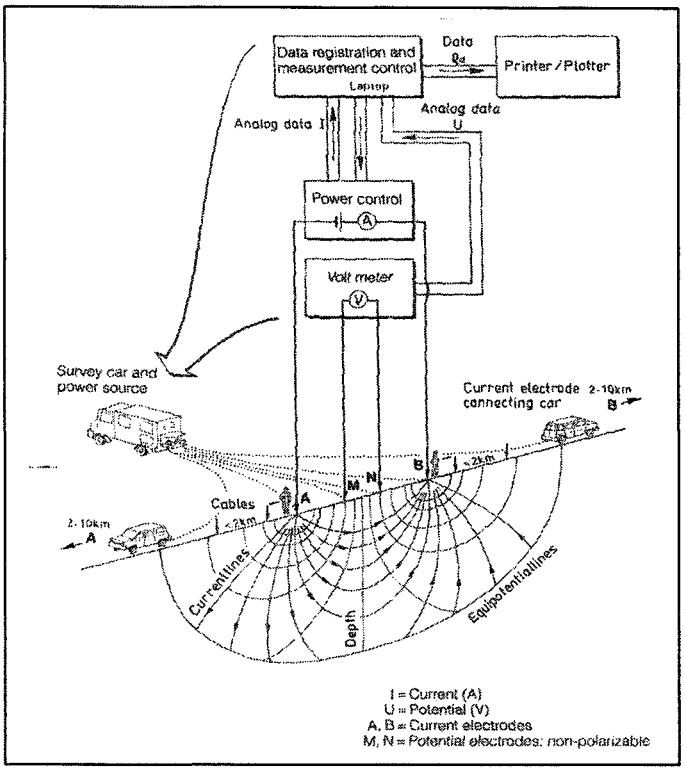

Figure 3.2. Principle of measurement and potential field for DC Resistivity surveys.

When two current electrodes, A and B, are used and the potential difference, δV, is measured between two measuring electrodes M and N, we will obtain :

$$V_M^A = \frac{\rho I}{2\pi}\frac{1}{\overline{AM}}$$ = potential at M due to positive electrode A,

$$V_N^A = \frac{\rho I}{2\pi}\frac{1}{\overline{AN}}$$ = potential at N due to positive electrode A,

$$V_M^B = \frac{\rho I}{2\pi}\frac{1}{\overline{BM}}$$ = potential at M due to negative electrode B,

$$V_N^B = \frac{\rho I}{2\pi}\frac{1}{\overline{BN}}$$ = potential at N due to negative electrode B,

$$V_M^{A,B} = \frac{\rho I}{2\pi}\left(\frac{1}{AM} - \frac{1}{BM}\right)$$

= total potential at M due to A and B,

$V_N^{A,B} = \frac{\rho I}{2\pi}\left(\frac{1}{AN} - \frac{1}{BN}\right)$ = total potential at N due to A and B,

and therefore, the net potential difference is:

$$\Delta V_{MN}^{A,B} = V_M^{A,B} - V_N^{A,B} = \frac{\rho I}{2\pi}\left(\frac{1}{AM} - \frac{1}{BM} - \frac{1}{AN} + \frac{1}{BN}\right) \quad (8)$$

Rearranging equation 8, we express the resistivity ρ by:

$$\rho = \frac{2\pi}{\frac{1}{AM} - \frac{1}{BM} - \frac{1}{AN} + \frac{1}{BN}} \cdot \frac{\Delta V}{I} \quad (9)$$

Equation 9 is a fundamental equation in direct current (DC) electrical prospecting. The factor

$$\frac{2\pi}{\frac{1}{AM} - \frac{1}{BM} - \frac{1}{AN} + \frac{1}{BN}}$$

is called the geometrical factor of the electrode arrangement and generally is designated by the letter K. Therefore,

$$\rho = K.\frac{\Delta V}{I} \quad (10)$$

If the measurement of ρ is made over a semi-infinite space of homogeneous and isotropic material, then the value of ρ computed from equation 9 will be the true resistivity of that material. However, if the medium is inhomogeneous and (or) anisotropic then the resistivity computed from the equation 9 is called an apparent resistivity $\bar{\rho}$.

The value of apparent resistivity is a function of several variables: the electrode spacing AM, AN, BM, and BN, the geometry of the electrode array, and the true resistivity and other characteristics of the sub-surface materials, such as layer thickness, angle of dip and anisotropic properties. The apparent resistivity -- depending on the electrode configuration and on the geology – may be a crude average of the true resistivities in the section, may be larger or smaller than any of the true resistivities, or may even be negative (Al'pin, 1950; Zohdy, 1969).

3.1.4. Electrode Configurations

The value of $\bar{\rho}$ (equation 9) depends on the four distance-variables AM, AN, BM, and BN. If it is made to depend on only one distance-variable the number of theoretical curves can be greatly reduced. Several electrode arrays have been invented to fulfill this goal:

1. Wenner Array
2. Lee Partitioning Array
3. Schlumberger Array
4. Dipole-dipole Array.

In this chapter, only Schlumberger Array would be discussed, since this is the most widely used in electrical prospecting and this array was used for the fieldwork.

Schlumberger Array

This array is the most famous and widely utilized in any geophysical project. Four electrodes are placed along a straight line on the earth surface (Figure 3.3) in the same order, AMNB.

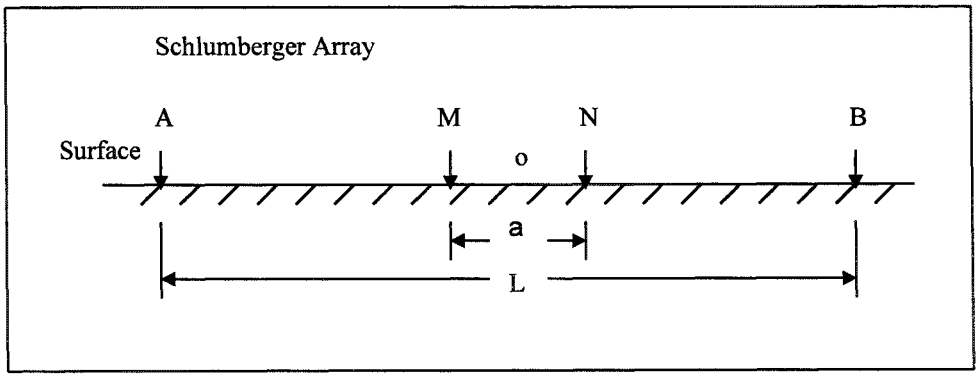

Figure 3.3. Array for geo-electric soundings.

For any linear, symmetric array AMNB of electrodes, equation 9 can be written in the form:

$$\rho = \pi \frac{(AB/2)^2 - (MN/2)^2}{MN} \cdot \frac{\Delta V}{I} \qquad (11)$$

but if MN approaches 0, then equation 12 can be written as

$$\rho_s = \pi (AB/2)^2 \cdot \frac{E}{I} \qquad (12)$$

where $E = \lim_{MN \to 0} \frac{\Delta V}{MN}$ = electric field.

Conrad Schlumberger defined the resistivity in terms of the electric field E rather than the potential difference ΔV. It can be seen from equation 13 that the Schlumberger apparent resistivity ρ_s is a function of a single distance-variable (AB/2). In practice it is possible to measure ρ_s according to equation 12, but only in an approximate manner. The apparent resistivity ρ_s usually is calculated by using equation 11 provided that AB ≥ 5 MN (Deppermann, 1954).

3.2. Geo-magnetic Method

The magnetic method of geophysical exploration involves measurement of the direction, gradient, or intensity of the Earth's magnetic field and interpretation of variations in these quantities over the area of investigation. Magnetic surveys can be made on land surface, from an aircraft, or from a ship. Most exploration surveys made today measure either the relative or absolute intensity of the total field or the vertical component. Measurement of magnetic intensity can be made with a simple mechanical balance or with elaborate electronic instruments.

The unit of magnetic intensity used almost exclusively in exploration geophysics is a gamma (γ). A gamma is defined as 10^{-5} oersted; an oersted is the magnetic intensity at a point that will exert a force of 1 dyne on a unit magnetic pole. The intensity of the magnetic field on or above the surface is dependent upon the location of the observation point in the primary magnetic field of the earth and local or regional concentration of magnetic material. The intensity of the earth's undisturbed magnetic field ranges from a minimum of about 25,000 γ at the magnetic equator to more than 69,000 γ near the magnetic poles.

Magnetic anomalies are distortions of the magnetic field produced by magnetic material in the earth's crust or perhaps upper mantle. Magnetic anomalies of geologic interest are two types: induced anomalies and remanent anomalies. Induced anomalies are the result of magnetization induced in a body by the earth's magnetic field. The anomaly produced is dependent upon the geometry

orientation, and magnetic properties of the body, and the direction and intensity of the earth's field. Because of the dependence on the direction of the earth's field, magnetic anomalies produced by similar bodies may differ widely with geographic location. Remanent anomalies are the result of 'permanent' magnetization of a body and are controlled by the direction and intensity of remanent magnetization and the geometry of the disturbing mass. Most magnetic anomalies are a combination of the two types, but usually one type of magnetization is dominant and the other can be ignored in the approximate interpretation of the results.

Several types of information can be obtained from magnetic surveys. The character of a magnetic anomaly is often indicative of the type of the rock producing the anomaly, and an experienced interpreter can identify a general rock type on the basis of the magnetic anomalies observed. Quantitative interpretation of individual magnetic anomalies yields information on the depth of burial, extent, structure, and magnetic properties of rock units. The most common use of magnetic data in ground-water studies is to map the depth to the magnetic basement rock.

Sedimentary rocks are the most common aquifers. However, most sedimentary rocks are essentially nonmagnetic and thus not amenable to direct study by magnetic methods. A few clastic rocks, e.g. some stream deposits and beach sands, do contain magnetic minerals and can be studied directly.

Igneous and metamorphic rocks generally contain a larger proportion of magnetic minerals and therefore more magnetic than sedimentary rocks but of less interest in ground-water investigations. However, determination of the configuration of the surface of a basement complex composed of igneous and metamorphic rock underlying water-bearing sediments is important in nearby ground-water studies. In general the darker, more basic, rocks are more magnetic than the light colored, acidic rocks. Some volcanic rocks, basalts, are important aquifers.

Magnetic Properties

The magnetic susceptibility and remanent magnetization of rocks are the properties of interest in magnetic surveys. Susceptibility is a measure of the ability of a rock to acquire a magnetization in the presence of a magnetic field. Remanent magnetization is the permanent magnetization of rock and is not dependent on any contemporary external field. The ratio of the remanent magnetization to reduce magnetization is the Q ratio.

Induced magnetization is defined by the formula:

$$M = K.H_0.10^{-5} \qquad (13)$$

where,

K = the susceptibility in cgs units
H_0 = the intensity of the applied field in gammas.

Susceptibility of a rock is primarily dependent upon the composition and internal structure of the rock. The magnetic susceptibility of most rocks depends primarily on the content of magnetite and pyrhotite, the two most common magnetic minerals.

Although remanent magnetization can be acquired by a rock in several ways, thermoremanent magnetization is the most important type. As an igneous rock cools through the Curie temperature (585^0C for magnetite), it acquires a magnetization parallel to the earth's field. This thermoremanent magnetization is usually stable and remains with the rock through subsequent changes in the direction of the earth's field. **Most volcanic rocks are magnetic and many have strong remanent magnetization.** Over near surface volcanic rocks the magnetic intensity may vary widely over short distances, and detailed observations are required to define the magnetic field near the surface. Although in many places the presence of volcanic rocks can be inferred from the character of the magnetic field, the geologic significance of many of the very local magnetic features over volcanic rocks is not determined easily.

3.3. Geohydrology

The morphology of the rift valley has affected surface drainage. Most of the surface drainage occurs within the rift valley. The Naivasha catchment is separated from the Nakuru-Elementeita catchment mainly by the Eburru volcanic system, which is linked to the Mau Escarpment by a ridge at an altitude of around 2600 meter.

To the south of the Lake Naivasha surface drainage, at least at lower altitudes, is limited. Only the river Karati provides perennial flow in its upper reaches, and cuts a deep gully as it descends the step platforms east of Naivasha Town.

The drainage originating on the Olkaria Complex includes the Hell's Gate up to Njorowa Gorge. All the above drainage system, except those from the Kinangop Plateau, terminate as alluvial fans on the Akira plains.

In general the permeability of rocks in the rift valley is low, although there is considerable local variation. Aquifers are normally found in fractured volcanics, or along the weathered contacts between different lithological units. These aquifers are often confined or semi-confined and storage coefficients are likely to be low. In addition aquifers with relatively high permeabilities are found in sediments covering parts of the rift floor (particularly around the lake). Such aquifers are often unconfined and will have relatively high specific yields.

Another limitation is that boreholes can only provide information concerning groundwater conditions within limited depths. In the case of the Rift Valley boreholes this usually implies depths less than 250 m. This means that to a large extent the hydrogeology of the rift valley at depths relevant to recharge of geothermal fields (several kilometers) has to be inferred from information such as piezometric and chemical data. In particular the degree of connection between aquifers intercepted by boreholes on the rift sides, and those at depth beneath the rift is poorly known.

3.4. The impact of the faults on groundwater table

As already mentioned before, the study area is situated in the Kenya Rift Valley. In this rift valley, the geological structure is clearly related to the regional tectonic setting. The azimuths of the faults are normally northwest-southeastern. Most of this faulting has probably occurred prior to the development of the volcanic centers on the rift floor.

Tectonic movements of the Rift Valley have important effects on aquifer properties, both on a small scale by creating the local fracture systems which comprise many aquifers, and on the large scale by forming hydraulic barriers or shatter zones of enhanced permeability.

The faults system also may become a medium for groundwater to move to the deeper aquifers. In the case of Lake Naivasha basin, groundwater circulation was determined according to geodynamic trends and piezometric reconstruction. A general outline was obtained on groundwater recharge in the lake area.

In this case, groundwater recharge is very low. Figure 3.4 shows hypothetical circuits of groundwater in the western part of Lake Naivasha. According to the piezometric and morphological trend, recharge from the east is unlikely since the waters flow downwards towards the deep circuits, through the fault systems that characterize these slopes, as shown by the groundwater contour lines.

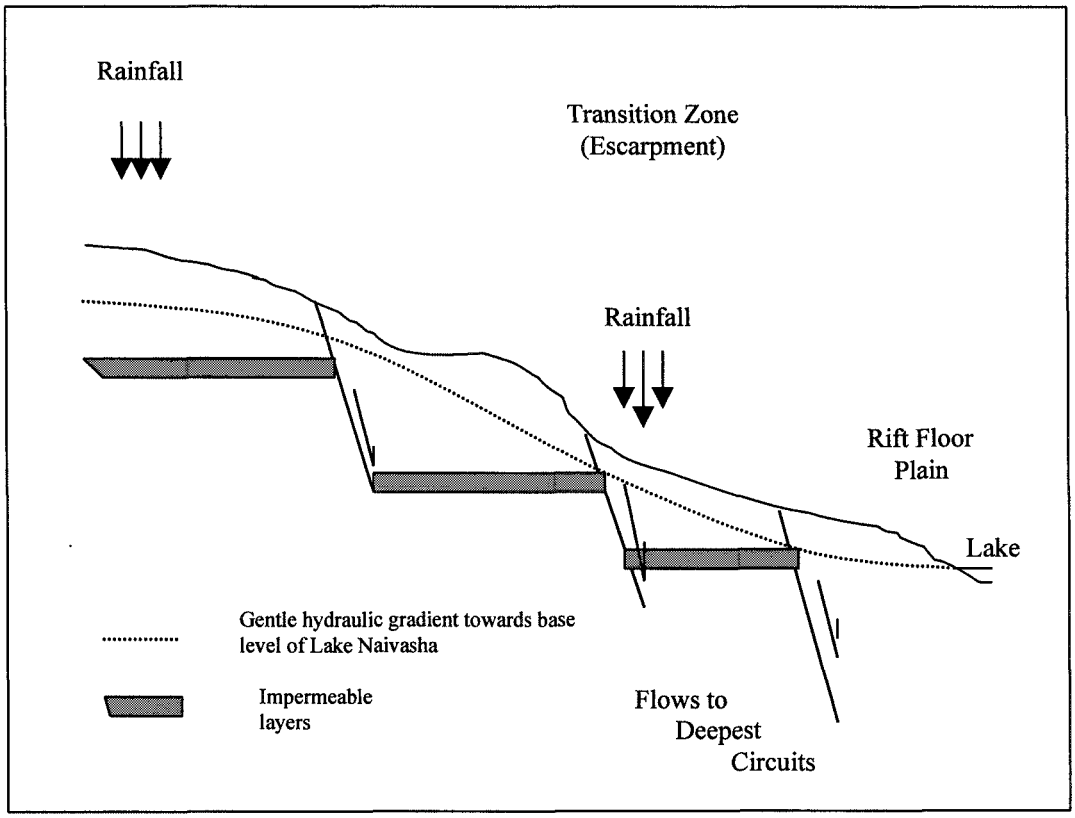

Figure 3.4 Hydrogeological scheme in the Lake Naivasha Area.

Chapter 4
Previous Work

4.1. Geology and Structural Geology

4.1.1. Geology

The oldest dated rocks in the area are sediments and pyroclastics on the Kinangop (Clarke et al., 1990). They are dated as belonging to the Kanjeran stage of the upper middle Pleistocene. Below are rocks of the upper members which are believed to be of Kamasian age. Whilst the oldest rocks found *in situ* in the Naivasha area may belong to the Tertiary era, they are taken to be of lower Pleistocene age because there is a lack of decisive evidence. Some rock fragments ejected by the numerous volcanoes in the area may be Tertiary or older in age.

According to their age from younger to older, the rocks in the Naivasha area are thus succesively classified as follows:
1. Holocene volcanics, lake and fluviatile sediments.
2. Upper Pleistocene volcanics and lake sediments.
3. Upper Middle Pleistocene volcanics and lacustrine sediments.
4. Lower Middle Pleistocene (?) volcanics and lake sediments.
5. Pleistocene (?) volcanics.

The volcanic rocks in the area consist of tephrites, basalts, trachytes phonolites, ashes, tuffs, agglomerats and the acid lavas rhyolite, comendite and obsidian. The lake beds are mainly composed of reworked volcanic material or sub-aqueously deposited pyroclastics. Details of stratigraphy are presented in Table 4.1.

4.1.2. Structural Geology

The tectonic of the Rift Valley have interested large numbers of investigators. Several theories have been put forward to explain the rifting invoke tension, compression and volcanism. Scott (1953) put forward the theory that rifting was due to a squeezing effect towards the equator, caused by the weight of fully developed polar ice-caps during periodic ice ages. He considered that cracks so formed were longitudinal and oblique to the earth's surface, so that in time collapse as a suitable wedge-shaped block could give rise to the floor to the rift valley. This theory must be considered unlikely, as it is not consistent with geological fact.

Table 4.1. The Summary of the Succession in the Naivasha Area

Age	Archaeological Stages	Rock Types Approximate Thickness	Main Locality	Remarks
Holocene	Neolithic	Trachytes and ashes Obsidians	Longonot Southern slopes of Eburru and Cedar Hill	Climate as present day
	Mesolithic	Basaltic ash cones Basaltic flows Silts 3.1 meter	Badlands Badlands Ndenit River	Wetter than present
		Ashes	Longonot	Drier than present day
		Gravels and silts 8.1 meter Trachytes	Ndenit Longonot	Slightly wetter than present day Lake Naivasha 36.6 feet higher than present lake
Upper Pleistocene	Upper Paleolithic	Obsidians	Eburru	Drier that present day
		Lake beds 30.5 meter	Lake Naivasha	Lake Naivasha terraces
	Middle Paleolithic	Basaltic ash cones Rhyolites Phonolites Trachytes Basalts Comendites Phonolites Trachytes (with intercalated pyroclastic)	Badlands Eburu & S.W. Naivasha Eburru Eburru Badlands Lower Eburru Lower Eburru East of Karterit	Drier than present day Faulting Much volcanic activity in the Rift floor
		Swamp deposits minimum Pyroclastics 15 meter	Kinangop and Mau Escarpments (diatomite) of Kariandus	Intense rifting and faulting Wetter than present day Erosion
Middle Pleistocene	Lower Paleolithic	Welded tuff 90 cm Pyroclastics & sediments 122 meter Trachytes 30.5 meter Pyroclastics & sediments w/ intercalated trachytes 122 meter	Rift Walls	Wetter than present day
Lower Pleistocene		Kijabe-type basalt 45.7 meter		

As opposed to the more popular theories invoking tension and compression, Shand (1936) visualized the Gregory rift valley as caused by a trench-like subsidence in a fissure volcano, much as cauldron subsidence takes place in volcanoes. He pointed out that the rift valley is deepest, although the floor elevation is the greatest, where the volcanic sequence was the thickest, and that, as the volcanic rocks thin to the north and south, the valleys flatten out. The most obvious objection to this hypothetis is that the Gregory Rift Valley is only a small part of an enermous rift system extending from Palestine through East Africa, possibly as far as South-West Africa (Brock, 1953). Furthermore, vast strecthes of the rift valleys are free of volcanics.

In the Naivasha area there is evidence of near-vertical step-faulting. These fault-scarps are often well preserved and marker horizon can be progressively traced on lower steps. It is notable that the majority of the fault-blocks plunge southward.

The age of the faulting as a whole presents a problem. Shackleton (1955) considered the main faulting took place just before the lower Pleistocene while Kent (1944) suggested that the earliest rifting of the Gregory Rift Valley took place in the Upper Miocene, and either the Pliocene or Pleistocene. Baker (1958) found evidence of pre-Pleistocene faulting in the Magadi area. In the present area evidence of pre-Pleistocene rifting is lacking, as there are no pre-Pleistocene rocks and as the nature of the subvolcanic floor is unknown. The bulk of the faulting apparently took place in late Middle Pleistocene times, either in late Kamasian times or possibly as late as Kanjeran stage, possibly along older fault lines. It can be observed that the Kamasian beds in the Kinangop escarpment have been cut by the faulting. The Kanjeran sediments capping the Kinangop, the best exposed at the stone-age horizon known as Cartwright's site, have also been preserved as they re-appear on the lower down-faulted shelf. There has been a great deal of slumping in this part of the area, however, and the lower occurrence is obscured by much overburden, so there is no definite proof of fault displacement. It should be noted , however, that if faulting did take place towards the close of the Kanjeran stage, the damp sediments might tend to slump rather than fracture cleanly along the fault-lines, which could account for disparity of dip-slopes quoted by Shackleton. The faulting that took place in middle Pleistocene times is also believed to be largely responsible for the intense disruption of the valley floor lavas.

The youngest phase of faulting is at least of late or post-Gamblian (Upper Pleistocene) age as it cuts through Gamblian sediments at the faulted ash craters in the Badlands area, and again in a single instance on the Ndabibi plains south of Eburru. This faulting is essentially tensional, the result being fissures of various dimensions. There is no indication of whether the Olgaria fissures, in which abundant steam-jets occur, are of the same age but their general appearance and condition of erosion suggest that they were contemporaneous with the Eburru

faults. The two main sets of faulting are quite distinctive, the rift faulting being aligned in a north-northwest to south-southeastern direction while the younger faults follow an approximate north-south alignment (Figure 4.1.)

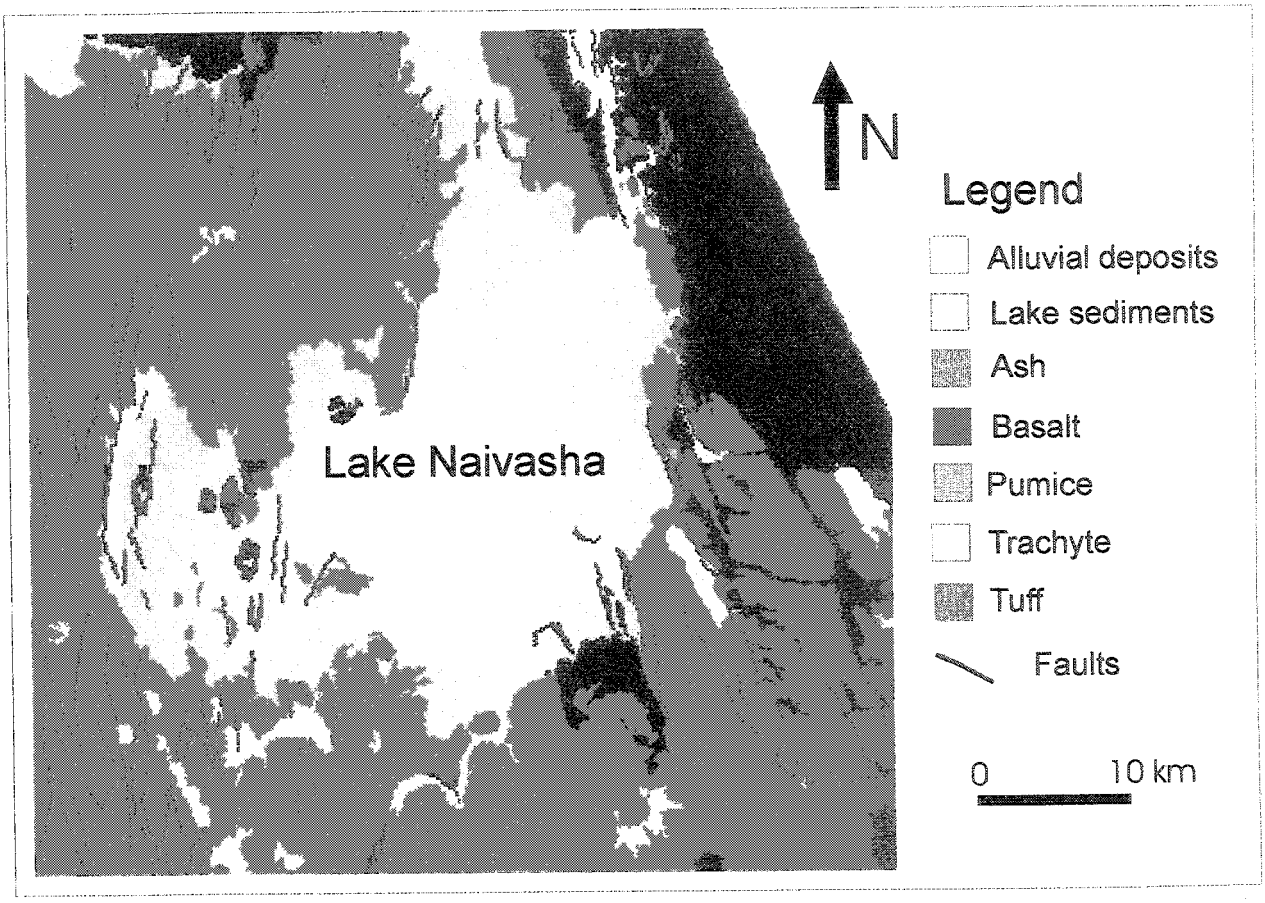

Fig. 4.1 Simplified geological map of the study area

There is a little evidence of folding in the area. Scott (1953) described anticlinal arching 'Kamasian' beds in the valley floor as a whole on a north-south axis. The only exposures of what are believed to be middle Pleistocene sediments of Kamasian age in the rift floor are in the Njorowa Gorge. There is a slight arch on approximate east-west axis, the dip of the limbs being of the order of 0.5^0. The bands of rock at the extremities of the gorge dip gently to the north and south respectively.

The slight tilting of the upper Pleistocene Gamblian Lake Beds – as a result of arching along an axis passing through Eburru – has already been described by Nilsson (1945) who found a fossil water buffalo *Bubalus nilssoni* sp in Quaternary lake beds near Malewa River, probably deposited by the Gamblian Lake. This tilting is taken as evidence of the north-south folding.

4.2. Geo-hydrology

The Naivasha catchment is a hydrogeologically complex feature, because while it is lower than Rift escarpments, it is at a culmination of the rift floor as well. The catchment is separated from the Nakuru-Elmenteita catchment mainly by the Eburru volcanic pile which is linked to the Mau Escarpment by a ridge at an altitude of around 2600 m. Between Eburru and the Bahati Escarpment, the surface drainage divide runs through Gilgil along the rift floor at an altitude of approximately 2000 m. Flow towards Lake Naivasha from the Mau escarpment and the Kinangop Plateau is unambiguous and some of the groundwater from the western side of the rift must eventually form part of the discharges at Olkaria and Eburru. However, the groundwater flow along the N-S axis of the Rift Valley is more difficult to assess.

Southeast of the drainage divide the perennial Gilgil and Malewa Rivers provide much of the recharge to Lake Naivasha. The slope of Bahati Escarpment provides runoff to some of the tributaries of the much larger Malewa River. Most of the discharge of the Malewa River, however, at least in its upper reaches, is derived from the western slopes of the high Nyandarua Range. Further downstream the Malewa is joined by the Turasha River which is also perennial and drains the north Kinangop Plateau through deeply incised tributaries.

To the north of Naivasha the surface water divide runs approximately east-west through Eburru, and then north through Gilgil. Accordding to Clarke et al. (1990) there is no evidence that the groundwater divide follows this route. However, recent investigations (Ramirez, 1999, Behar, 1999) have shown that the shallow groundwater flow divide coincides with the surface water divide. There appears to be some evidence for deep groundwater outflow towards Lake Elmenteita in the north. However, the dominant deep groundwater outflow from the lake (if any) appears to be towards the South.

To the south of Lake Naivasha the surface water divide runs from the Mau Escarpment in the West, through Olkaria and Longonot to the Kinangop Plateau and finally to the Nyandarua Mountains. Surface drainage and shallow groundwater flow in the vicinity of the lake appear to be towards the lake. Drainage south of this divide originates on downfaulted platforms of the western rift margin of the Sakutiek settlement, on the Olkaria Volcanic Complex, on Longonot Volcano, and on and adjacent to the southernmost part of the Kinangop Plateau. The drainage originating on the Olkaria Complex includes the Hell's Gate – Ol Njorowa Gorge. All the above drainage systems, except those from Kinangop Plateau, terminate as alluvial fans on the Akira Plains.

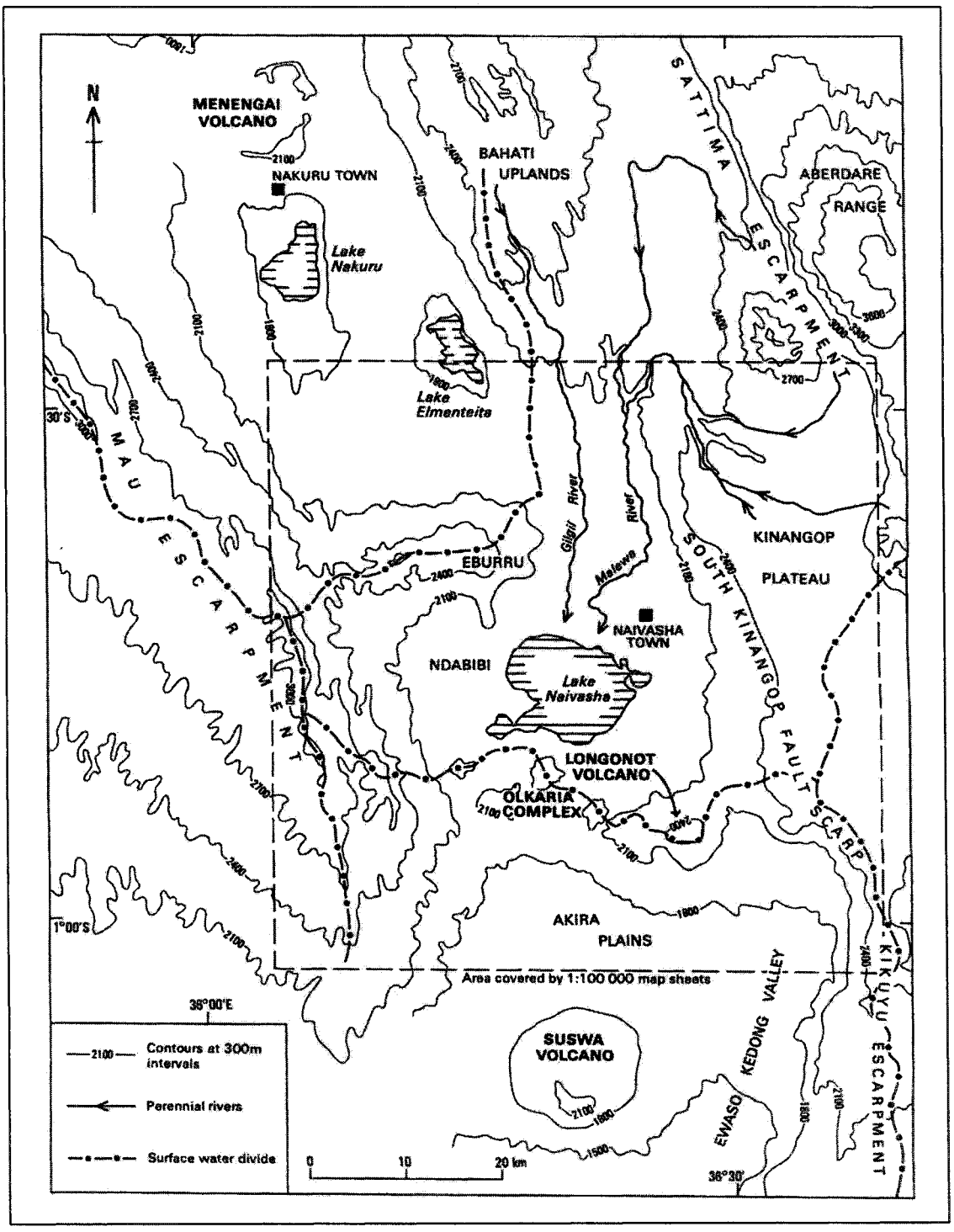

Figure 4.2. Surface runoff in the study area

Around Lake Naivasha itself the groundwater level is between approximately 1880 and 1890 m, similar to that of the lake itself. East and west of the lake the groundwater contours rise, indicating flow towards the lake, while to the south they remain at about the same level as far as the latitude of the Longonot and Olkaria Complexes. South of this region the piezometric surface must drop by several hundreds of meters according to the level information provided by the few boreholes drilled between Longonot and Suswa, which all proved to be dry or have produced steam. The data indicate a fall of at least 450 m in piezometric level or a distance of around 10 km (i.e. a gradient of at least 0.05). At depth a north-south pressure gradient of 11 bars/km has been reported in the Olkaria geothermal field (Bodbarsson et al., 1987) which corresponds to a freshwater head gradient of 0.1 (Fig. 4.3).

Groundwater appears to flow away from Lake Naivasha because the lake water is fresh, even though the lake has no outlet and lies in an area of high evaporation. The position of the lake, at a culmination of the rift floor, suggests flow both to the north and to the south (i.e. a regional groundwater divide runs east-west in the vicinity of the lake). Southerly flow must also occur, following the hydraulic gradient. However, piezometric evidence shows that close to the lake, shallow groundwater flow directions are towards the lake, even on the northern and southern ends.

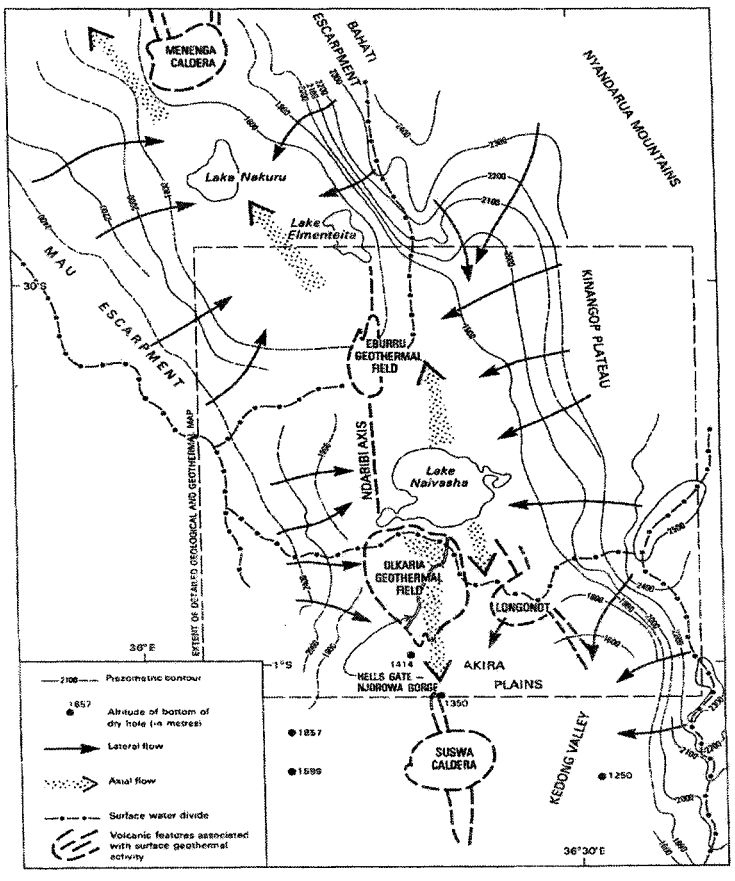

Figure 4.3. Piezometric map of the study area

4.3. Geophysics - Gravity

As already mentioned in previous chapters, the Kenyan Rift Valley conforms closely to an early stage of plate margin construction, where oceanic crust is created at spreading centers. This rift is part of a worldwide system of sublinear belts of active seismicity, volcanicity and heat flux defining the edges of the lithosphere.

In this particular area, however, separation is not complete although geophysical evidence strongly suggests that the lithosphere is anomalously thin representing the incipient nature of the breakup process (Wendland and Morgan, 1982).

The lithosphere, in continental areas away from rift zones and high mountain belts, consists of an upper layer of crustal rocks averaging 40 km in thickness underlain by seismic discontinuity marking the transition to less dense, partially melted mantle (Windley, 1984). A combination of gravity, seismic and heat flow data indicates that the East African Rift system, which has relatively normal crustal thickness, characterizes the rift shoulders. However, it is reduced to 20 km within the rift. Furthermore, the seismic data can be interpreted as indicating that the zone of partial melting – top of the asthenosphere – may be in direct contact with the lower crust (Fig. 4.4).

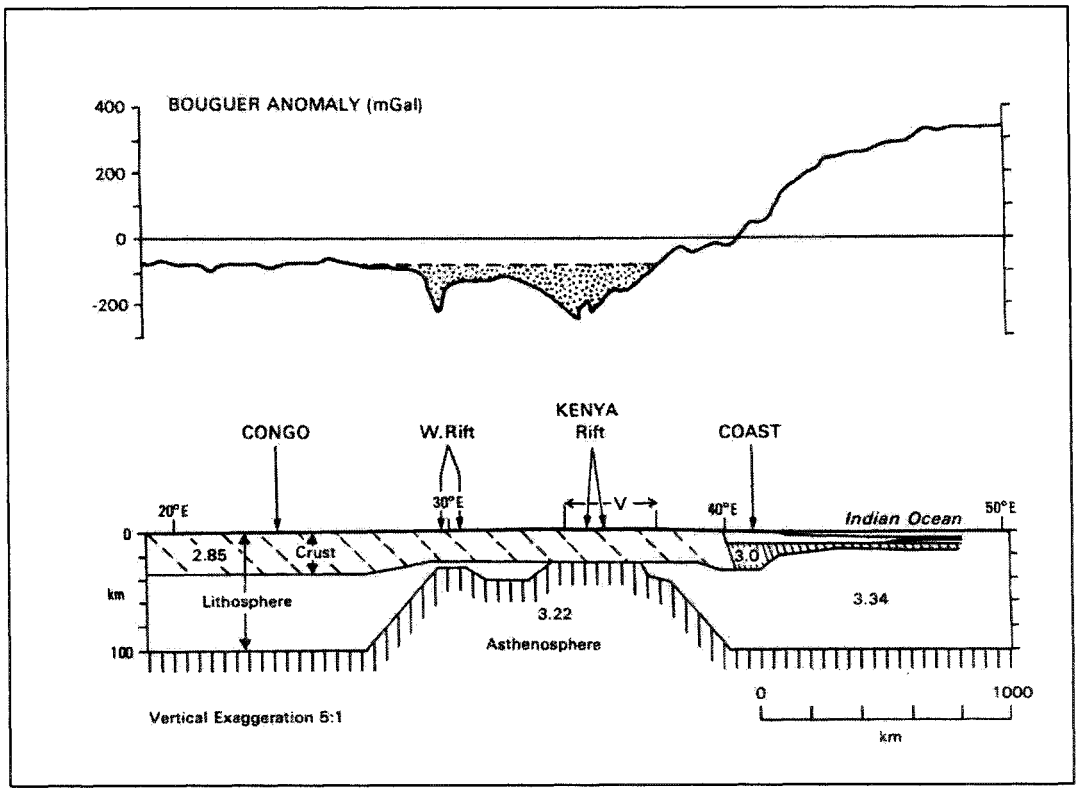

Figure 4.4. Regional E-W Bouguer anomaly profile and lithospheric model through Central and Eastern Africa (after Fairhead, 1986).
The general effect is of an approach to breakup involving close contact of the crust and updoming asthenosphere.

The evidence for structural doming was based on quite scattered occurrences of Miocene sediments that in turn lead to the concept of a pre-Miocene erosion surface (Shackleton, 1951; Pulfrey, 1960). This was believed to show a gradual rise towards the rift with a relatively sharp reversal of dip on the shoulders. The domal structure and another coinciding with the Ethiopian highlands are frequently related to explanation of some of the broad gravity anomalies of the region. Refinement of the gravity database, however, shows that the rift axis coincides with a linear zone within the regional gravity low (Fig. 4.4).

During the Pliocene (5-2 Ma BP) the junction area may well have been the locus of highest mantle activity and therefore volcanism. It can be argued, however, that by the later Pleistocene and continuing to the present, the locus of most intense mantle activity has moved South and now corresponds to the western side of the rift in the Elmenteita-Naivasha area. The following facts support this view:

1. The rift floor reaches its highest elevation (nearly 2000 m) in the Elmenteita-Naivasha area.
2. The western rift escarpment (Mau) reaches its highest elevation due West of Lake Naivasha.
3. Three large (and highly evolved) volcanic complexes (Longonot, Olkaria and Eburru) occur around Lake Naivasha within an area of 50x30 km – a much greater concentration of Pleistocene to recent volcanoes than exists elsewhere in the rift.
4. The regional gravity minimum corresponds with the highest portion of the Mau escarpment, and therefore with the Olkaria and Eburru centers.
5. Olkaria and Eburru are the only Late Quaternary (i.e. still active), centers in the rift where rhyolitic volcanism is present. Rhyolites represent the most evolved composition in terms of fractional crystallization. Alternatively they may have resulted from partial melting.

Chapter 5
Methodology

5.1. Equipment and Materials

For the fieldwork, the equipment consisted of the following:
1. Electrical Resistivity, Abem Terrameter (Figure 5.1.)
2. Geophysical Well Logging, Terrameter SAS Log 200.
3. Hand Auger

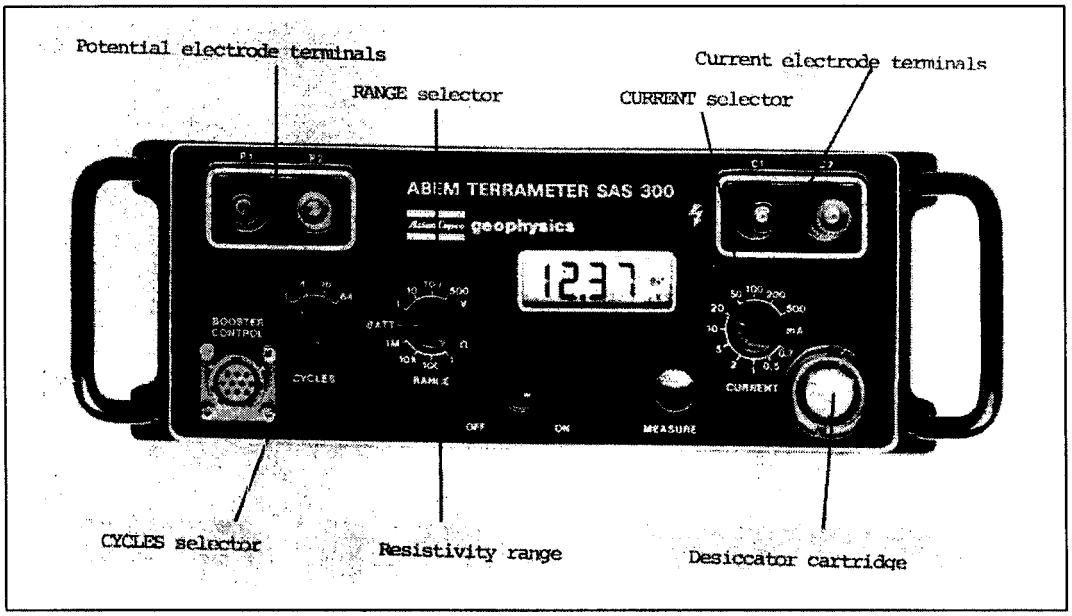

Figure 5.1. Abem Terrameter SAS 300 used in the fieldwork

While the materials used include the following:
1. A set of aerial photographs of approximately 1 : 50,000 scale, run 1 to7.
2. Stereoscope
3. Topographic map of Naivasha (sheet South A-37/A-III-NE, 133/2) and Longonot (133/4) Area. Both at scale 1:50,000.
4. Geological map of Longonot Volcano, The Greater Olkaria and Eburru Volcanic Complex and Adjacent Areas, scale of 1 : 100,000.
5. Personal computer (hardware).

6. Computer softwares:
   - Word processor: Microsoft® Word 97 SR-1.
   - Spreadsheet: Microsoft® Excel 97 SR-1.
   - Grapher v.1.30
   - Surfer v.6.03
   - ILWIS 2.2 (GIS)
   - Adobe Photoshop
   - Corel Photopaint v.7.0
   - Resist87 v.1.0
   - Geosoft-Oasis Montaj v.4.0
   - Map Maker v.2.0

5.2. Research Methods

5.2.1. Methodological Background

As groundwater becomes one of the most important commodities in many African countries, methods for locating and controlling good aquifers at low cost must become more efficient. For this reason, geophysical methods are playing an important role in groundwater investigations. The methods, which are considered in this study and which are widely used in groundwater exploration, are electrical prospecting as well as geophysical well logging techniques. The application of the geophysical methods in groundwater investigations support:

- Determination of the subsurface structures of the basins
- Determination of the horizontal and vertical distribution of aquifers and their regional boundaries
- Detailed investigation of areas of artificial groundwater recharge
- Tracing groundwater movements
- Locating groundwater discharge areas below seas, lakes, rivers, etc.
- Mapping promising groundwater zones like thick saturated weathered rock, fracture zones, solution cavities and fissures in hard rocks.

In recent years, in addition to the aspects mentioned above, contributions have been made to develop a relationship between the geophysical and the hydrogeological parameters of aquifers. The contribution of geo-electrical methods especially vertical electrical sounding (VES), and geophysical well logging are discussed. Both methods are comprehensively discussed in this chapter.

5.2.2. Techniques of Data Collection

The data collection started at the ITC (Enschede) and continued in the field during October 1998.

5.2.2.1. Pre-fieldwork

In the office, existing maps and aerial photographs were interpreted to determine relevant geological features. The approach was based on integration of drainage pattern, geology and geomorphology to delineate the fault in preparation of the field work. Having completed this step, observation points were then selected.

5.2.2.2. Fieldwork Techniques

The fieldwork consisted of geophysical exploration and the identification of present water depth by making some boreholes (in the work carried out close to the lake where the water table is close to the surface)

5.2.2.2.1. Resistivity

The resistivity surveying mode, i.e. Schlumberger Array, that was applied for the survey is shown in the Figure 5.2., with ample separation (>5m) between potential and current cables to avoid crosstalk.

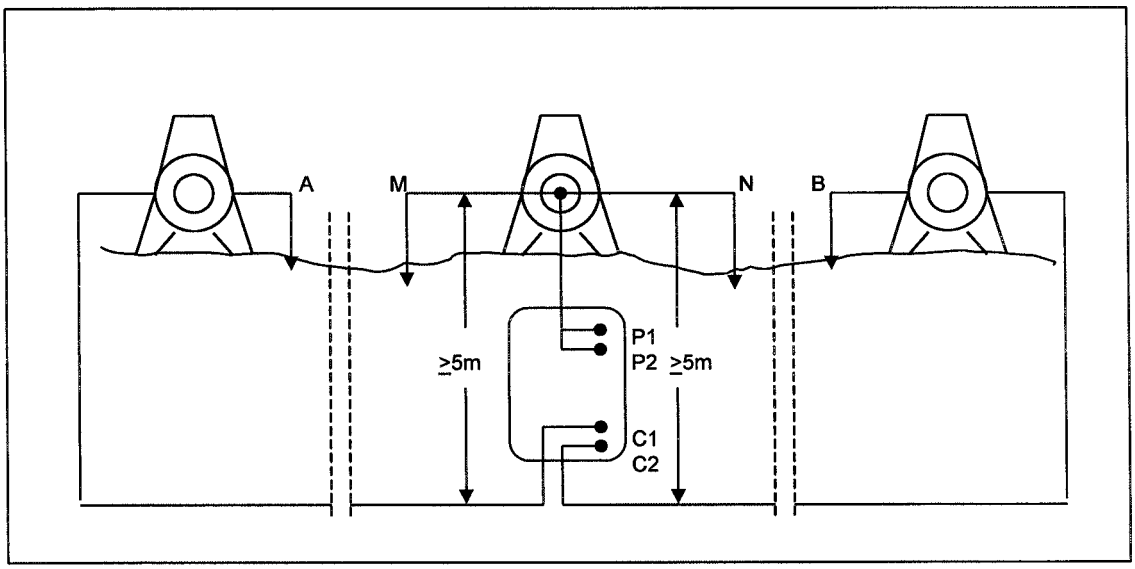

Figure 5.2. Resistivity surveying setup

Non-polarizing potential electrodes are preferable above metal electrodes because of the self potential effect. However, only steel electrodes were available.

The following points must be observed during the field work.

- Position of ABEM terrameter is half way between the potential electrodes M and N. Terminals P1 and P2 are connected to M and N respectively. ABEM sounding cables set unit or 2-conductor cable of good quality are used with the conductors separated at the electrode end.
- The current electrodes A and B are connected to terminals C1 and C2 respectively. These cables are run in parallel adjacent to the terrameter, and are arranged symmetrically with respect to the potential electrodes.
- The RANGE selector is turned to the 1 ohm position, the CYCLE selector to position 4, and the CURRENT selector to position 20, before switching on the power and pressing the MEASURE button.
- When the 'error 1' code appears and the beeper sounds repeatedly, the current can be reduced step by step until the beeper stops sounding, then the reading will appear on the display afterwards. In the case of the beeping does not stop, the transmitter cables and current electrodes should be checked for bad connections.
- When the 'error 2' code appears and the beeper sounds repeatedly, the setting of the RANGE selector can be increased in steps to obtain higher resistance ranges until the beeper stops sounding. The reading will appear on the display afterwards.
- The four readings that appear successively on the display have to be observed. When they are nearly equal, the noise level is low and the setting of the CYCLES selector can be reduced to 1. However, if the third and fourth readings differ significantly from the previous ones, the CYCLES selector can be turned to position 16 or even 64 (to obtain 16 or 64 cycles). Alternatively, the current can be increased by improving the current electrode grounding or using the SAS 2000 Booster.
- Negative resistance readings can occur for two reasons:
  - ➢ The current or the potential electrodes have been connected with reversed polarities.
  - ➢ The noise level may be much higher than the signal level (long distance between A and B and low current)

  If this is causing single negative readings, signal averaging must be used.

5.2.2.2.2. Geophysical Well Logging

Geophysical well logging equipment used for the survey was Terrameter SAS Log 200. This equipment consists of a 200-m long logging cable with a logging probe, a 6-position MODE selector and circuitry for connecting a Terrameter SAS 300, a current return electrode and a potential reference electrode.

The stainless steel upper end of the logging probe serves as an electrode D. The lower inside end of the probe – the chamber – has one ring electrode E and a centre electrode F. A control cable connects the 10-position connector on the SAS 200 to the connector on the SAS 300. A 4-conductor cable is permanently attached to the SAS LOG 200. It is connected to the potential (P1, P2) and current (C1,C2) terminals on the Terrameter SAS 300. The return current terminal is connected to a return current electrode placed not less than 75 m from the well to be surveyed. This electrode must be properly grounded.

The potential reference terminal is connected to a reference potential electrode, i.e. ABEM stainless steel electrode, not less than 50 m from the well and in the opposite position from the return current electrode (Figure 5.4.)

Resistivity is measured while the SAS 300 is in the resistivity-surveying mode. The RANGE selector is normally set to 1 ohm and the CURRENT selector to 20 mA. To take the measurements, the logging probe is lowered to the desired depth below the ground water table and the 6-position MODE selector is set to the desired position. The Terrameter SAS 300 is turned on and measurements are taken as follows.

A number of different electrode configuratiuons are used in resistivity logging. (Fetter, 1994). These include the short-normal, long-normal and lateral configurations, as shown in Figure 5.3. The short-normal resistivity curve indicates the resisistivity of the zone close to the borehole where drilling fluids have possibly invaded the drilling formations. The long-normal method has more spacing between the electrodes and thus measures the resistivity farther away from the borehole – presumably beyong the influence of the drilling fluid. Lateral devices have very widely spaced electrodes for measuring zones that are far from the borehole. Because of the wide spacing, lateral devices will have a lower resolution and will therefore not pick out thin beds of different resistivity. With the equipment used, these methods can be applied with a single set of electrodes lowered down the borehole.

a. Short Normal Logging

The MODE selector is set to the NORMAL 16" position and the MEASURE button is pressed on the SAS 300. Current is then injected via the upper probe electrode. The corresponding signal voltage is measured between the ground potential reference and the ring electrode at the bottom of the probe. A network in the SAS LOG 200 causes the SAS 300 to display R_{displ} in ohms or milliohms. This value is proportional to the resistivity of the surrounding medium (no hole corrections).

$$\rho = 100 \times R_{displ} \text{ (ohm-metres)}$$

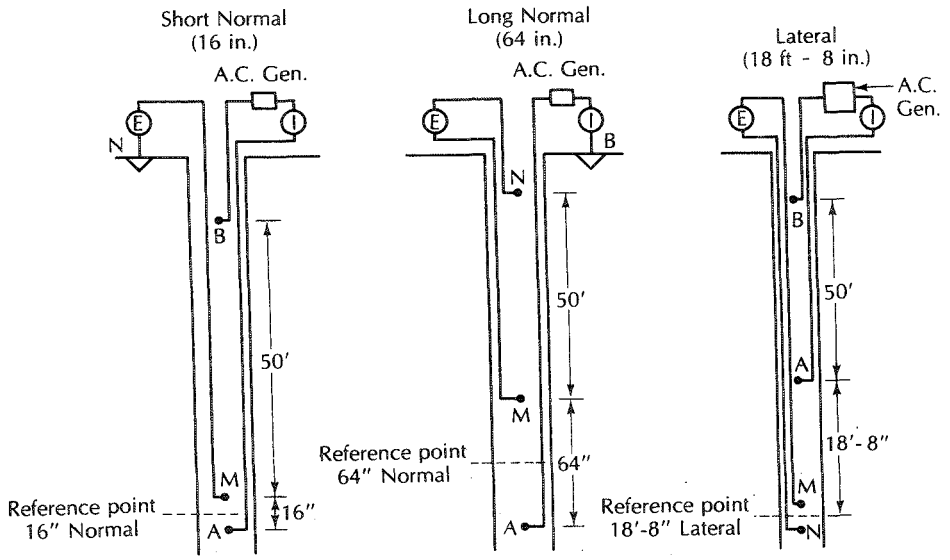

Fig. 5.3 Electrode configurations for short-normal, long-normal and lateral resistivity logging devices.

If the displayed value is 175 milliohms, the resistivity will be 100 x 0.175 = 17.5 ohm-metres.

b. Long Normal Logging

The MODE selector is set to the NORMAL 64" position and the MEASURE button is pressed on the SAS 300. Current is then injected via the cable electrode while potential is measured at the ring electrode at the bottom of the probe. A network is the SAS LOG 200 provides the same conversion constant as that used for short normal logging (see section a).

$$\rho = 100 \times R_{displ} \text{ (ohm-metres)}$$

c. Long Lateral Logging

The MODE selector is set to the NORMAL 18" position and the MEASURE button is pressed on the SAS 300. Current is injected via the cable electrode and the potential is measured between the ring chamber electrode at the bottom of the probe and cable electrode.

The network in the SAS LOG 200 now provides a conversion factor that differs from that used for short normal and long normal logging. As a result:

$$\rho = 1000 \times R_{displ} \text{ (ohm-metres)}$$

d. Fluid Resistivity Logging

Set the mode selector to the FLUID position and the MEASURE button is pressed on the SAS 300. Current (20mA) is injected via the ring electrode, while the potential is measured between the upper probe electrode and the centre electrode. The SAS LOG 200 needs no conversion factor here.

$$\rho \text{ fluid} = R_{displ} \text{ (ohm-metres)}$$

The following corrections should be made for small-diameter wells:

Well diamater (mm)	Multiply R_{displ} by
50 – 60	1.08
60 – 70	1.06
70 – 80	1.04
80 – 90	1.03
90 – 100	1.01

e. Temperature Logging

Temperature is measured while the SAS 300 is in the resistivity-surveying mode and the MODE selector on the SAS 200 is at the TEMP°C position. The 1-ohm scale and 0.5 mA current are used, and 1°C is equivalent to 1 ohm. If the CURRENT selector is not at the 0.5 mA position, the SAS 300 issues an alarm (beeper signal) and error code 1 appears. Temperature is measured to an accuracy of $\pm$1°C within the 0° ...+50°C range. The usable precision is 0.01 °C within the 0° ...+50°C range and 0.1°C within the +20°C ... + 50°C range, thus permitting local temperature gradients to be studied in detail.
When using the high precision for temperature gradient studies, ample time must be allowed to permit the probe to reach thermal equilibrium in relation with the fluid. The probe is moved slightly up and down a few times while waiting for equilibrium to be established.

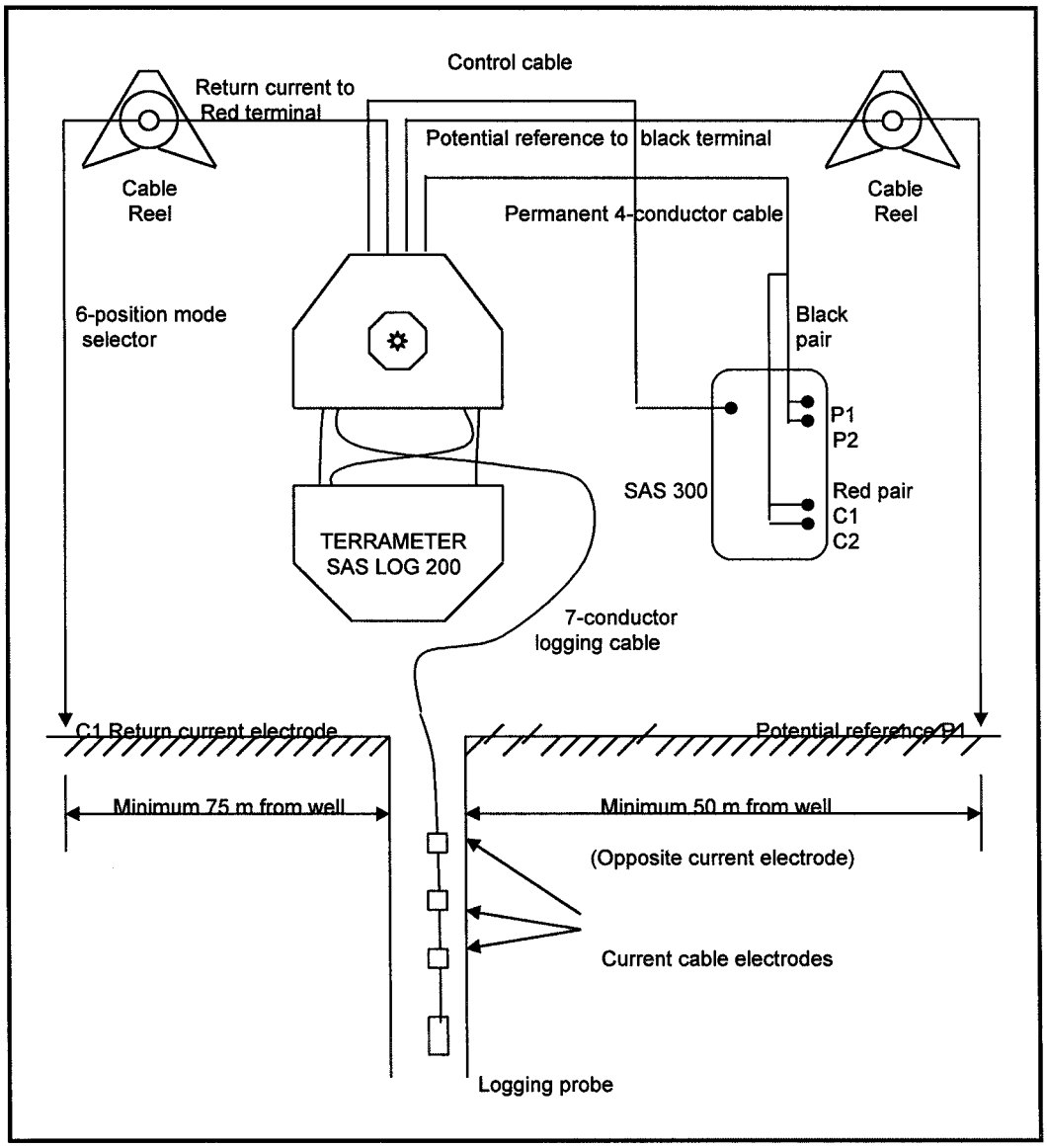

Figure 5.4. Terrameter SAS LOG 200 well logging setup

5.2.3.2. Technique of Data Processing/Interpretation

5.2.3.2.1. Map Handling

Maps compiled for this study had a basic scale of 1: 50,000. For easy manipulation need and GIS use, they were digitized and handled with ILWIS 2.2 software (ITC, 1993). ILWIS is an Integrated Land and Water Information Systems developed by ITC. This program can be used interactively to integrate spatial and non-spatial data using both raster and vector input.

5.2.3.2.2. Vertical Electrical Soundings (VES)

In geoelectrical prospecting, experience has shown that apparent resistivity sounding curves often have high frequency noise components because of disturbance due to localized inhomogenities of surface and near surface materials, errors in measurements, etc. It is therefore worthwhile to use a method, which allows smoothing of field sounding curves. It seems to be generally accepted that noise filtering may be accomplished somewhat by discarding and replacing outlying data. In the analysis of the VES sounding curves the RESIST software was used (Van der Velpen, 1988).

The stages in the data processing can be summarized as follows :

Single Point Correction

Raw field data need to be corrected both for high and low frequency noise components, originating from from disturbances due to localized inhomogeneities, near surface materials and errors in measurement. Several filtering techniques are available to accomplish this :

- *visual inspection of experimental curves and removal of outliers*

  This technique is straightforward. However, much depends on the geophysicist's assessment of potential errors.

- *Interpolation*

  It has been shown that cubic spline interpolation is more suitable for treatment of VES sounding curves than the simultaneous polynomial interpolation of all observation points. Several cubic spline interpolation methods may be tried with the RESIST Software.

- *Extrapolation*

  Automatic extrapolation techniques are applied to correct the starting and ending points of an apparent resistivity sounding curve. It is not very often the case that the asymptotic values on both sides of the curves have been reached during field work. The extrapolation to the left does not present much problems because the resistivity would always be that of the top layer. The extrapolation to the right gives more problems because it rarely happens that the survey is completed up to an electrode distance at which the asymptotic value for the resistivity of the bottom layer is obtained. A choice is possible between hyperbolic extrapolation and the more conventional horizontal straight line technique.

<u>eccentricity correction and vertical shift of branches</u>

In resistivity measurements for a Schlumberger array it is occasionally necessary to increase the distance between the potential electrodes as the distance between the current electrodes increases. Without this stepwise increase the potential difference would become too small to allow reliable measurements. The eccentricity is defined as the ratio between the potential and current electrode spacings. Changes in eccentricity values cause shifts in the apparent resistivity values of a given layer stratification.

The lack of tie-in between adjacent segments of an apparent resistivity curve may also be caused by the occurrence of near-surface inhomogeneities in the ground. These inhomogeneities affect the current density and distribution pattern, depending on the position of the potential electrodes.

The software applies eccentricity corrections to a standardized eccentricity value.

The vertical shift of an entire segment on the logarithmic scale is the adjustment of the tie-in between the segments of an apparent resistivity curve caused by near-surface irregularities. It is normally assumed that changes in

current density are independent of current electrode spacing. This allows the user to shift the entire curve-segment vertically. In the software this can be done interactively on-screen.

Inverse modelling

The method used by RESIST to calculate the theoretical curves, is the linear filter technique, which was first introduced by Ghosh (1971). Resistivity inversion is the technique to fit a theoretical curve to the experimental data. Usually this is accomplished with non-linear least squares techniques, such as, for example, the Marquardt-Levenberg technique. However, solutions will always depend on the selection of the initial model, i.e. the number of layers.

Fig. 5.5 illustrates the different steps in the modelling process with RESIST.

5.2.3.2.3. Resistivity Profiling

The interpretation of horizontal profiling data is generally qualitative and the primary value of the data is to locate geologic structures. Quantitative interpretation is obtained by making a sufficient number of profiles with different electrode spacings. Best results are obtained generally from a combination of horizontal profiling and electrical sounding data.

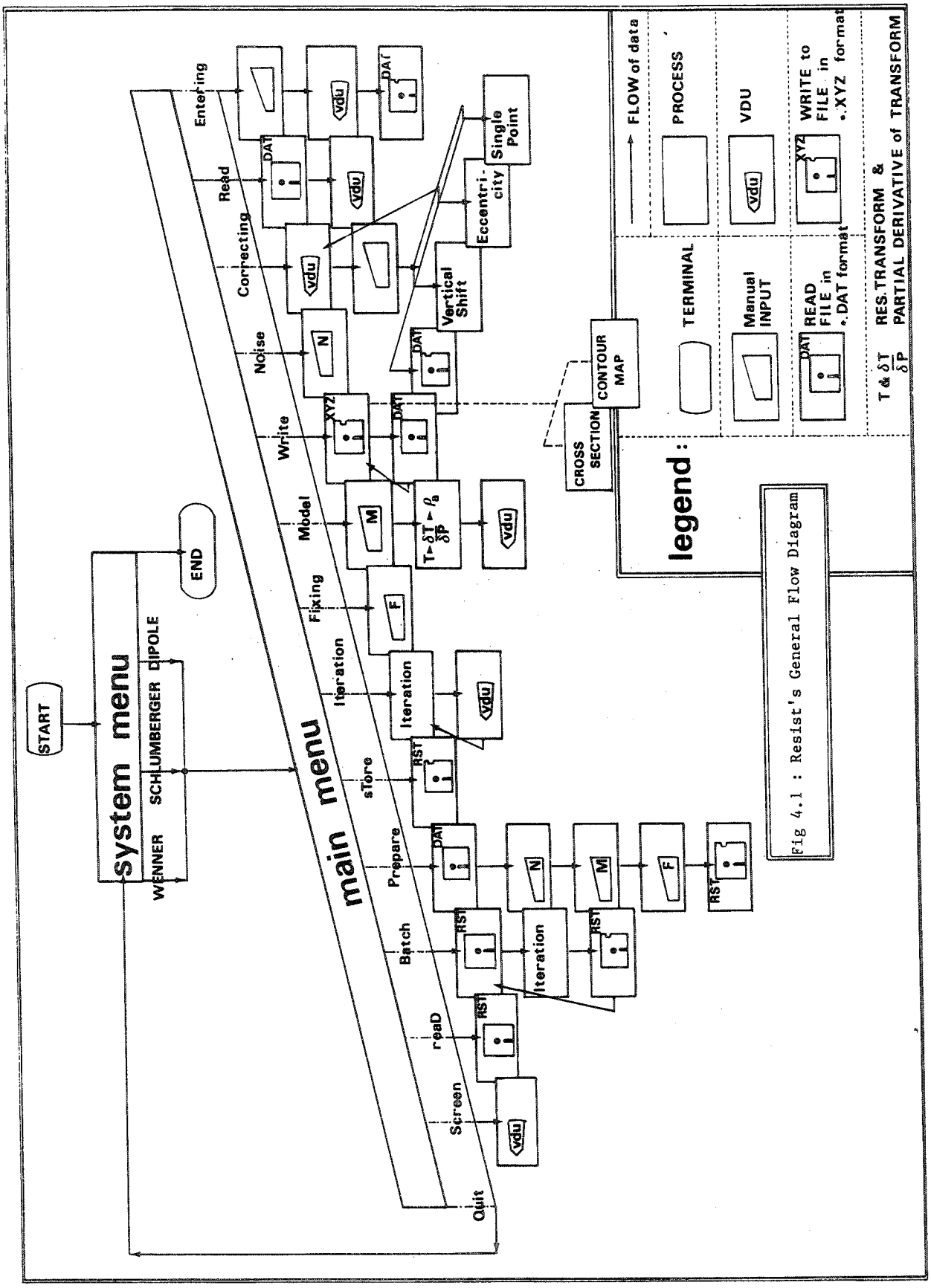

Fig. 5.5 General Flow Diagram of RESIST Software.

Chapter 6
Results and Analysis

6.1. Field Data

Electrical geophysical techniques, vertical electrical sounding (VES), horizontal profiling and well logging were used in the study area. The objectives were:

- To investigate the relation between the geophysical response and the height of the groundwater table.
- To study the geophysical signature of faults and lineaments in the area.

In order to approach the first objective of the study, special effort was put on the Vertical Electrical Sounding (VES) method, since this method has the capability to describe the subsurface vertical variations with respect to electrical property of the rocks. Twenty-five VES soundings were made in the selected observation points. They were spread out in the study area from Lake Naivasha shore (swamp zone) to Suswa in the southeast and the Malewa catchment in the northeast of the study area (Fig. 6.1).

Furthermore, the horizontal profiling method (CST) was used – as already described in a previous chapter –to obtain the lateral variations of the subsurface lithology. The aerial photograph interpretation suggested a number of fault lineations and it guided us where the horizontal profiling had to be located. Five horizontal profiles were located in the hilly part of the survey area where the topographic contrast could be clearly found.

Geophysical well logging was employed in this survey, to compare the electrical response of the subsurface with some independently obtained well lithologies.

The observation points of all methods are shown in Figure 6.1 and the general data with respect to dates and coordinates can be found in appendix A. The VES data are available in appendix C, the horizontal profiling data in appendix B and well logging data in appendix D.

In addition to that, borehole data are also given, as these are the only reliable source of data on the subsurface aquifer. Behar (1999) and Ramirez (1999) carried out the hydrogeological investigations. However, because they are really needed for the study as control points, they have been taken up as Appendix E. The location map of the wells is illustrated in Figure 6.2.

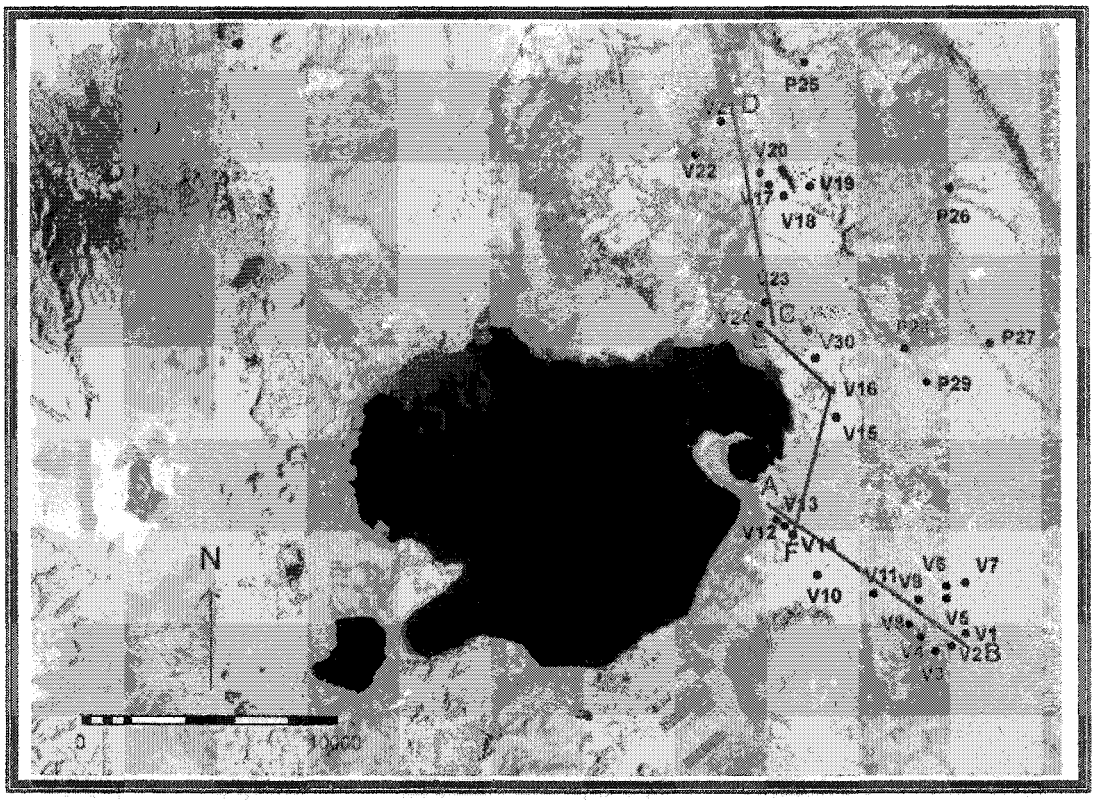

Figure 6.1. Map showing positions of VES and CST measurements. The 'V' are VES points, the 'P' are horizontal profiling points.

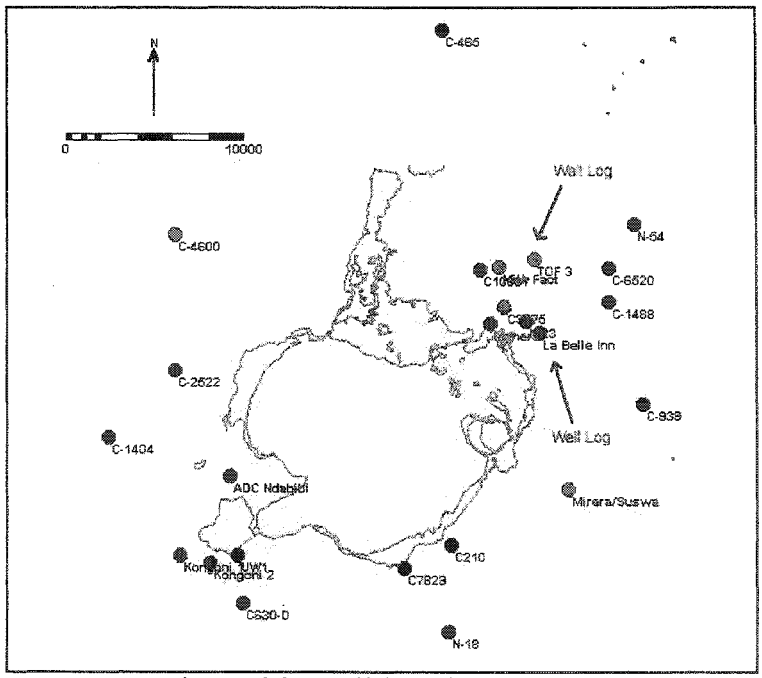

Figure 6.2. Well location map.

6.2. Vertical Electrical Soundings (VES)

6.2.1. Introduction

Vertical Electrical Sounding (VES) is the method easily applied on the ground, very flexible and immediately adaptable to many field problems. It results in relatively cheap and quick surveying.

In the Naivasha area VES measurements were made using four electrodes, a Schlumberger Array arrangement with maximum current electrodes AB/2 varying between 1.5 to 200 meters and potential electrodes MN/2 separation between 0.5 to 20 meters. The measurements were conducted using an ABEM-Terrameter SAS 300 resistivity meter (Figure 5.1.).

The resistivity curves of all observation points were prepared by plotting the apparent resistivity values (ρ) as ordinate against AB/2 as abscissa on a log-log graph. The field curves are generally three and four layer models, while five layers are also encountered. The preliminary and final interpretation of the VES was made using the curve matching technique of the RESIST program (Van der Velpen, 1988).

The data were collected manually in the field. Therefore they have to be input as the database in 'Resist software' format. The software allows us to enter the field data manually through the keyboard and correct wrongly entered data during the process, such as changing, inserting and / or moving. See Figure 6.3.

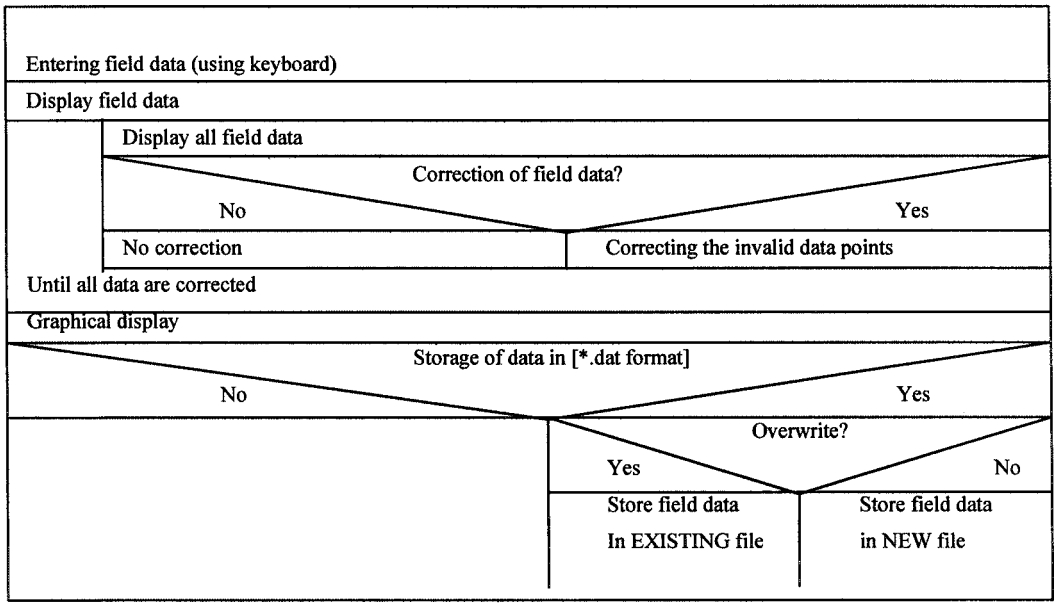

Figure 6.3. Diagram: Entering and editing the field data (Vander Velpen, 1988)

The program gives the possibility to correct raw field data for high and low frequency noise. Field apparent resistivity curves are not free of noise, due to near surface inhomogeneities, instrumental noise, observation errors etc. Filtering of high frequency noise may be accomplished by single point corrections. In order to correct the noise, resist program gives us the choice between the manual or automatic correction. The latter is accomplished by discarding some outlying data points and replacing them by interpolating or extrapolating of the remaining observations. Another choice of correction is a curve-segment shifting. This option allows us to adjust the lack of tie-in between different adjacent segments of an apparent resistivity curve caused by inhomogeneities in the ground. The technique is based on the vertical shift of whole branches.

Having completed the first step of the processing, the next analysis step is the model entering. In this case, we enter a possible model for a specific set of data. The method which is used in Resist for the computation of the apparent resistivity curve for the entered layer is the linear filtered method, introduced by Ghosh (1971).

The results of the resistivity modeling of all VES are given in Appendix C. Three geoelectric section profiles AB, CD and EF were constructed and further discussed here. The location of these profiles is shown in Figure 6.1.

6.2.2 *Profile AB from the Lake towards Suswa area (VES14-VES11-VES-1)*

Profile AB with the bearing of N 125° E plotted from VES-14 in Sanctuary Farm near Lake Naivasha towards southeast direction to VES-11 and VES-1 in Suswa Area. The summary of the VES involved is shown in Table 6.1 as follows:

Table 6.1. The summary table of VES-14, VES-11 and VES-1

VES No.	Coordinate		Bearing	VES length	Spacing	
	X	Y	(degree)	(m)	AB/2	MN/2
VES-14	212566	9912513	N 288 W	200	1.5 - 200	0.5 - 10
VES-11	214984	9910071	S 178 E	200	1.5 - 200	0.5 - 20
VES-1	218274	9908296	S 258 W	200	1.5 - 200	0.5 - 20

The three main VES apparent resistivity models are displayed in Tables 6.2 – 6.4 and Figs 6.4 – 6.7 as follows:

Table 6.2. VES-14

Layer No.	ohm-m	Thickness (m)	Depth (m)
1	195.4	3.2	3.2
2	74.8	37	40.2
3	6.7	-	-

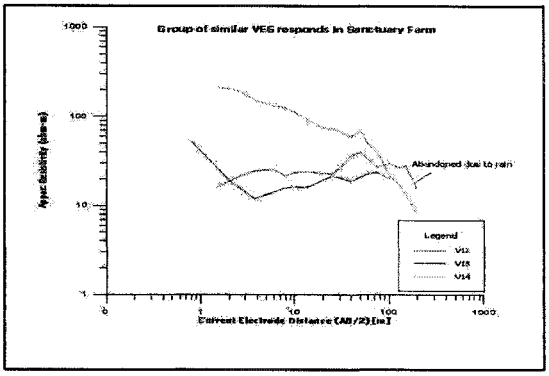

Figure 6.4

Table 6.3. VES-11

Layer No.	ohm-m	Thickness (m)	Depth (m)
1	620.6	1.1	1.1
2	42.3	2.6	3.8
3	210.8	31.9	35.7
4	81.3	91	126.6
5	222.3	-	-

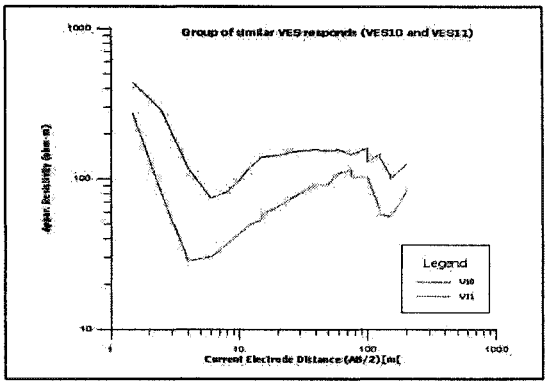

Figure 6.5

Table 6.4. VES-1

Layer No.	ohm-m	Thickness (m)	Depth (m)
1	855	0.8	0.8
2	35	2.6	3.4
3	334.8	43.2	46.6
4	66	-	-

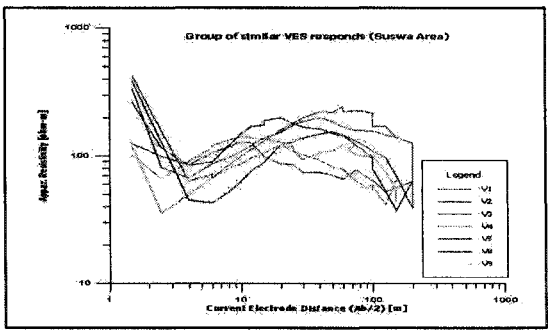

Figure 6.6.

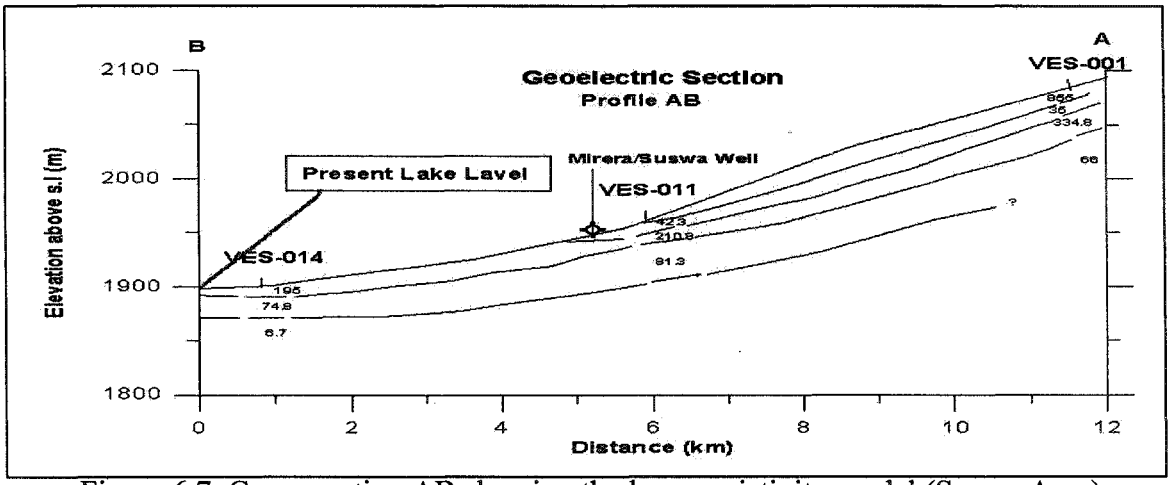

Figure 6.7. Cross-section AB showing the layer resistivity model (Suswa Area).

Figure 6.7. shows the geoelectric cross section of the profile AB. There are several VES crossed by the profile. However, they can be grouped into three main models as follows:

1. VES-12, VES-13 and VES-14 in one group. They were situated in the lake riparian zone. From this group, VES-14 was selected to be put in profile AB, as it seems characteristic of the subsurface rock properties at this particular location. It has to be noted that VES-12 is disqualified because of rain during the fieldwork. As we know the rain would cause noise in. the apparent resistivity result.

2. VES-10 and VES-11 as one group. Both curves look similar. The upper layer gave a resistivity value of 500 to 600 ohm-m. They dropped to about 40 – 50 ohm-m, before rising again to the next resistivity layer of 200 – 300 ohm-m. They fluctuate to 500 – 600 ohm-m and the last layers detected gave the resistivity value of 200 ohm-m. Arbitrarily, VES-11 was chosen to represent the profile AB in Fig. 6.4.

3. VES-1, VES-2,VES-3, VES-4, VES-8 and VES-9 were put in the third group. From this group, VES-1 was selected to be located in profile AB, since the location of VES-1 is furthest away point from the lake.

See Tables 6.2, 6.3 and 6.4.

Figure 6.7 shows the interpretation of geoelectric cross-section of profile AB. The first layer with less than 1 m thickness and resistivity values up to 190 ohm-m in the southern riparian zone of the Lake Naivasha (VES-014) represents the loose lacustrine sediment material as the top soil layer. Further away from the lake, a second thin layer of 2 to 3 m is found with resistivities ranging from 30 to 70 Ohm-m. Below this is a third layer with a thickness from 30 to 40 m and resistivities varying from 200-300 Ohm-m. No clear evidence of a groundwater table was found. However, the high resistivity of the third layer indicates a dry zone. Hence the groundwater table should be below this. Towards the lake the resistivity of the third layer becomes less, indicative of increasing moisture content and/or clay layers. Again, close to the lake, no clear signature was found of the groundwater table.

Table 6.5. The summary table of VES-23, VES-17, VES-20 and VES-21

VES No.	Coordinate		Bearing	VES length	Spacing	
	X	Y	(degree)	(m)	AB/2	MN/2
VES-23	211331	9921888	S 220 W	200	1.5 - 200	0.5 - 20
VES-17	213854	9924903	S 152 E	200	1.5 - 200	0.5 - 20
VES-20	213590	9925296	S 160 E	200	1.5 - 200	0.5 - 20
VES-21	212248	9927325	S 216 W	200	1.5 - 200	0.5 - 20

Table 6.6 VES-23

Layer No.	ohm-m	Thickness (m)	Depth (m)
1	64.8	0.8	0.8
2	7.3	31.0	31.8
3	17.9	-	-

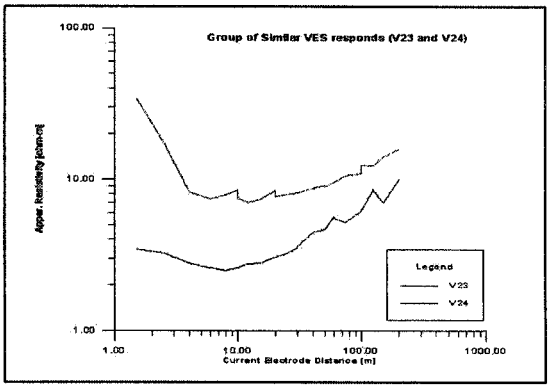

Figure 6.8.

Table 6.7 VES-17

Layer No.	ohm-m	Thickness (m)	Depth (m)
1	36.5	2.5	2.5
2	104.6	4.8	7.3
3	31.6	43.3	50.5
4	55.2	98.0	148.5
5	18.9	-	-

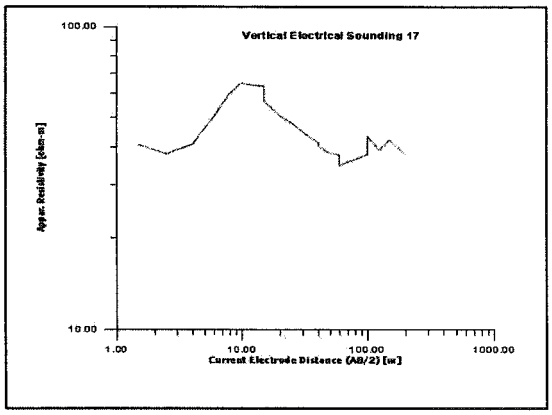

Figure 6.9.

Table 6.8 VES-20

Layer No.	ohm-m	Thickness (m)	Depth (m)
1	171.1	0.8	0.8
2	38.4	2.6	3.4
3	50.1	6.6	10.0
4	33.8	-	-

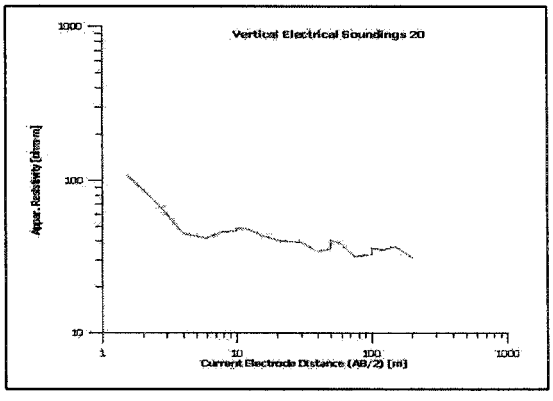

Figure 6.10

Table 6.9 VES-21

Layer No.	ohm-m	Thickness (m)	Depth (m)
1	70.3	0.5	0.5
2	11.9	1.6	2.1
3	19.2	17.3	19.4
4	60	15.6	35.1
5	19.9	-	-

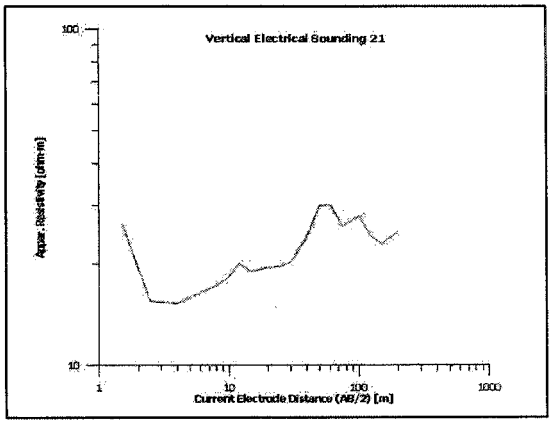

Fig. 6.11

6.2.3 Profile CD, Malewa Alluvial Fan (VES-23,VES-17,VES-20, VES-21)

These soundings extend from Lake Naivasha into the alluvial aquifers around the Malewa River. Most of the boreholes in the area are high yielding, as a result of the coarse sedimentary material deposited by the Malewa River. In general these layers are embedded in less conductive caly/silt layers. The multiple-layer leaky confined aquifers have high transmissivities, because of the high conductivity production zones. From a geophysical point of view, however, there is not much difference in response between the high conductivity layers and the less conductive confining layers.

This is apparent when studying the sequence of soundings VES23-VES17-VES20-VES21, Table 6.5 gives an overview of the coordinates (see also Fig. 6.1). The individual results are shown in Tables 6.6-6.9 and the attached graphs (Figs 6.8-6.11). Detailed model results may be found in Appendix C as mentioned before.

The curves generally show low resistivity (between 10 and 100 Ohm-m) with a shallow (dry) surface layer with a higher resistivity. Not much difference is found between the soundings close to the Lake (VES-23) and those further inland (VES-21).

This confirms the generally similar conditions found in the alluvial fan of the Malewa River. No clear signature of a groundwater table was found.

6.2.4 Profile EF, Soundings along the Lake (VES-24, VES-30, VES-16, VES-14).

These soundings are summarized in Table 6.10 (see also Fig. 6.1). Individual results are shown in Tables 6.11- 6.14 with the attached graphs. As was the case with the soundings on the Malewa Fan, resistivities are generally low (10-50 Ohm-m) without clear layering structures, probably due to the fact these alternating sand/clay sequences do not have very different resistivities.

It can be concluded therefore that electrical resistivity surveying cannot be used to detect the shallow groundwater tables around the Lake and on the Malewa Fan. On the other hand, on volcanic ground in the Suswa area, it was found that high resistivities at depth show that the groundwater table must be at least below this high resistivity zone. However, with the methods used, not enough power and cable length was available to measure resistivities at the depths required.

Table 6.10. The summary table of VES-24, VES-30, VES-16 and VES-15 and VES-14.

VES No.	Coordinate		Bearing	VES length	Spacing	
	X	Y	(degree)	(m)	AB/2	MN/2
VES-24	210785	9920719	S 208 W	200	1.5 - 200	0.5 - 20
VES-30	214384	9918656	S 065 E	200	1.5 - 200	0.5 - 20
VES-16	215010	9917431	S 096 E	200	1.5 - 200	0.5 - 20
VES-15	214791	9916508	S 200 W	200	1.5 - 200	0.5 - 20
VES-14	212566	9912513	S 288 W	200	1.5 - 200	0.5 - 20

Table 6.11. VES-24

Layer No.	ohm-m	Thickness (m)	Depth (m)
1	3.9	0.9	0.9
2	2.5	18.7	19.6
3	13.4	-	-

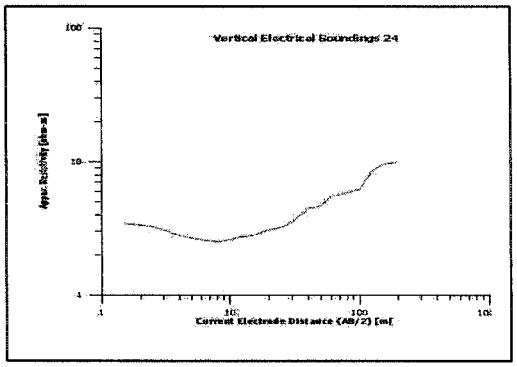

Figure 6.13.

Table 6.12. VES 30

Layer No.	ohm-m	Thickness (m)	Depth (m)
1	55.8	0.6	0.6
2	7.8	4.0	4.6
3	8.8	22.0	26.6
4	22.4	94.2	120.8
5	10.3	-	-

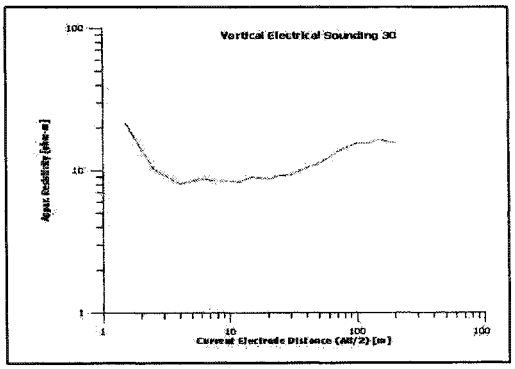

Figure 6.14.

Table 6.13. VES-16

Layer No.	ohm-m	Thickness (m)	Depth (m)
1	10.8	0.8	0.8
2	24.8	3.8	4.6
3	15.1	73.4	78.0
4	2.1	-	-

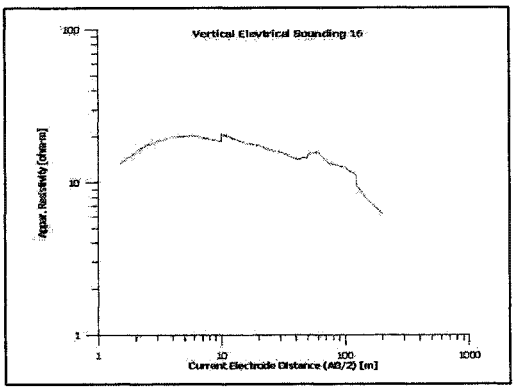

Figure 6.15.

Table 6.14. VES-14

Layer No.	ohm-m	Thickness (m)	Depth (m)
1	70.3	0.5	0.5
2	11.9	1.6	2.1
3	19.2	17.3	19.4
4	60	15.6	35.1
5	19.9	-	-

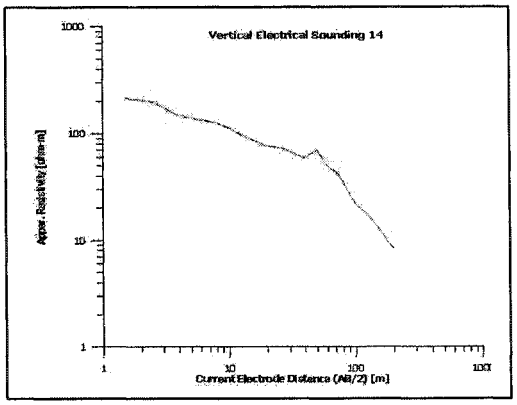

Figure 6.16.

6.3 Horizontal Profiling

As already mentioned in chapters 3 and 5, a resistivity horizontal profiling is a resistivity method in which the electrode spacing is kept fixed, preferably on the basis of studying the results of electrical soundings. The entire electrode array is moved along a profile after each measurement is made. The value of apparent resistivity is plotted at the geometric center of the array. Maximum apparent resistivity anomalies are obtained by orienting the profiles at right angles to the strike of the geologic structure.

Horizontal profiling has been carried out in the study area using a Schlumberger Array arrangement with a current electrode spacing AB/2 of 0.5 meter and a potential electrode MN/2 separation of 10 meter. The sites of the locations were selected by aerial photograph interpretation through tracing of fault lineations. However these lineations have to be verified in the field. Obviously, in the study area, the faulting was recognized by the topographic contrast where the flat land abruptly changed to relatively undulating ground.

Five geoelectric profiles were constructed across the western part of the area where geologic structure is very much controlled by geology. Data of all 5 profiles are given in Appendix B. Three profiles will be discussed briefly.

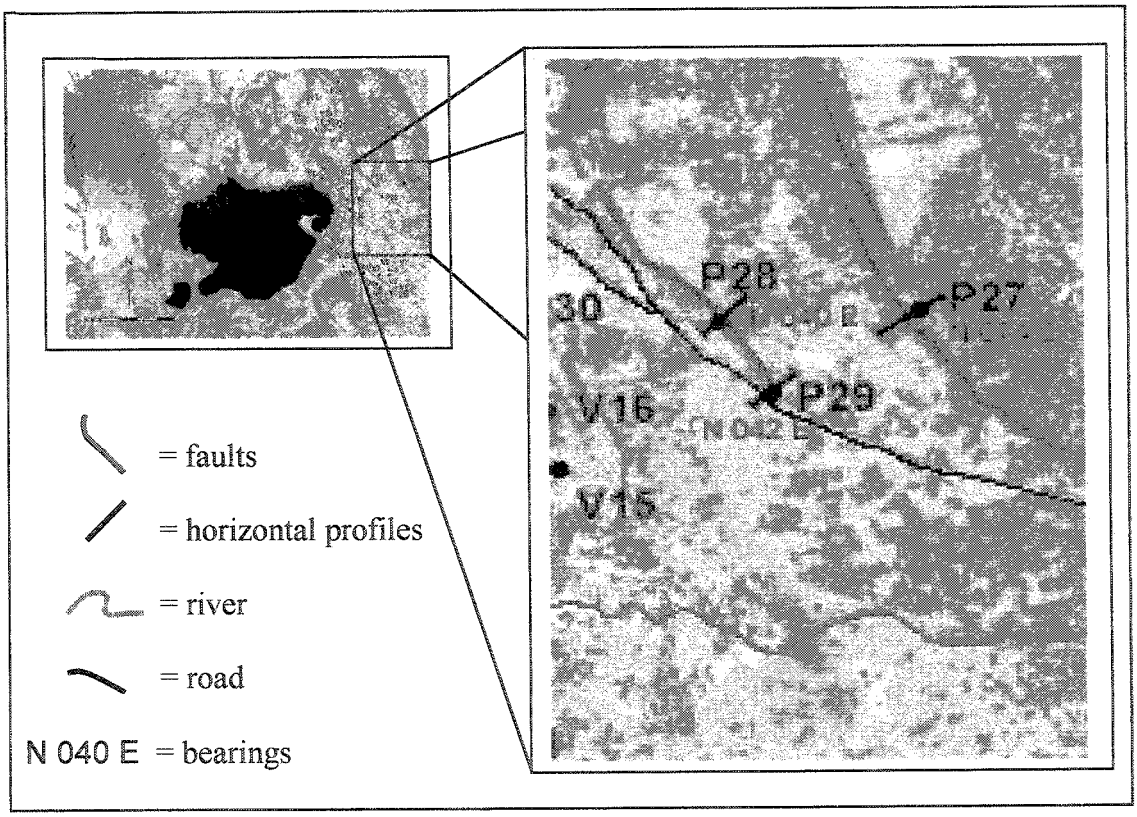

Figure 6.17. The location map of the three profiles P27, P28 and P29.

Profile P27 was measured along the small track to Njabini. The length of the profile was 250 meters with a of 10 m between the measurements. The raw data can be found in appendix B. It shows the response of the lateral variations in lithology from a resistivity point of view. It can be seen from the graph (Fig. 6.18) that from –150 to 40m, the resistivity curve does not show very much fluctuation. The values are ranging from 28 to 67 ohm-m. This specific range of resistivity values reflects the lithologic condition below the surface that consisting of sand with clay material (Springer, 1995). The hand specimens taken from the field can be described as weathered fine-grained sandstone, grey-yellowish color with clayey materials. This type of sediment was originally deposited as lake floor sediments.

The high resistivity values of 127 to 195 ohm-m were obtained from 50 to 100 meters along the profile. This represents the presence of the trachyte intrusions which can be found in the field as a lineation of hills with the azimuth of approximately N 165° E. In other words, the change of resistivity values from 60 ohm-m of lacustrine sediments to 162 ohm-m of trachyte lavas in the distance from 40-50 m, is probrably the location of the fault where the structural contact between lacustrine lake deposits and trachyte lavas is found as the change of terrain in the field (Fig. 6.18).

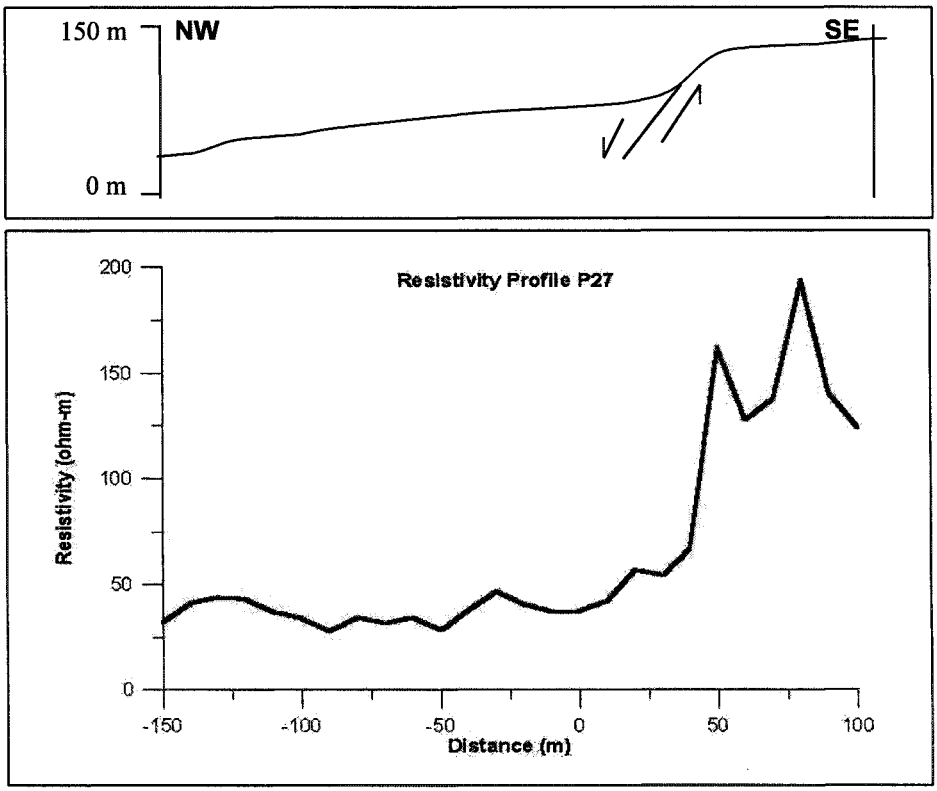

Figure 6.18. Profile P27

Another interesting observation point was found in the location of Profile P28. The terrain of this location is shown in Fig. 2.2 where the road was situated on relatively plain surface leading towards the northeast. The road is then crossing a small hill. We could distinguish lithological differences between the plain and the hills.

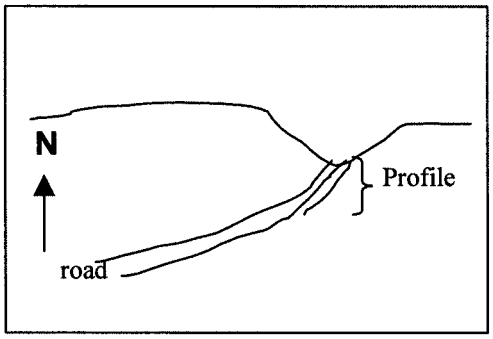

Figure 6.19. The horizontal profiling was done to the other side of the hill.

Again, a similar curve response was observed as in Profile P27 (Fig. 6.18).

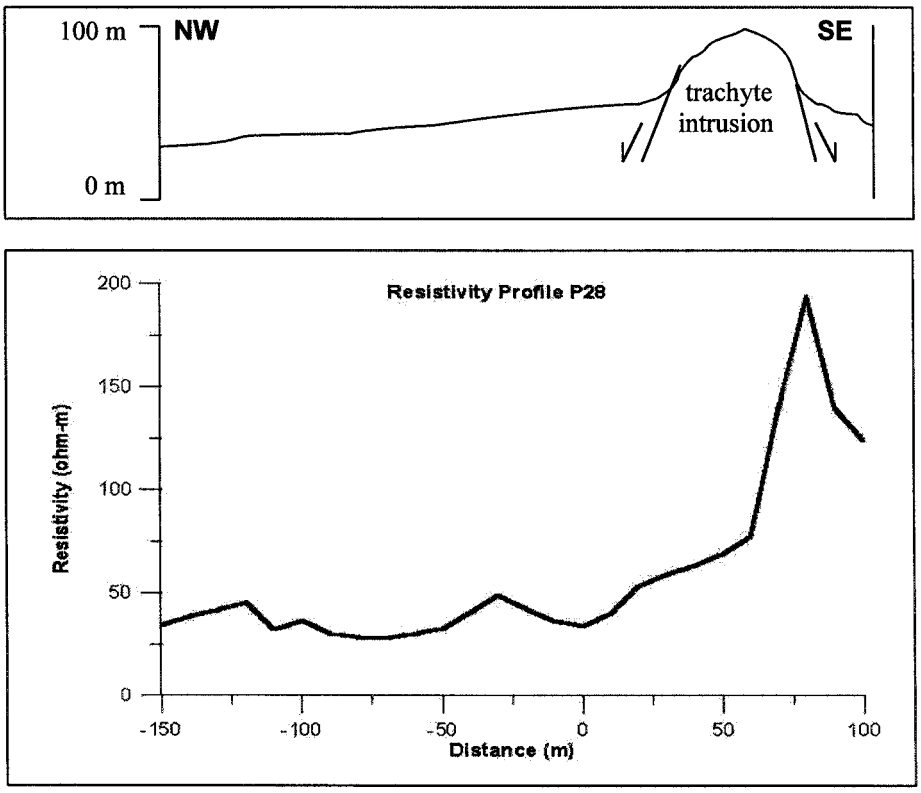

Figure 6.20. Profile P28

Profile P29 (Fig. 6.21) was done crossing the old main road from Naivasha Town to Nairobi. In the southern part of the road (distance 0 to 150 meters), the range of resistivity values ranged from 32 – 85 ohm-m. These relatively homogenous resistivity values are probably due to the dry fine material of the lacustrine sediments. The abrupt change of the resistivity curve can be seen at the distance of 80 meter in northern part of the road where the resistivity increase to 184 ohm-m and getting higher up to 343 ohm-m. This represents the presence of the trachyte lavas which intruded the lacustrine sediments through the weak zone of the fractures.

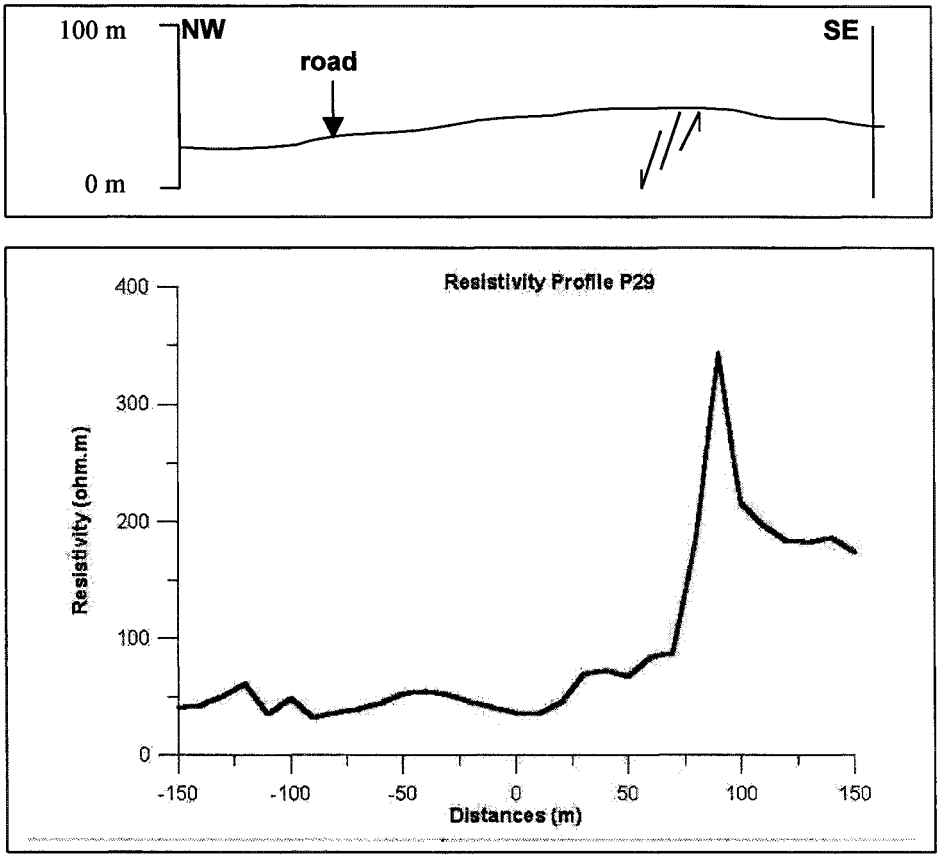

Figure 6.21. Profile P29.

It can be observed from this figure that the lateral resistivity variations in this point no longer appeared in the geomorphology. The reason for this is that the profile was directed along the edge of the trachyte intrusion (See again Fig. 6.17). The trachyte lavas have eroded away from the surface. However, the trachyte is still present below the surface. Event though in this case the peak of the curve is relatively narrow, due to the narrowing upper part of the intrusive body, the response of the subsurface features, as evidenced by the resistivity curve, reveals the presence of the intrusion through the fault.

6.4 Geophysical Well Logging

Two geophysical logging tests were carried out from a depth of 20-46 m, using a one-meter interval. The following parameters were measured: longnormal, shortnormal and latero-log electrical resistivity, fluid resistance, self-potential and temperature. Fluid TDS can be determined through the use of the EC values. The first test was carried out at La Belle Inn (Borehole 20, Appendix E) in Naivasha town during the 1997 field work, and has not been reported on before. The second test was carried out at Three Ostrich Farm (Borehole 18, Appendix E) during the fieldwork in 1998. The location of the two wells is indicated in Fig. 6.2. All data concerning the two tests are taken up in Appendix D. The theory and equipment have been described on pages 35-39 of this thesis.

6.4.1 La Belle Inn Well Log

The well is located at coordinates [214127, 9920848] (Arc 1960/ UTM coordinates, zone 37), at an elevation of approximately 1905 m above sea level (masl). The measured depth of the well is 46 and at the time of visit, the rest water level was 19.97 m below ground level. Water was reportedly struck at 24 m depth.

Unfortunately the temperature probe was not working during the survey. The borehole stratigraphic log results are shown in Fig.6.21 together with two plots of the geophysical well log, i.e. the resistivity and EC as a function of depth. It is clear from the stratigraphic log that the aquifer was encountered below the basalt at 24 m. Since the static water level is 19.97 m below ground level, pressure conditions were (semi)confined.

In sedimentary formations the higher the resistivity, the better the aquifer potential as a high resistivity indicates a lower percentage of clay, which is not good aquifer material. Based on the resistivity logs, the aquifer is thus located between 26-32 m depth. Figure 6.21 shows the change in water quality (EC – electrical conductivity/salt content) with depth. It appears as if the water quality is best at greater depths. The portion under the pumice layer has the best water quality and is well protected against contamination. However, from a salinity point of view, the water quality is acceptable.

It seems that under the pumice another 4 meters of lacustrine deposits occur. At a depth of 36-40 meters, the weathered zone of the underlying basalt starts, while at the bottom of the hole fresh basalt is encountered. The weathered basalt may constitute a reasonable aquifer, but it is not certain if it can support or sustain the desired yield.

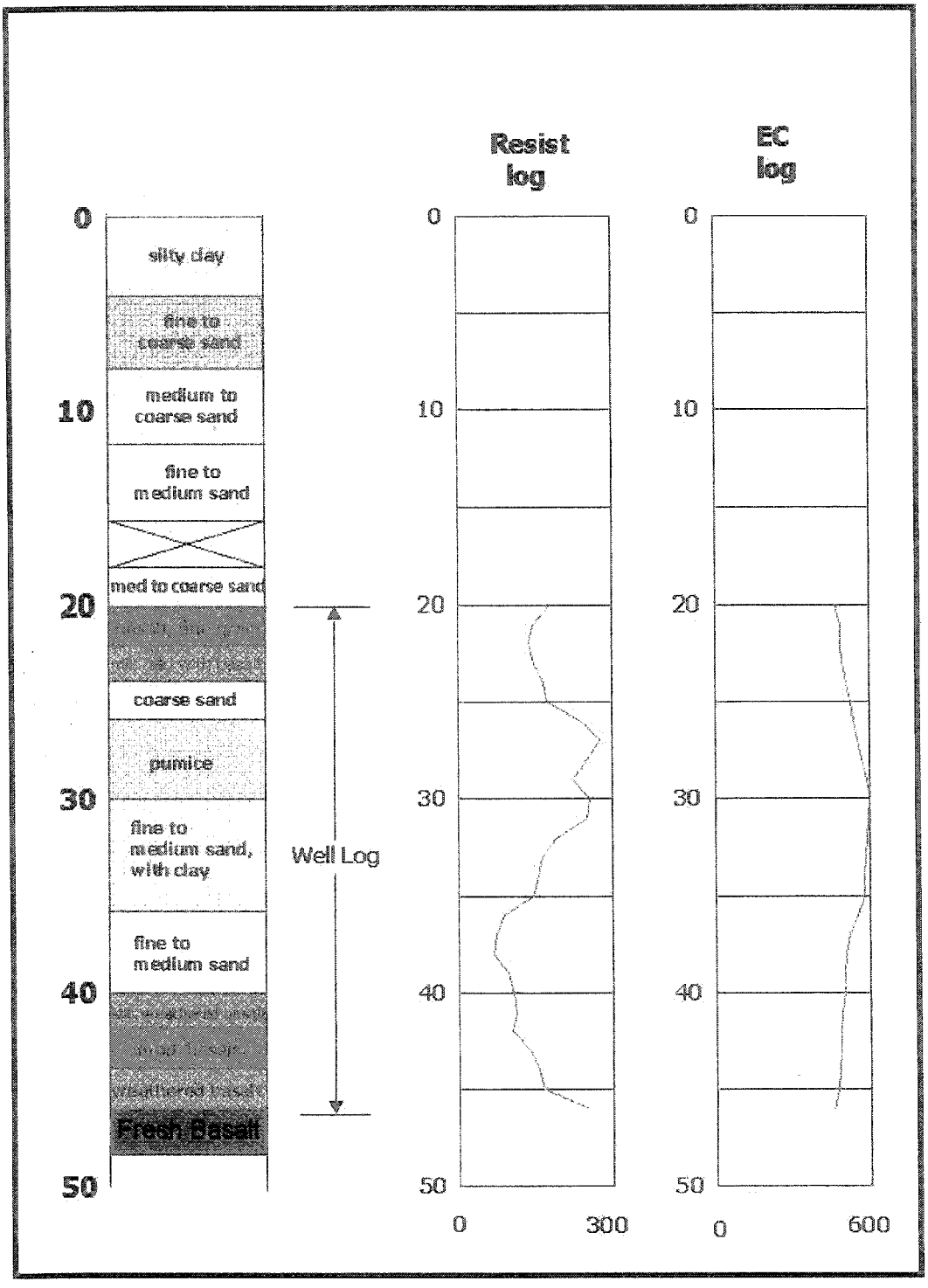

Fig. 6.21 Stratigraphic and geophysical well log of the borehole at La Belle Inn.

6.4.2 Well Log at Three Ostrich Farm

The well is located at coordinates [213854, 9924903] (Arc 1960/ UTM coordinates, zone 37), at an elevation of approximately 1910 m above sea level (masl). The measured depth of the well was 40m at the time of construction (due to borehole collapse and subsequent further drilling this may have changed later) and at the time of visit, the rest water level was at 24.56 m below ground level. Water was reportedly struck at 28 m depth.

The borehole stratigraphic log results are shown in Fig.6.23 together with four plots of the geophysical well log, i.e. the short-normal, long-normal, resistivity and TDS as a function of depth. It is clear from the stratigraphic log that the major aquifer was encountered in the pebble zone at about 30 m depth. Since the static water level is 24.56 m below ground level, pressure conditions were (semi)confined. Probably the overlying layer of fine to medium sand contained some silts and fines, which is difficult to determine exactly because the drill samples are washed.

Several strikes have occurred here which emphasizes the multi-layered semi-confined nature of these aquifers. Highly productives zones occur at the zones with pebbles and coarse sand and gravel. The best zone seems to occur at about 40 m, just above the clasts of siltstone. The angular material indicates a high-energy depositional environment. The resistivity goes up in this zone. Unfortunately, it was not possible to extend the log to a depth of 60 m because of borehole collapse during construction. It should be noted that the poorest water quality seems to occur near the top of the aquifer, as recorded by the TDS log.

The correlation with VES-17 resistivity sounding (50 m away from this borehole) is poor. Fig. 6.22 below shows that the sounding was modelled with 5 layers. However, the detailed aquifer structure as recorded by the drill samples cannot be reproduced. It seems likely that the individual aquifer layers have very small differences in apparent electrical resistivity.

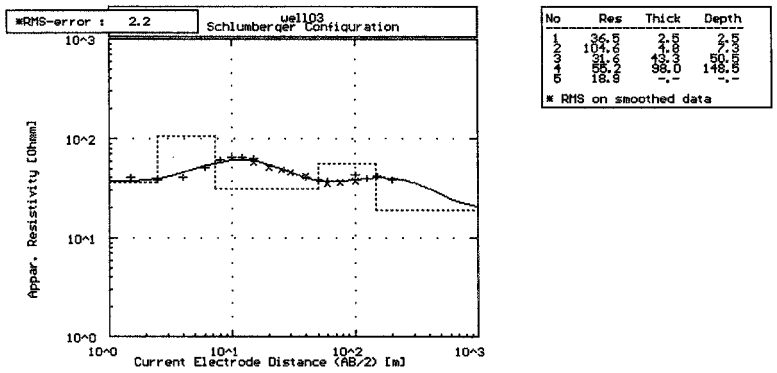

Fig. 6.22 Electrical Resistivity sounding VES-17 at Three Ostrich Farm.

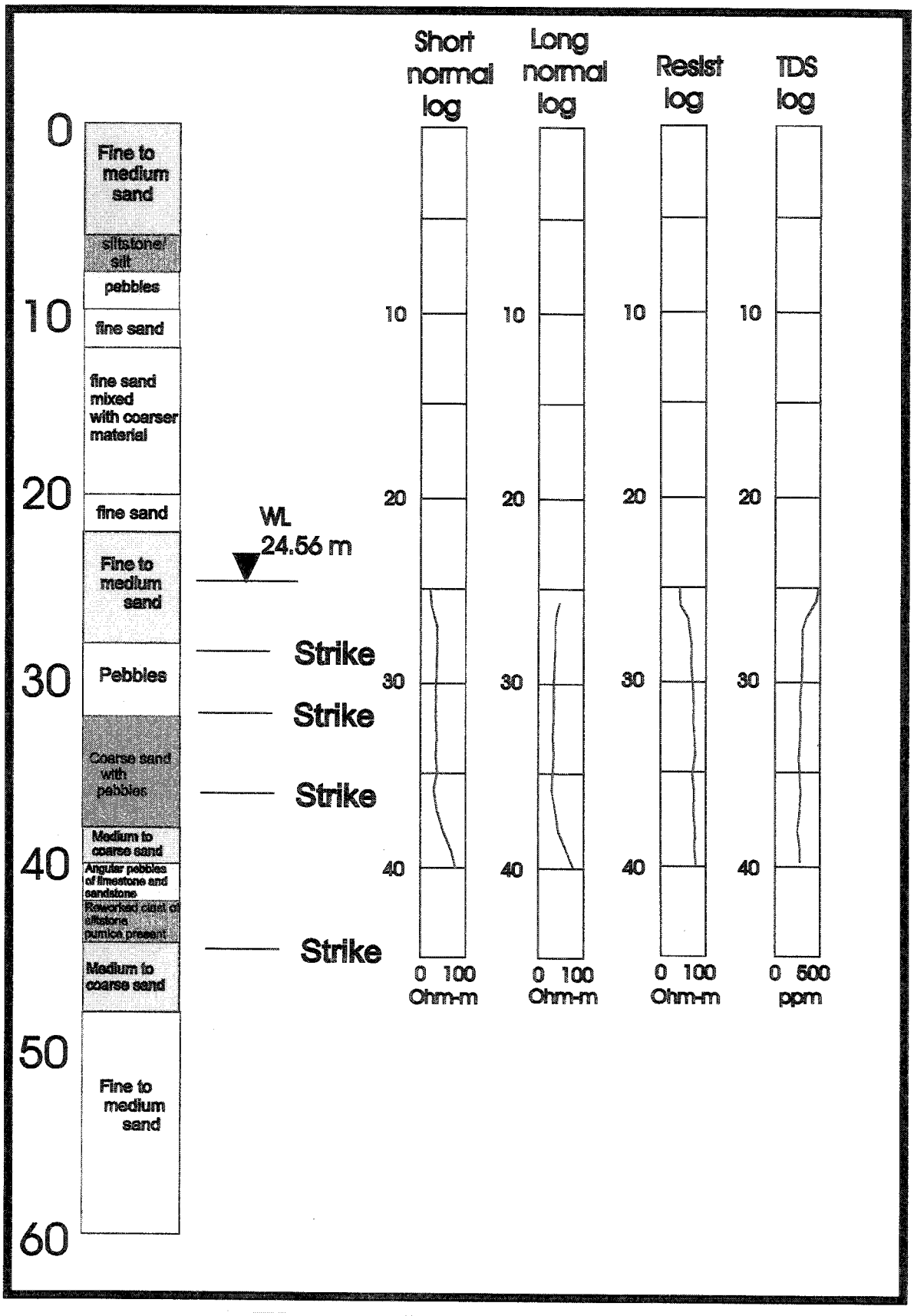

Fig. 6.23 Stratigraphic and geophysical well log at Three Ostrich Farm.

6.5 Magnetic Field Study

As the final part in this study East African magnetic field data were collected from the African DataBase (Barrett, ITC Delft, private communication). In this database the regional magnetic anomalies of several African countries have been merged. The data for the Naivasha region are shown in Fig. 6.24, which shows that the data, more especially the gaps in the data, are clearly linked to the national boundaries. Fortunately the Kenyan and Nyanza Rift areas are well covered. These rift areas show up as areas with large field anomalies at short distances, typical of volcanic terrain. This was already discussed in Section 3.2. In the area of Fig. 6.24, the field anomalies lie between –800 and +1200 nT.

The original database was given as a GeoSoft textfile, with the x- and y-coordinates in metre in the Equatorial Mercator System (Clarke 1880 Ellipsoid). The files were then transferred into an ILWIS 2.2 raster map with the same co-ordinate system. The Kenyan boundary was imported into ILWIS as an ArcInfo .E00 file, obtained from the Pennsylvania State University (website: www.libraries.psu.edu). The outline of Lake Naivasha was obtained through digitization of existing topographical maps, followed by georectification to the Arc 1960 UTM coordinate System. Crosschecks between these maps show that the error in the coordinates of the magnetic field map is in the order of one to two pixels with a pixel size of 1 km.

Fig. 6.25 shows a detailed section of the Magnetic Field Anomalies in the Lake Naivasha area. The yellow lines indicate the Rift Valley System. The topographical contours (in red) and the drainage features (in blue) were downloaded as ArcInfo files as dicussed earlier from the Pennsylvania State University website. Shades of grey indicate variations in the magnetic field. As mentioned before, the rift valley magnetism is characterized by relatively large variations at short distances, which is usually the case in volcanic terrain. The magnetic anomalies appear to be related to the topography of the rift valley. The Aberdare Range shows up as a white area, i.e. with high positive anomalies, at the eastern edge of the rift. Remarkable is also the large negative anomaly zone, north of Lake Naivasha and Eburru Hill, south of Lake Elmenteita. This area coincides with the surface and groundwater divide between the northern and southern parts of the rift valley.

The resolution is too low to distinguish the individual smaller rift faults and lineaments

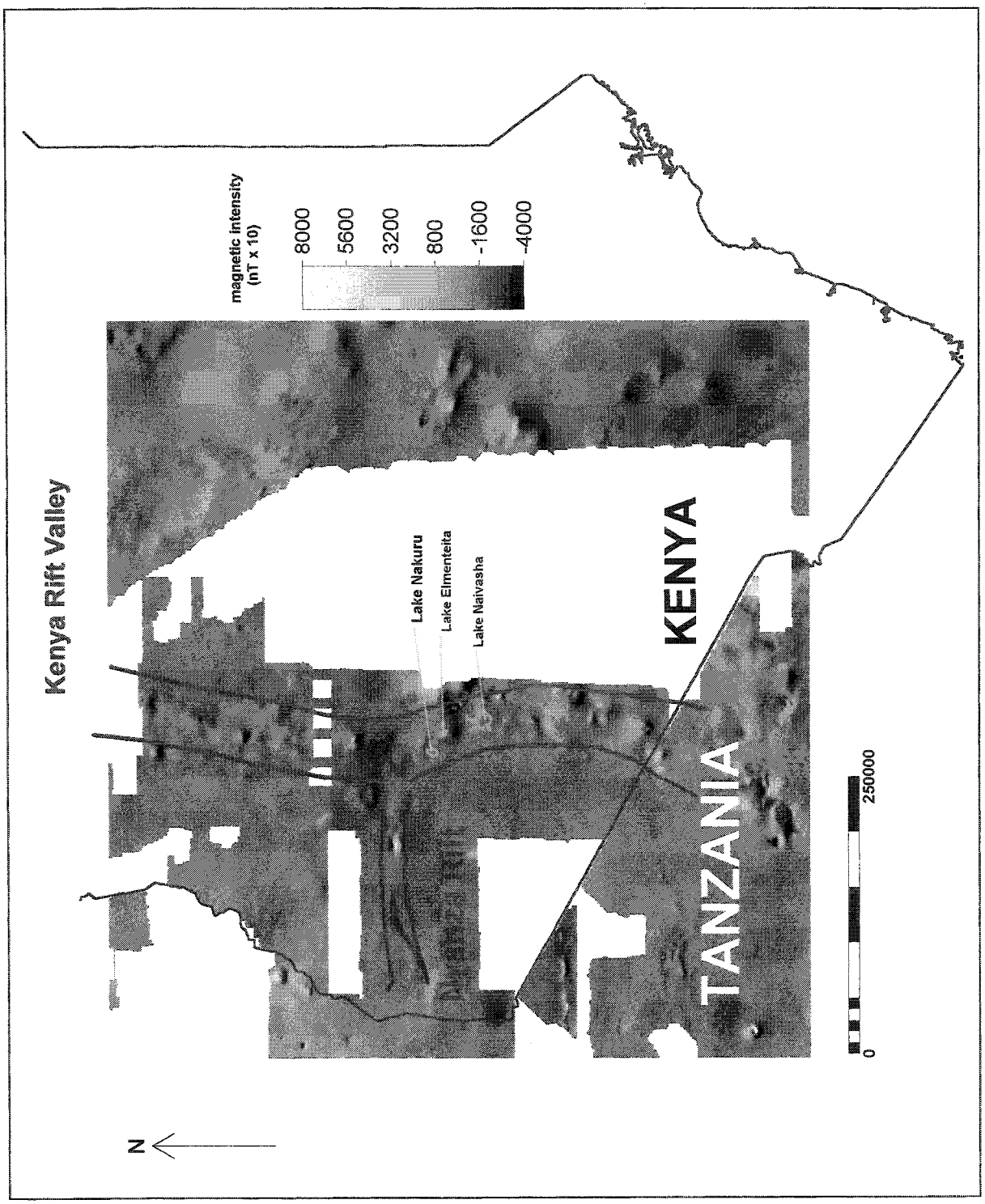

Fig. 6.24. Map of the magnetic field anomalies in the Kenya-Tanzania area. Data of several African countries have been combined. White areas mark absence of data or data rejected because of poor quality.

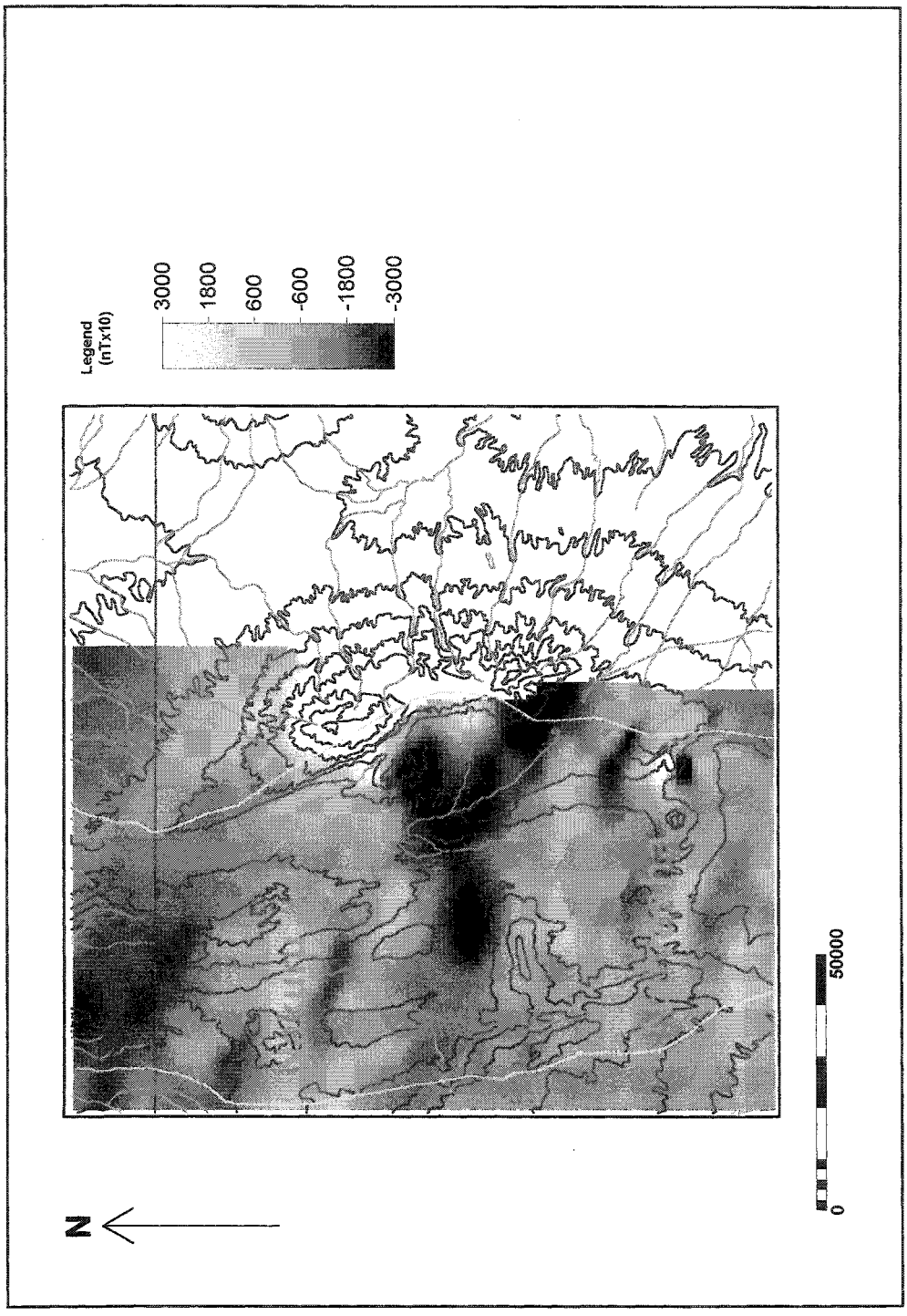

Fig. 6.25 Detailed map of the magnetic field anomalies in the Lake Naivasha area. Anomalies range from –3000 nT to + 3000 nT. The area north of Eburru Hill and south of Lake Elmenteita shows up as a region with a large negative anomaly.

Chapter 7
Final Considerations and Conclusions

Two objectives were mentioned in the previous chapters. Firstly, it was required to study the relation between electrical resistivity and groundwater table depth. Second, it was proposed to study the geophysical response of rift faults in the area.

Four different geophysical techniques have been applied in this study. The first three are variations of electrical resistivity surveying: Vertical Electrical Sounding (VES), Profiling (or Constant Separation Traversing, CST) and Well Logging. The fourth technique was based on the East African Residual Magnetic Field Database (ITC, Delft).

It was concluded that electrical resistivity surveying cannot be used to detect the shallow groundwater tables around the Lake and on the Malewa Fan. The various clay and saturated sand layers do not have sufficiently different apparent resistivities. All resistivities near the Lakeshore and on the Malewa fan were found to be within 10 to 100 Ohm-m. On the other hand, on volcanic ground in the Suswa area, it was found that high resistivities (above 100 Ohm-m) at depth show that the groundwater table must be at least below this zone. However, with the methods used, not enough power and cable length was available to measure resistivities at the depths required.

With regard to the horizontal profiling technique, it can be concluded that the rift faults can very well be detected because the contrast between the resistivities of the lacustrine sediments and the intrusive trachyte lavas is high. It appears likely that these faults are aquifer boundaries because of the generally impermeable nature of the lavas.

The interpretation of the geophysical well logs has shown that these could be of considerable practical use in assessing the multiple layered aquifer structures in the area.

With regard to the interpretation of the regional magnetic anomalies, it should be noted that their resolution (1-km pixel size) is insufficient to detect the smaller rift faults. On a regional basis, however, they seem to be of interest in the analysis of large-scale rift features.

Due to the lithologic complexity of the study area, agricultural development and the rapid increase of groundwater using, it is suggested that geophysical techniques in the study area are applied in more detail in the future. The author found that the quality of small-scale geophysical data is rather poor. A well-integrated geophysical database would be of great value in delineating aquifer boundaries and studying stratification.

References

Al'pin, L.M., 1950, *The Theory of dipole sounding: Moscow, Gostoptekhizdat [Translation in Dipole methods for measuring earth conductivity,* New York, Plenum Press, 1966.

Baker, B.H., 1958, *The Geology of the Magadi Area,* report No. 42, Geological Survey, Kenya.

Behar Abdulahi, B.H., 1999, *Surface Water – Groundwater Interaction, Lake Naivasha, Kenya,* MSc Thesis, ITC Enschede, The Netherlands.

Bodvarsson, S., Pruess, K., Stefansson, V., Bjornsson, S., Ojiambo, S.B., 1987, *East Olkaria Geothermal Field, Kenya 1: History Match with Production and Pressure Data Decline,* Journal of Geophysical Research, vol. 92, No. B1, 521-539.

Brock, B.B., 1952, *An Approach to the Rift Valley Problem,* Comptes Rendus, XIXth International Geology Congress, section 3, 225-238.

Clarke, M.C.G., Woodhall, D. G., Allen, D., Darling, G., 1990, *Geological, Volcanological and hydrogeological controls on the occurrence of geothermal activity in the area surrounding Lake Naivasha, Kenya,* Ministry of Energy, Republic of Kenya.

Deppermann, K., 1954, *Die Abhangigkeit des scheinbaren Widerstandes von Sondenabstand bei der Vierpunkt-Method: Geophys. Prosp.,* vol.2.

Fairhead, J.D., 1976, *The Structure of the Lithosphere beneath the Eastern Rift, East Africa – a gravity study,* Tectonophysics, No. 30. 269-298

Fetter, C.W., 1994, *Applied Hydrogeology,* Prentice Hall, Upper Saddle River, New Jersey 07458, USA.

Ghosh, D.P., 1971, *Inverse Filter Coefficient for the Computation of Apparent Resistivity Standard Curves for a Horizontally Stratified Earth: Geophysical Prospecting,* vol. 19, pp 769 – 795.

Kent, P.E., 1944, *The Age and Tectonic Relationship of East African Volcanic Rocks,* Geol. Mag., vol. LXXXI, 15-27.

Kinyariro, J.K., Clarke, C.G., 1988, *Geological Map of Longonot, The Creater Olkaria and Eburru Volcanic Complexes and adjacent areas,* Geothermal Section – Ministry of Energy, Government of Kenya.

Leakey, L.S.B., 1931, *The Stone Age Cultures of Kenya, C*ambridge University Press, Cambridge, England.

Nilsson, E., 1945, *Quaternary Glaciations and Pluvial Lakes in British East Africa,* Geog. Annaler, Stockholm, 13, 249-348.

Pulfrey, W., 1960, *Shape of the Submiocene Erosion Level in Kenya,* Bulletin of Geological Survey of Kenya, No. 3.

Ramirez, R.H., 1999, *Groundwater Flow Modeling of Naivasha Basin, Kenya,* MSc Thesis, ITC Enschede, The Netherlands.

Scott, J., 1953, *The Great Rift Valley and its Economic Possibilities*, Nairobi.

Shackleton, R.M., 1951, *A Contribution to the Geology of the Kavirondo Rift Valley,* Quarterly Journal of the Geological Society of London, vol. 106, 345 – 389.

Shackleton, R.M., 1955, *Pleistocene Movements in the Gregory Rift Valley,* Geol. Runds., Bd. 43, Heft 1, 257-263.

Shand, S.J., 1936, *Rift Valley Impressions,* Geol. Mag., vol. LXXIII, 307-312.

Springer, J., 1995, *Environmental Geophysics,* John Wiley and Sons Inc., Canada.

Stuttard, M.J., Hayball, J.B., Narsico, G., Suppo, Oroda, A.M., 1993, *Monitoring Lakes in Kenya, an Environmental Analysis Methodology for Developing Countries,* Proceeding International Symposium on Operationalization of Remote Sensing, vol.4.

Telford, W.M., Geldart, L.P., Sheriff, R.E., 1996, *Applied Geophysics-second edition,* Cambridge University Press.

Thompson, A.O., Dodson, R.G., 1958, *Geology of the Naivasha Area,* explanation of degree sheet 43 S.W. (with colored geological map), Directorate Survey of Kenya, Nairobi.

Topographic sheet Naivasha, 1960, no. 50 A-37/A-III-NE(133/II), scale of 1:50000, Directorate Survey of Kenya, P.O. Box 1766, Naerobi.

Topographic sheet Longonot, 1974, no. 133/4, scale of 1:50000, , Directorate Survey of Kenya, P.O. Box 1766, Naerobi.

Van der Velpen, B.P.A., 1988, *Resist: A Computer Processing Package for DC Resistivity Interpretation for the IBM PC and Compatible,* MSc Thesis, ITC Delft, The Nederlands.

Wendlandt, R.F., Morgan, P., 1982, *Lithosphere Thinning Associated with Rifting in East Africa,* Nature, London, vol. 298, 734-736.

Windley, B.F., 1984, *The evolving continents* (2nd edition), Chichester: Wiley.

Zohdy, A.A.R., 1969, *Application of Deep Electrical Soundings for Groundwater Exploration in Hawaii,* Geophysics, v.34.

Zohdy, A.A.R., Eaton, G.P., Mabey, D.R., 1980, *Application od Surface Geophysics to Groundwater Investigation,* Washington D.C.: United States Department of the Interior.

INTERNATIONAL INSTITUTE FOR AEROSPACE SURVEY AND EARTH SCIENCES

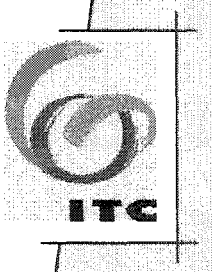

APPENDIX A

Coordinates of observation points

INTERNATIONAAL INSTITUUT VOOR LUCHT – EN RUIMTEKAARTERING EN AARDKUNDE

INSTITUTO INTERNACIONAL PARA LEVANTAMIENTOS AEROESPACIALES Y CIENCIAS TERRESTRES

INSTITUT INTERNATIONAL DE LEVES AEROSPATIAUX ET SCIENCES DE LA TERRE

Coordinates Data

No	Code	Date	Time (GMT)	Bearing (degree)	UTM Coordinate X	UTM Coordinate Y	Remarks
1	VES-1/V1	4-Oct-98	7:00	S 258 W	218274	9908296	perpendicular to the main road in suswa area
2	VES-2/V2	4-Oct-98	8:43	S 256 W	217359	9907997	perpendicular to the main road in suswa area
3	VES-3/V3	4-Oct-98	10:31	S 256 W	217012	9907853	perpendicular to main road to nairobi in suswa area
4	VES-4/V4	4-Oct-98	12:14	S 258 W	216622	9908834	western side of the rail-way track in suswa area
5	VES-5/V5	4-Oct-98	13:23	S 258 W	217758	9909634	perpendicular to main road to nairobi in suswa area
6	VES-6/V6	5-Oct-98	7:13	S 240 W	217705	9909892	parallel to the VES-4 about 2 km
7	VES-7/V7	5-Oct-98	8:49	S 248 W	218427	9910104	eastern side of the river & also near the main road to nairobi
8	VES-8/V8	5-Oct-98	11:21	S 258 W	216533	9908928	western side of the railway track
9	VES-9/V9	5-Oct-98	13:18	S 260 W	216778	9909404	near the bend of railway track
10	VES-10/V10	6-Oct-98	11:05	S 178 E	213276	9911117	small track to the airstrip
11	VES-11/V11	6-Oct-98	12:53	S 178 E	214984	9910071	small track towards longonot direction
12	VES-12/V12	7-Oct-98	15.36	S 160 E	212178	9913224	inside the sanctuary farm
13	VES-13/V13	6-Oct-98	9:00	N 070 E	212084	9913422	polo field in the sanctuary farm
14	VES-14/V14	8-Oct-98	9:52	N 288 W	212566	9912513	entrance track to sanctuary farm
15	VES-15/V15	12-Oct-98	9:39	S 200 W	214791	9916508	south lake road, 1.5 km from the junction to the left
16	VES-16/V16	16-Oct-98	6:39	S 096 E	215010	9917431	arbadare farm
17	VES-17/V17	9-Oct-98	6:51	S 152 E	213854	9924903	three austriche farm in north east of lake naivasha
18	VES-18/V18	9-Oct-98	11:20	N 332 W	214169	9924489	200 m from the river in the three austriche farm
19	VES-19/V19	9-Oct-98	13:06	N 342 W	215065	9924793	eastern part of the ridge in the three austriche farm
20	VES-20/V20	12-Oct-98	13:07	S 160 E	213590	9925296	in the western part of the VES-17
21	VES-21/V21	13-Oct-98	7:49	S 216 W	212248	9927325	about 75 meter towards eastern direction from malewa river
22	VES-22/V22	13-Oct-98	11:10	S 230 W	211380	9926518	homegrown farm (near malewa river)
23	VES-23/V23	15-Oct-98	13:17	S 220 W	211331	9921888	manera farm along the road
24	VES-24/V24	13-Oct-98	13:26	S 208 W	210785	9920719	manera farm near the lake in the north eastern part of the lake
25	CST-25/P25	15-Oct-98	6:39	S 235 W	215235	9929149	The coordinates were measured at the starting point
26	CST-26/P26	14-Oct-98	13:17	S 220 W	211331	9921888	The coordinates were measured at the starting point
27	CST-27/P27	14-Oct-98	9:19	N 074 E	220808	9919026	The coordinates were measured at the starting point
28	CST-28/P28	14-Oct-98	13:46	N 040 E	217674	9918582	The coordinates were measured at the starting point
29	CST-29/P29	15-Oct-98	11:26	N 042 E	218498	9916653	The coordinates were measured at the starting point
30	VES-30/V30	16-Oct-98	7:48	S 065 E	214384	9918656	next to the main road to naerobi

INTERNATIONAL INSTITUTE FOR AEROSPACE SURVEY AND EARTH SCIENCES

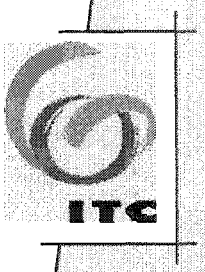

APPENDIX B

Resistivity Horizontal Profiling Data

INTERNATIONAAL INSTITUUT VOOR LUCHT – EN RUIMTEKAARTERING EN AARDKUNDE

INSTITUTO INTERNACIONAL PARA LEVANTAMIENTOS AEROESPACIALES Y CIENCIAS TERRESTRES

INSTITUT INTERNATIONAL DE LEVES AEROSPATIAUX ET SCIENCES DE LA TERRE

Horisontal Profile / P-25

Station (m)	Ohm-m
320	23.348
310	24.132
300	24.132
290	24.915
280	36.668
270	29.303
260	27.893
250	25.7
240	27.736
230	24.132
220	21.468
210	19.117
200	21.781
190	17.864
180	18.491
170	23.035
160	20.058
150	21.155
140	22.565
130	18.961
120	17.55
110	17.08
100	14.103
90	15.827
80	13.79
70	15.983
60	14.73
50	15.2
40	20.371
30	24.445
20	22.251
10	18.491
0	32.907
-10	28.833
-20	35.414
-30	26.012
-40	28.363
-50	29.773
-60	26.326

Horisontal Profile / P-26

Station (m)	Ohm-m
-130	40.742
-120	48.577
-110	29.616
-100	38.235
-90	24.132
-80	28.519
-70	29.93
-60	32.124
-50	33.064
-40	43.87
-30	47.01
-20	40.115
-10	34.32
0	31
10	38.235
20	50.77
30	68.165
40	67.851
50	60.8
60	78.66
70	77.41
80	223.611
90	140.09
100	184.593

Horisontal Profile / P-27

Station (m)	Ohm-m
-150	32.129
-140	41.758
-130	43.926
-120	42.904
-110	37.418
-100	33.920
-90	28.092
-80	34.459
-70	31.761
-60	34.743
-50	28.603
-40	38.499
-30	46.890
-20	40.679
-10	37.43
0	37.597
10	42.723
20	56.9
30	54.58
40	67.189
50	162.325
60	127.698
70	138.093
80	193.918
90	140.509
100	124.57

Horisontal Profile / P-28

Station (m)	Ohm-m
-150	34.47
-140	38.39
-130	41.63
-120	45.258
-110	32.1
-100	36.549
-90	30.328
-80	28.724
-70	27.795
-60	29.985
-50	32.684
-40	40.452
-30	48.917
-20	42.195
-10	36.327
0	33.87
10	40.235
20	52.954
30	58.984
40	63.157
50	68.852
60	77.169
70	138.284
80	193.846
90	140.09
100	124.937

Horisontal Profile / P-29

Station (m)	Ohm-m
-150	40.742
-140	43.093
-130	50.457
-120	61.426
-110	35.728
-100	48.577
-90	32.124
-80	36.041
-70	39.802
-60	44.66
-50	53.278
-40	54.845
-30	51.711
-20	45.6
-10	40.742
0	36.354
10	35.571
20	45.756
30	69.731
40	72.395
50	67.538
60	84.148
70	87.439
80	183.652
90	343.486
100	216.716
110	196.659
120	184.279
130	182.399
140	186.473
150	174.564

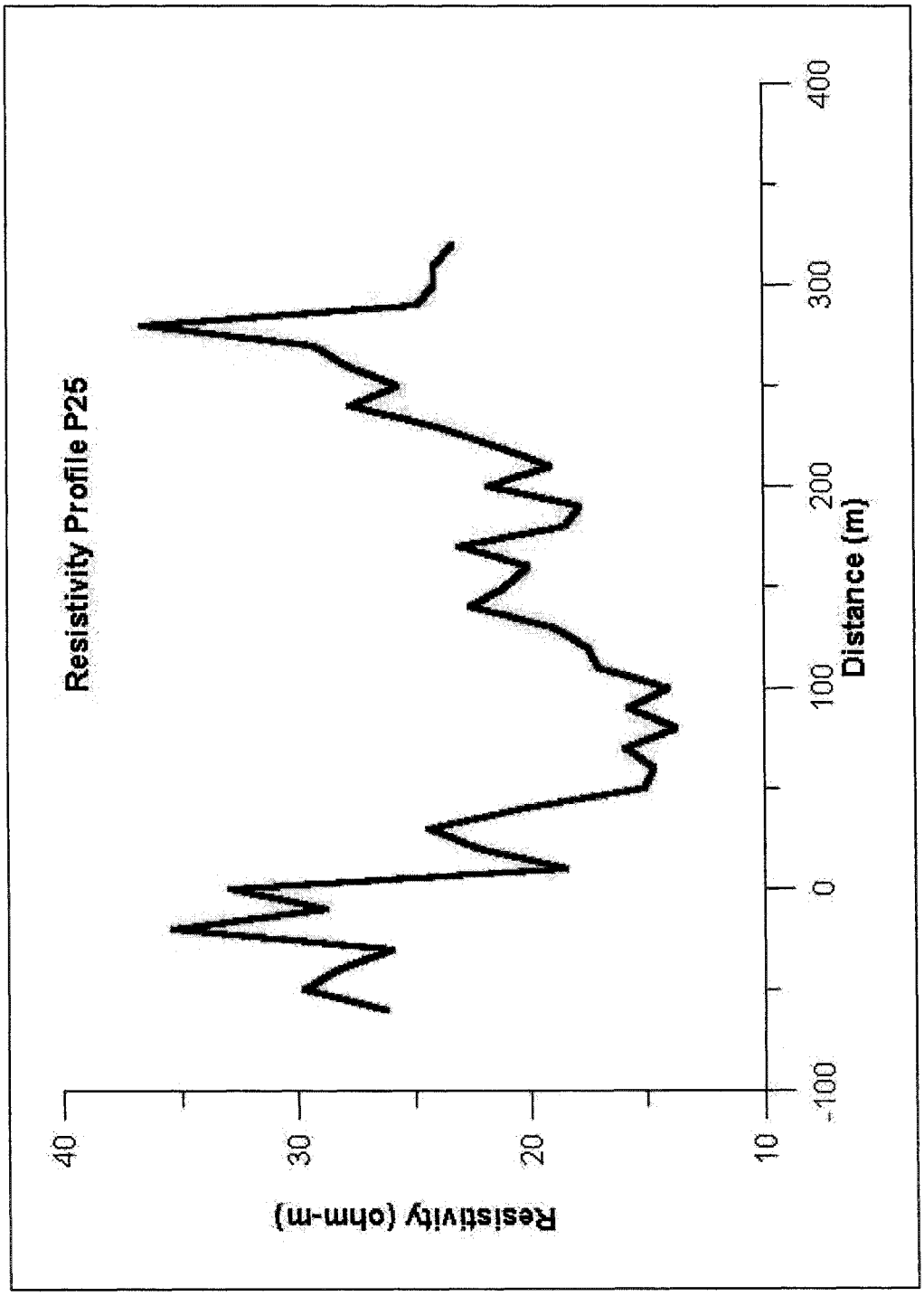
Resistivity Profile P25
Resistivity (ohm-m)
40
30
20
10
-100
0
100
200
300
400
Distance (m)

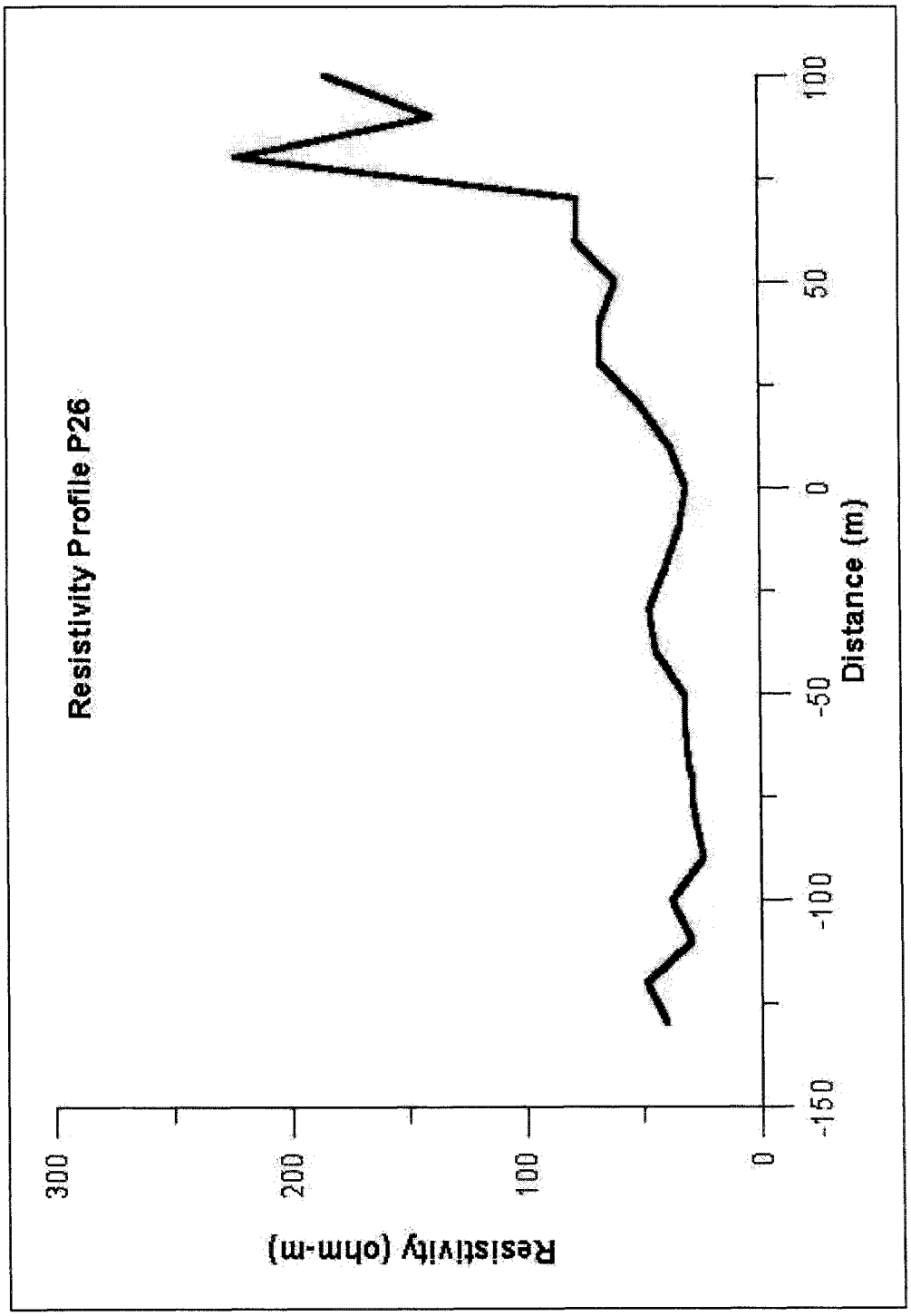
Resistivity Profile P26
Resistivity (ohm-m)
300
200
100
0
-150
-100
-50
0
50
100
Distance (m)

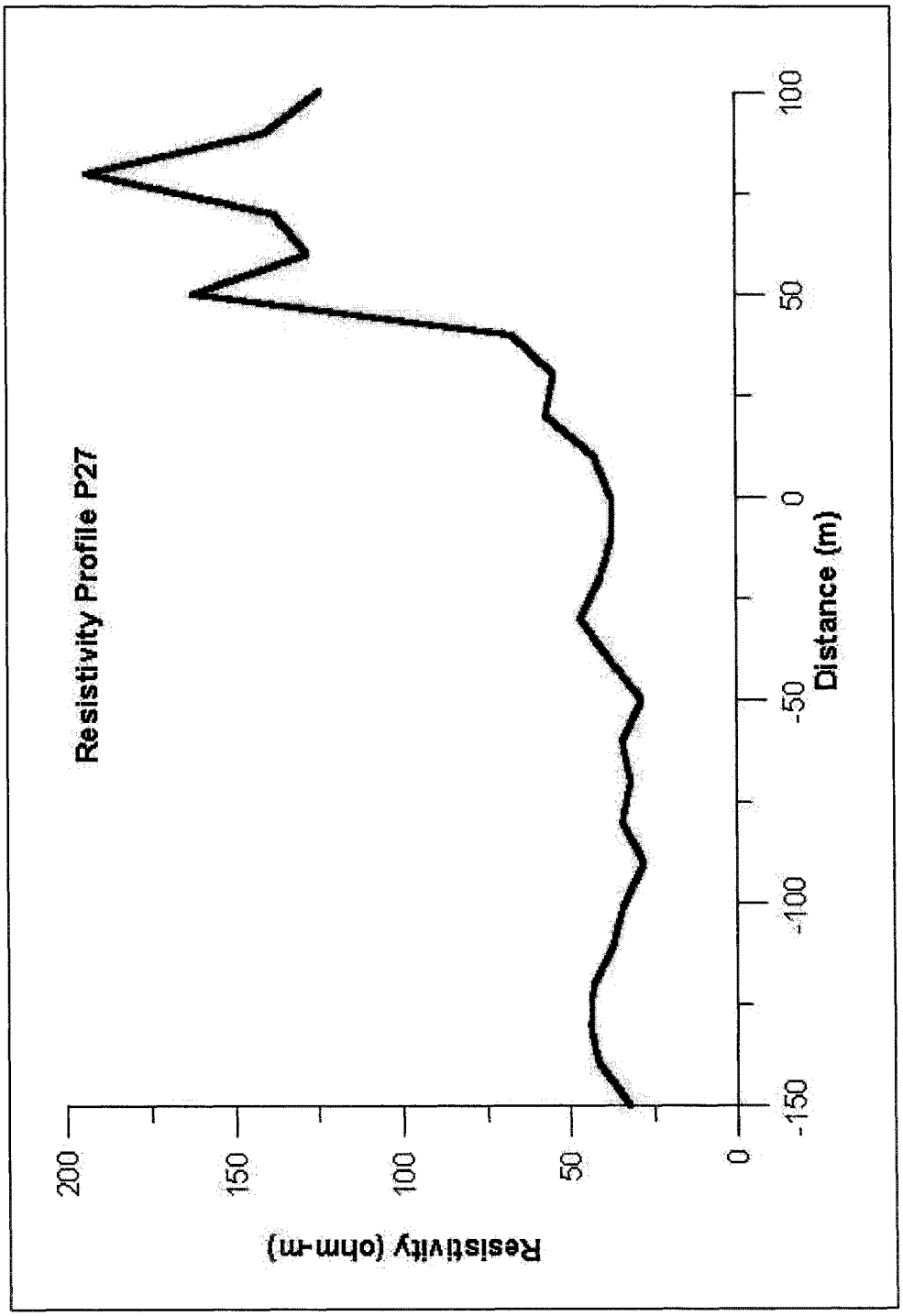
Resistivity Profile P27
Resistivity (ohm-m)
200
150
100
50
0
-150
-100
-50
0
50
100
Distance (m)

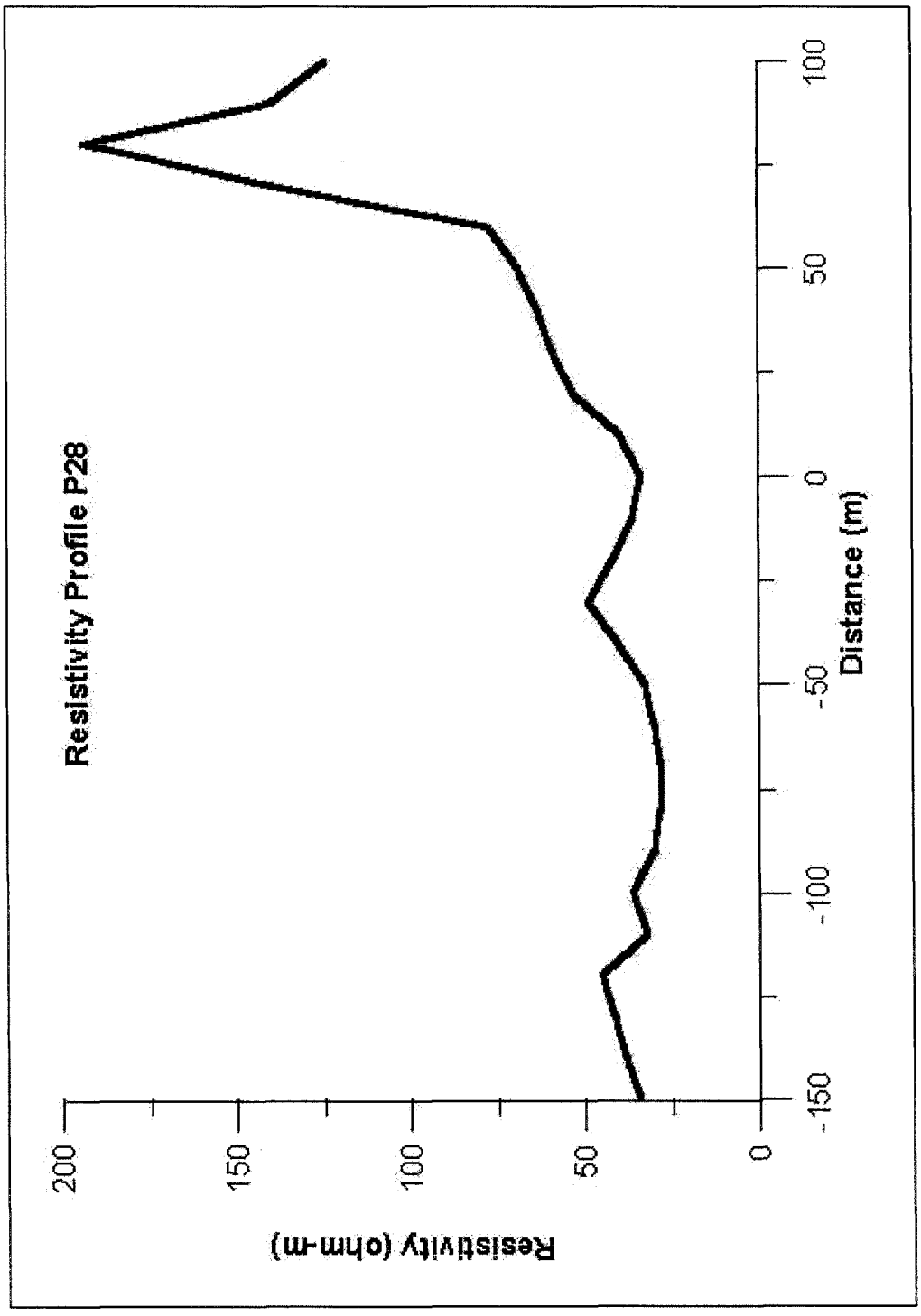
Resistivity Profile P28
Resistivity (ohm-m)
200
150
100
50
0
-150
-100
-50
0
50
100
Distance (m)

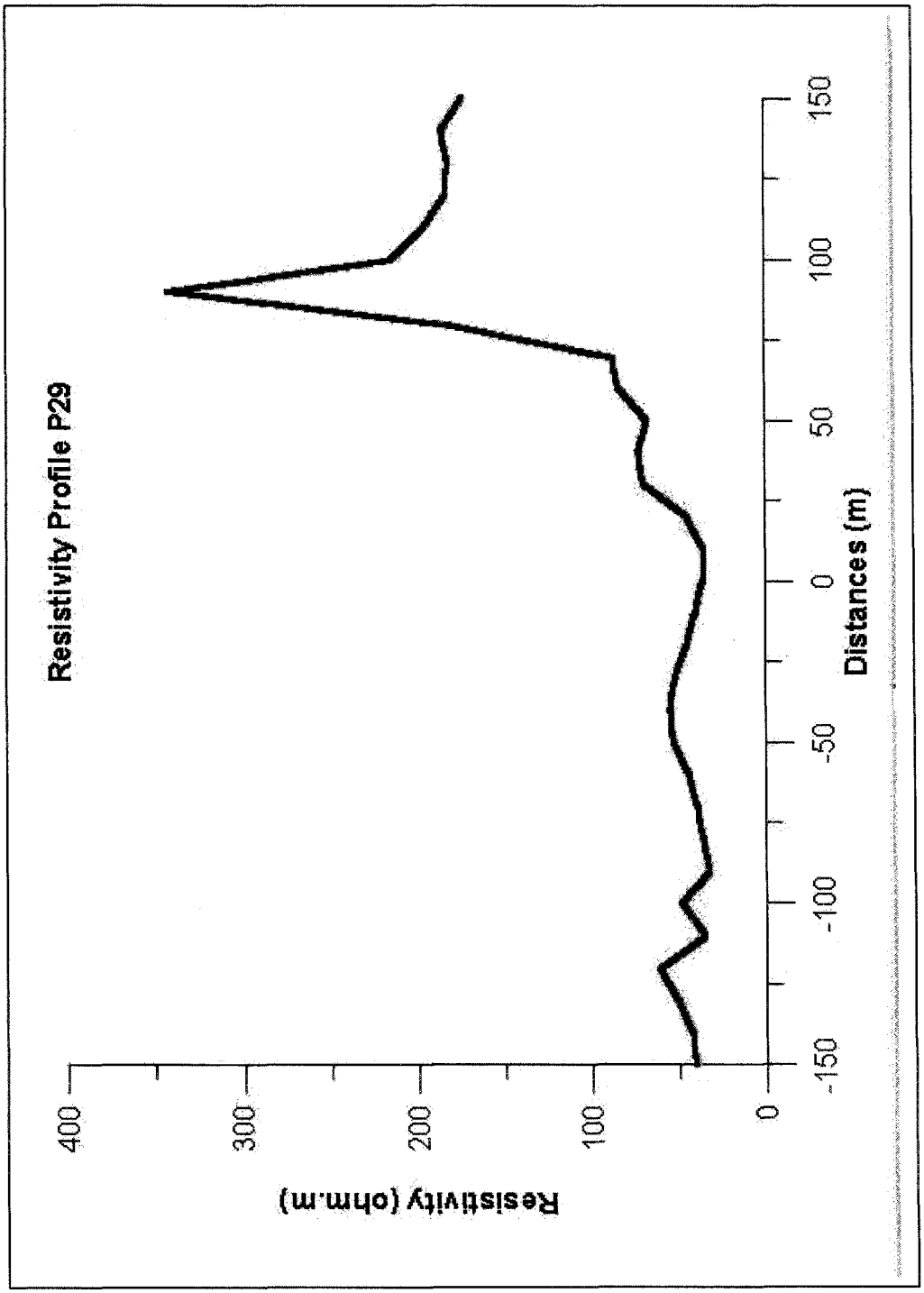
Resistivity Profile P29
Resistivity (ohm.m)
400
300
200
100
0
-150
-100
-50
0
50
100
150
Distances (m)

INTERNATIONAL INSTITUTE FOR AEROSPACE SURVEY AND EARTH SCIENCES

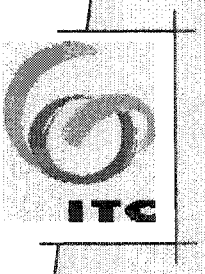

APPENDIX C

Vertical Electrical Sounding Data

INTERNATIONAAL INSTITUUT VOOR LUCHT – EN RUIMTEKAARTERING EN AARDKUNDE

INSTITUTO INTERNACIONAL PARA LEVANTAMIENTOS AEROESPACIALES Y CIENCIAS TERRESTRES

INSTITUT INTERNATIONAL DE LEVES AEROSPATIAUX ET SCIENCES DE LA TERRE

VES-1

perpendicular to the main road to Naerobi (in suswa area)
Schlumberger Array

AB/2	RES
1.5000	425.7800
2.5000	157.9600
4.0000	63.3300
6.0000	71.8700
6.0000	66.8500
8.0000	83.8800
10.0000	99.5300
12.0000	113.3000
12.0000	111.7000
15.0000	131.2000
20.0000	159.6700
25.0000	180.6000
30.0000	200.6000
40.0000	224.9000
50.0000	221.7000
60.0000	244.4000
60.0000	224.6000
75.0000	228.7000
100.0000	219.3800
100.0000	171.0500
125.0000	170.7300
150.0000	140.7600
200.0000	125.3400

VES-2

perpendicular to the main road to Naerobi (in suswa area)
Smoothed Schlumberger Array

AB/2	RES	SmoothedAB/2	SmoothedRES
1.5000	387.4800	1.5000	387.4800
2.5000	128.1800	2.5000	128.1800
4.0000	44.5000	4.0000	44.5000
6.0000	44.9000	6.0000	42.5550
6.0000	40.2100	6.0000	42.5550
8.0000	51.8300	8.0000	51.8300
10.0000	63.3400	10.0000	63.3400
12.0000	77.0000	12.0000	77.0000
15.0000	90.2700	15.0000	89.2450
15.0000	88.2200	15.0000	89.2450
20.0000	122.8200	20.0000	122.8200
25.0000	129.0000	25.0000	129.0000
30.0000	139.9500	30.0000	138.7000
30.0000	137.4500	30.0000	138.7000
40.0000	148.4000	40.0000	148.4000
50.0000	155.5000	50.0000	155.5000
60.0000	146.0000	60.0000	146.0000
75.0000	140.7000	75.0000	131.1050
75.0000	121.5100	75.0000	131.1050
100.0000	108.8500	100.0000	108.8500
125.0000	97.5600	125.0000	97.5600
150.0000	70.3800	150.0000	70.3800
200.0000	125.3000	200.0000	39.4334

VES-3

perpendicular to main road to Naerobi in suswa area
Schlumberger Array

AB/2	RES
1.5000	337.8600
2.5000	81.8100
4.0000	67.2900
6.0000	89.8400
6.0000	82.6800
8.0000	96.1300
10.0000	108.5800
12.0000	121.0000
15.0000	138.8800
20.0000	155.5000
20.0000	151.4800
25.0000	174.1500
30.0000	186.6000
40.0000	199.9200
50.0000	195.6000
50.0000	178.8300
60.0000	145.9900
75.0000	158.3100
100.0000	156.7000
125.0000	147.0300
150.0000	141.2200
200.0000	125.6000

VES-4

western side of the rail-way track in suswa area
Schlumberger Array

AB/2	RES
1.5000	136.5900
2.5000	41.0900
4.0000	57.4000
6.0000	78.6100
6.0000	67.8500
8.0000	80.1000
10.0000	86.7100
12.0000	96.8000
15.0000	107.6300
15.0000	102.9200
20.0000	122.8200
25.0000	109.6500
30.0000	93.3000
30.0000	112.7100
40.0000	128.6500
50.0000	132.1800
60.0000	146.0000
75.0000	123.1300
75.0000	130.1900
100.0000	124.4000
125.0000	97.5600
150.0000	70.3800
200.0000	62.6700

VES-5

perpendicular to main road to nairobi in suswa area
Smoothed Schlumberger Array

AB/2	RES	SmoothedAB/2	SmoothedRES
1.5000	262.5000	1.5000	262.5000
2.5000	116.1200	2.5000	116.1200
4.0000	84.1200	4.0000	84.1200
6.0000	105.5600	6.0000	105.5600
8.0000	120.1800	8.0000	117.5750
8.0000	114.9700	8.0000	117.5750
10.0000	128.1800	10.0000	128.1800
12.0000	125.4000	12.0000	125.4000
15.0000	104.1600	15.0000	98.4500
15.0000	92.7400	15.0000	98.4500
20.0000	85.9700	20.0000	85.9700
25.0000	87.0800	25.0000	85.0100
25.0000	82.9400	25.0000	85.0100
30.0000	74.2200	30.0000	74.2200
40.0000	74.2200	40.0000	74.2200
50.0000	69.9800	50.0000	70.8050
50.0000	71.6300	50.0000	70.8050
60.0000	65.9800	60.0000	65.9800
75.0000	78.1100	75.0000	77.5750
75.0000	41.0400	75.0000	77.5750
100.0000	94.2500	100.0000	64.2500
125.0000	514.2800	125.0000	52.6240
150.0000	374.9800	150.0000	43.4000
200.0000	406.7900	200.0000	40.4300

VES-6

parallel to the VES-4 about 2 km
Schlumberger Array

AB/2	RES
1.5000	107.5100
2.5000	95.9500
4.0000	129.6400
6.0000	138.1900
6.0000	106.0500
8.0000	127.6950
10.0000	141.3000
12.0000	145.6400
15.0000	144.6090
20.0000	120.9790
20.0000	127.3230
25.0000	121.5800
30.0000	115.2260
30.0000	122.0560
40.0000	96.4860
50.0000	84.7480
60.0000	75.2410
60.0000	73.6700
75.0000	69.4320
100.0000	76.1950
125.0000	63.4140
150.0000	70.3800
200.0000	62.6700

VES-7

eastern side of the river and also near thr main road to Naerobi
Schlumberger Array

AB/2	RES
1.5000	192.4820
2.5000	157.5860
4.0000	174.1700
6.0000	196.4130
6.0000	184.7060
8.0000	209.2130
10.0000	229.2160
12.0000	228.8000
15.0000	231.0620
20.0000	207.4370
20.0000	204.7000
25.0000	175.1180
30.0000	167.0070
40.0000	131.6140
50.0000	82.1520
50.0000	87.0800
60.0000	75.2410
75.0000	72.1190
100.0000	51.7110
100.0000	51.3150
125.0000	47.8340
150.0000	52.7850
200.0000	40.9630

VES-8

western side of the railway track
Schlumberger Array

AB/2	RES
1.5000	124.2180
2.5000	99.8110
4.0000	84.6740
6.0000	88.9600
6.0000	88.9600
8.0000	120.1560
10.0000	150.8000
12.0000	169.7850
15.0000	173.4260
15.0000	188.0850
20.0000	199.3780
25.0000	178.8260
30.0000	168.4070
40.0000	163.2680
40.0000	164.7680
50.0000	150.8350
60.0000	145.9900
75.0000	121.3710
100.0000	98.7210
100.0000	78.5280
125.0000	53.6580
150.0000	37.4680
200.0000	21.5340

VES-9

near the bend of railway track
Schlumberger Array

AB/2	RES
1.5000	100.5740
2.5000	66.8230
4.0000	90.5000
6.0000	115.4440
6.0000	119.8700
8.0000	132.4070
10.0000	142.2040
12.0000	138.6000
12.0000	137.5120
15.0000	135.3810
20.0000	128.5520
25.0000	116.7450
25.0000	108.4500
30.0000	102.7400
40.0000	93.5170
50.0000	81.6380
60.0000	78.6100
75.0000	63.3240
100.0000	53.2780
100.0000	59.0900
125.0000	41.4630
150.0000	63.3420
200.0000	62.6700

VES-10

small track to the airstrip
Schlumberger Array

AB/2	RES
1.5000	271.0000
2.5000	80.5000
4.0000	28.5000
6.0000	30.4000
8.0000	36.7000
10.0000	43.2000
12.0000	49.6000
15.0000	53.4000
15.0000	58.0000
20.0000	66.0000
25.0000	73.8000
30.0000	79.5000
40.0000	92.7000
50.0000	92.1000
60.0000	110.0000
75.0000	114.0000
75.0000	102.9000
100.0000	103.5000
125.0000	32.7000
125.0000	58.8000
150.0000	56.6000
150.0000	56.3000
200.0000	81.5000
200.0000	66.8000

VES-11

Small track towards longonot direction
Schlumberger Array

AB/2	RES
1.5000	438.3000
2.5000	288.0000
4.0000	116.7000
6.0000	74.1000
8.0000	82.2000
10.0000	97.9000
12.0000	118.3000
15.0000	139.8000
20.0000	143.8000
25.0000	150.1000
25.0000	150.2000
30.0000	153.4000
40.0000	157.8000
50.0000	153.8000
60.0000	158.1000
75.0000	145.7000
100.0000	160.9000
100.0000	129.4000
125.0000	147.2000
125.0000	139.7000
150.0000	105.9000
150.0000	100.3000
200.0000	125.3000

VES-12

inside the sanctuary farm
Smoothed Schlumberger Array

AB/2	RES	SmoothedAB/2	SmoothedRES
1.5000	16.0140	1.5000	16.0140
2.5000	20.9800	2.5000	20.9800
4.0000	25.0860	4.0000	25.0860
6.0000	25.6040	6.0000	25.6040
8.0000	21.8330	8.0000	21.8330
10.0000	23.6620	10.0000	23.6620
12.0000	24.0000	12.0000	24.0000
15.0000	25.4200	15.0000	23.8725
15.0000	22.3250	15.0000	23.8725
20.0000	23.3250	20.0000	23.3250
25.0000	22.9220	25.0000	22.9220
30.0000	26.7410	30.0000	26.7410
40.0000	36.3370	40.0000	36.3370
50.0000	40.1800	50.0000	40.1800
60.0000	39.5360	60.0000	34.1254
60.0000	23.5000	60.0000	34.1254
75.0000	23.5280	75.0000	26.9275
100.0000	36.2390	100.0000	29.7730
100.0000	29.7730	100.0000	29.7730
125.0000	26.9560	125.0000	26.9560
150.0000	28.2440	150.0000	28.1980
150.0000	28.1520	150.0000	28.1980
200.0000	15.6680	200.0000	15.6680

VES-13

polo field in the sanctuary farm
Smoothed Schlumberger Array

AB/2	RES	SmoothedAB/2	SmoothedRES
1.5000	52.2180	0.8000	52.3642
2.5000	18.3220	2.1145	18.2081
4.0000	11.9490	3.7800	11.9031
6.0000	14.2620	5.8577	14.2620
8.0000	15.7240	7.8844	15.7245
10.0000	16.2970	9.8906	16.2970
12.0000	14.0000	11.8866	15.9567
15.0000	15.1810	15.0000	16.4877
15.0000	19.2700	15.0000	16.4877
20.0000	19.7490	20.0000	19.7490
25.0000	21.4590	25.0000	21.4590
30.0000	18.2960	30.0000	20.5649
40.0000	15.4110	40.0000	18.8965
40.0000	22.3820	40.0000	18.8965
60.0000	25.2910	60.0000	22.9186
75.0000	16.4900	75.0000	24.0048
100.0000	20.2150	100.0000	20.2150

VES-14

entrance track to sanctuary farm
Schlumberger Array

AB/2	RES
1.5000	211.6360
2.5000	195.6630
4.0000	147.4500
6.0000	132.5140
8.0000	125.1880
10.0000	119.2490
10.0000	107.6710
12.0000	100.4300
15.0000	87.3210
20.0000	75.5730
25.0000	73.6430
30.0000	67.5550
40.0000	58.8910
50.0000	68.6000
50.0000	71.0680
60.0000	50.7600
60.0000	49.9740
75.0000	40.4570
100.0000	21.9380
100.0000	33.4330
125.0000	26.8290
150.0000	31.6710
200.0000	12.5340

VES-15

south lake road, 1.5 km from the junction to the left
Schlumberger Array

AB/2	RES
1.5000	44.0540
2.5000	42.4130
4.0000	48.5400
6.0000	46.6610
6.0000	56.2700
8.0000	51.9500
10.0000	42.3000
10.0000	48.9800
12.0000	46.5210
15.0000	42.0730
20.0000	39.0980
25.0000	34.1850
25.0000	36.0040
30.0000	35.0500
40.0000	34.3890
50.0000	34.9880
60.0000	37.0590
60.0000	39.5860
75.0000	32.1120

VES-16

arbadare farm
Schlumberger Array

AB/2	RES
1.5000	13.2510
2.5000	17.5870
4.0000	19.6930
6.0000	20.1020
8.0000	19.2290
10.0000	18.4910
10.0000	20.5470
12.0000	19.8000
15.0000	18.2280
20.0000	17.4160
25.0000	16.0940
25.0000	16.1250
30.0000	15.8610
40.0000	14.1610
50.0000	14.3440
50.0000	15.1610
60.0000	15.7220
75.0000	13.1930
100.0000	12.5360
100.0000	12.4400
125.0000	10.9750
125.0000	9.5680
150.0000	7.8120
200.0000	6.2200

VES-17

three austriche farm in north east of lake naivasha
Schlumberger Array

AB/2	RES
1.5000	40.5690
2.5000	37.8890
4.0000	40.8210
6.0000	50.4230
8.0000	60.0900
10.0000	65.1870
12.0000	64.1270
15.0000	63.5490
15.0000	56.7670
20.0000	50.6930
25.0000	47.7950
30.0000	45.0370
40.0000	41.3490
40.0000	40.4000
50.0000	37.8160
60.0000	37.6000
60.0000	34.8130
75.0000	36.0600
100.0000	37.6080
100.0000	43.5400
125.0000	39.0240
150.0000	42.2280
200.0000	37.6770

VES-18

200 m from the river in the three austriche farm
Schlumberger Array

AB/2	RES
1.5000	61.3240
2.5000	53.9110
4.0000	44.9770
6.0000	42.0560
8.0000	42.0630
10.0000	45.1300
12.0000	51.0310
15.0000	59.3120
15.0000	56.2460
20.0000	68.5760
25.0000	80.9580
30.0000	93.5920
40.0000	113.1460
50.0000	125.4400
60.0000	135.5520
60.0000	132.5400
75.0000	145.5800
100.0000	150.1330
100.0000	147.2980
125.0000	137.2280
150.0000	112.9760
150.0000	102.0510
200.0000	68.9370

VES-19

eastern part of the ridge in the three austriche farm
Schlumberger Array

AB/2	RES
1.5000	40.8830
2.5000	25.6080
4.0000	21.6480
6.0000	24.0880
8.0000	29.1440
10.0000	33.2200
12.0000	36.1280
12.0000	38.1700
15.0000	38.3660
20.0000	37.7860
25.0000	38.0410
30.0000	37.2960
40.0000	36.9640
40.0000	39.5680
50.0000	41.7280
60.0000	39.4800
60.0000	38.7440
75.0000	33.4210
100.0000	28.2060
100.0000	28.7680
125.0000	24.3900
150.0000	21.1100
200.0000	25.0680

VES-20

in the western part of the VES-17
Schlumberger Array

AB/2	RES
1.5000	108.5180
2.5000	71.6300
4.0000	44.8040
6.0000	41.8880
8.0000	46.2690
10.0000	46.8530
10.0000	48.5200
12.0000	48.2350
15.0000	44.4420
15.0000	43.7130
20.0000	40.5310
25.0000	39.8290
30.0000	39.1860
40.0000	34.1530
50.0000	35.8600
50.0000	40.4300
60.0000	38.1820
75.0000	31.6620
100.0000	32.9070
100.0000	35.7650
125.0000	35.3660
150.0000	36.9500
200.0000	31.3350

VES-21

about 75 meter towards eastern direction from Malewa river
Schlumberger Array

AB/2	RES
1.5000	26.3130
2.5000	15.4760
4.0000	15.2650
6.0000	18.5300
8.0000	17.2260
10.0000	17.2370
10.0000	19.6040
12.0000	20.1300
15.0000	19.0090
20.0000	19.5930
25.0000	19.9960
25.0000	19.3500
30.0000	24.2580
40.0000	24.1570
50.0000	29.9920
60.0000	30.0800
75.0000	26.4690
75.0000	22.8670
100.0000	25.0720
100.0000	27.9900
125.0000	24.3900
150.0000	22.8740
200.0000	25.0680

VES-22

homegrown farm (near malewa river)
Schlumberger Array

AB/2	RES
1.5000	27.3180
2.5000	30.2540
4.0000	29.2180
6.0000	23.3580
8.0000	18.7280
8.0000	22.3820
10.0000	16.2110
12.0000	11.7700
15.0000	9.5480
20.0000	9.9520
25.0000	9.2660
25.0000	10.3200
30.0000	12.8290
40.0000	15.8270
50.0000	15.6480
60.0000	17.8600
60.0000	17.9680
75.0000	20.2290
100.0000	20.3710
100.0000	19.4380
125.0000	20.7315
125.0000	19.1360
150.0000	19.0960
200.0000	27.9900

VES-23

Manera Farm along the road
Schlumberger Array

AB/2	RES
1.5000	34.2890
2.5000	17.3610
4.0000	8.2630
6.0000	7.4120
8.0000	7.8120
10.0000	8.4620
10.0000	7.4650
12.0000	6.9850
15.0000	7.3780
20.0000	8.3970
20.0000	7.6760
25.0000	7.9010
30.0000	8.1640
40.0000	8.7470
50.0000	9.1280
50.0000	8.9400
60.0000	9.5460
75.0000	10.5540
100.0000	10.9690
100.0000	12.4400
125.0000	12.1950
150.0000	14.0760
200.0000	15.6680

VES-24

manera farm near the lake in the north eastern part of the lake
Schlumberger Array

AB/2	RES
1.5000	3.4400
2.5000	3.2310
4.0000	2.8040
6.0000	2.5760
6.0000	2.6140
8.0000	2.5000
10.0000	2.6010
12.0000	2.7500
15.0000	2.7780
15.0000	2.8000
20.0000	3.0710
25.0000	3.2250
30.0000	3.5000
30.0000	3.5740
40.0000	4.4500
50.0000	4.6650
60.0000	5.6150
60.0000	5.4980
75.0000	5.2070
100.0000	6.2200
125.0000	8.5370
150.0000	7.0380
200.0000	10.0270

VES-30

next to the main road to naerobi
Schlumberger Array

AB/2	RES
1.5000	21.6660
2.5000	10.2360
4.0000	8.0900
6.0000	8.7590
8.0000	9.0140
8.0000	7.7750
10.0000	8.4450
12.0000	8.3600
15.0000	9.0270
20.0000	8.7080
25.0000	9.7540
25.0000	8.7080
30.0000	9.3300
40.0000	10.4130
50.0000	11.0840
50.0000	11.2740
60.0000	12.3530
75.0000	14.0720
75.0000	10.4150
100.0000	15.5500
125.0000	23.1710
125.0000	22.1260
150.0000	16.4920
200.0000	15.5600

VES-1

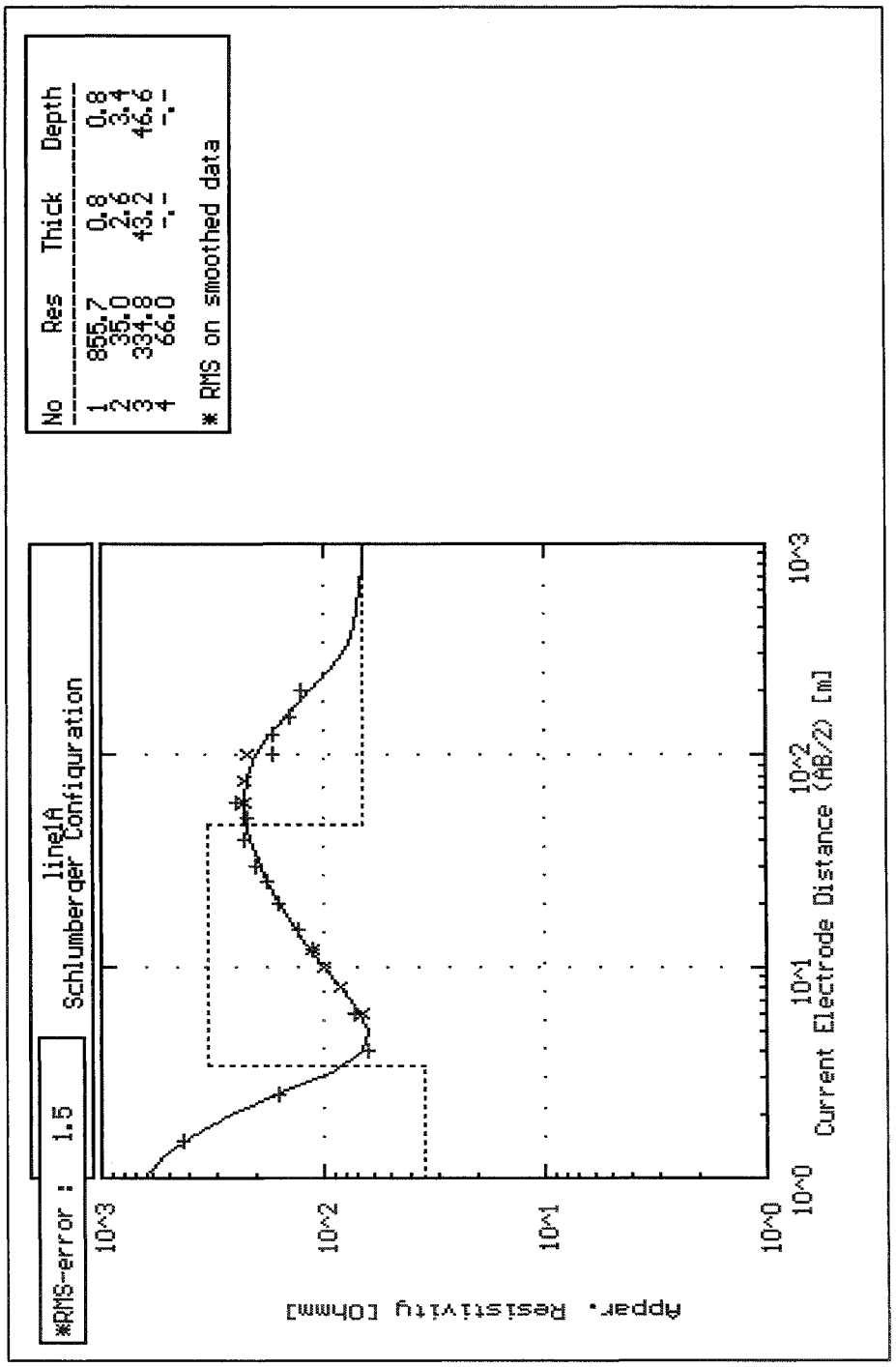
No Res Thick Depth
1 855.7 0.8 0.8
2 35.0 2.6 3.4
3 334.8 43.2 46.6
4 66.0 -.- -.-
* RMS on smoothed data
line1A
Schlumberger Configuration
*RMS-error : 1.5
Appar. Resistivity [Ohmm]
10^3
10^2
10^1
10^0
10^0
10^1
10^2
10^3
Current Electrode Distance (AB/2) [m]

VES-2

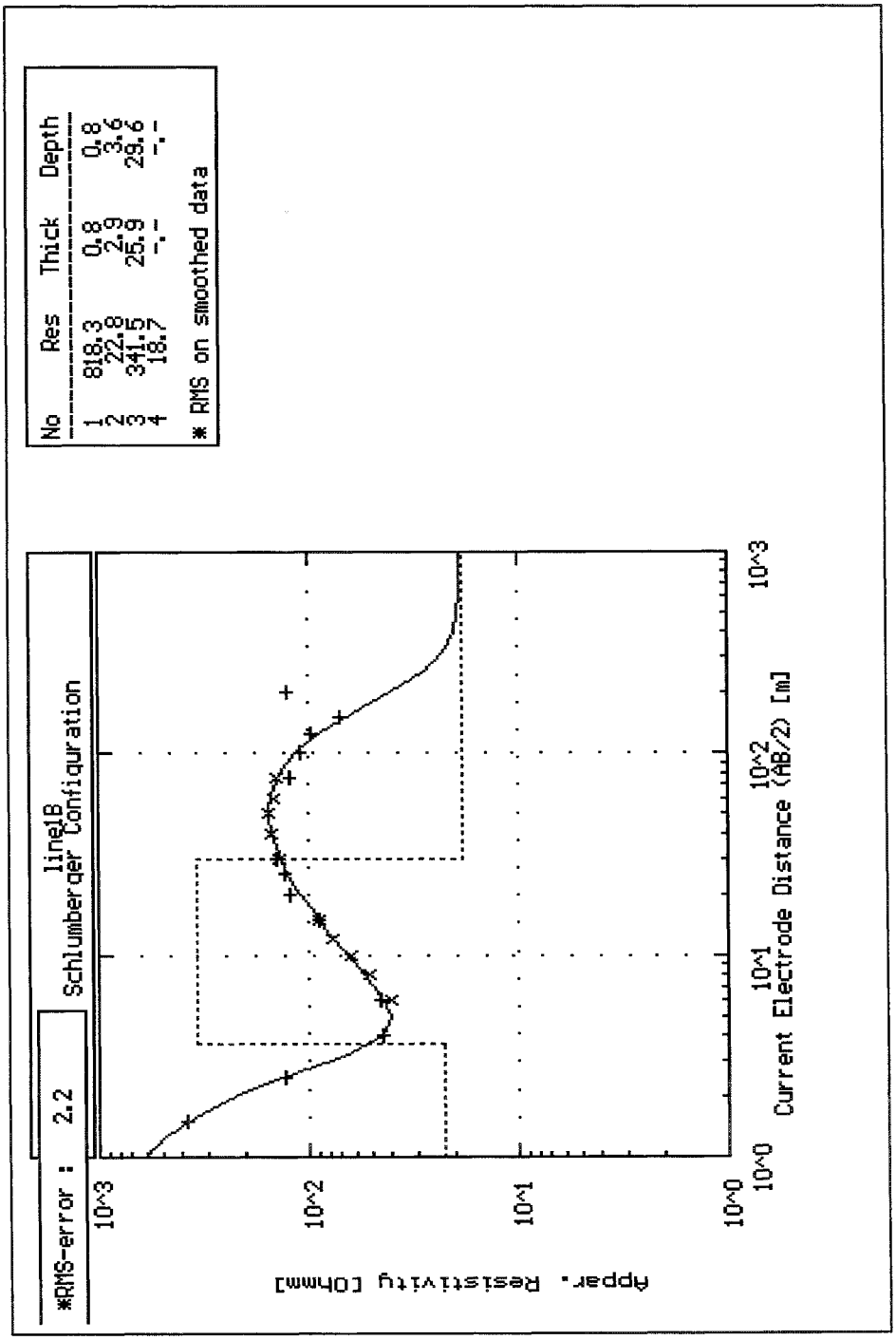
No Res Thick Depth
1 818.3 0.8 0.8
2 22.8 2.9 3.6
3 341.5 25.9 29.6
4 18.7 -.- -.-
* RMS on smoothed data
line1B
Schlumberger Configuration
*RMS-error : 2.2
Appar. Resistivity [Ohmm]
10^3
10^2
10^1
10^0
10^0 10^1 10^2 10^3
Current Electrode Distance (AB/2) [m]

VES-3

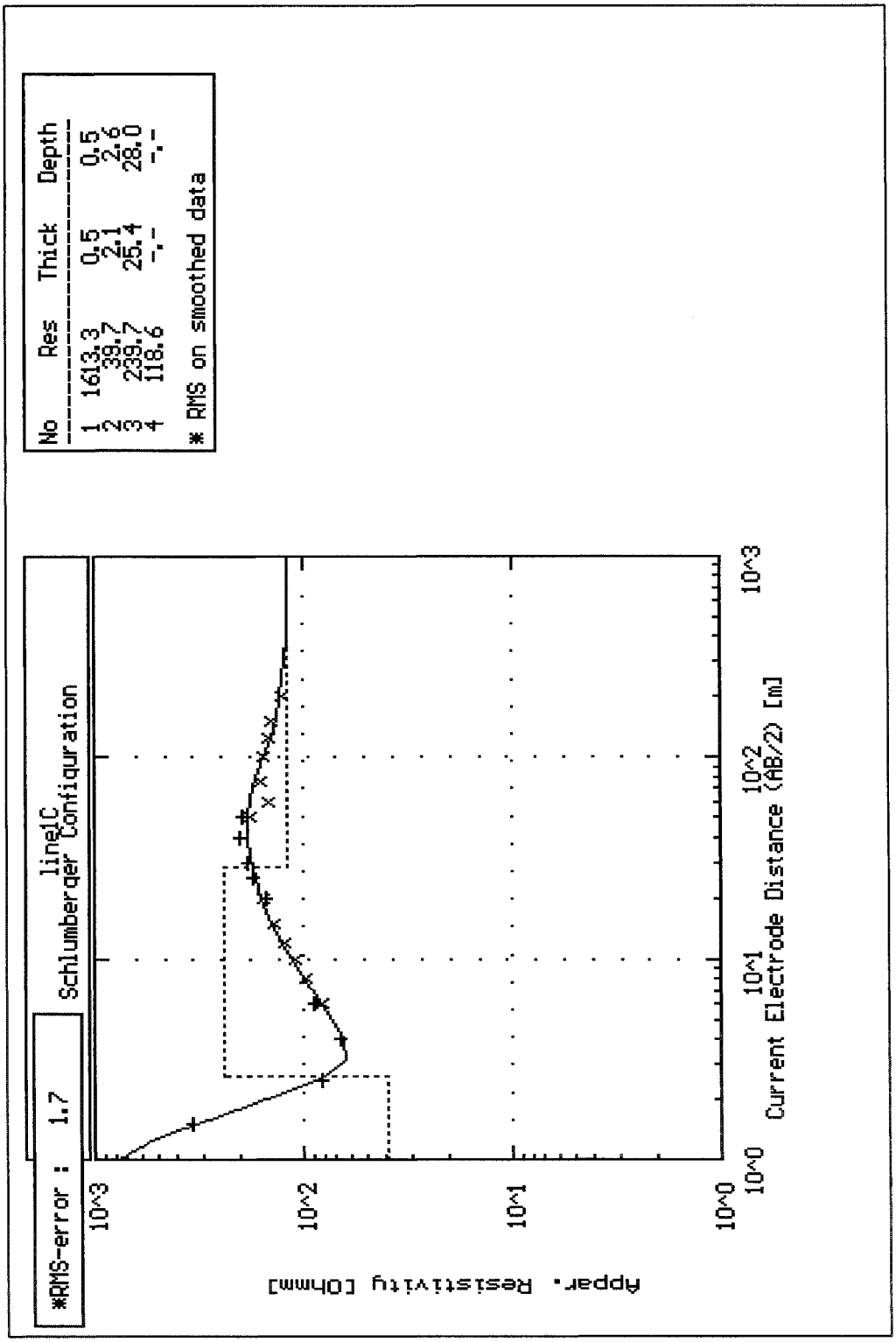
No Res Thick Depth
1 1613.3 0.5 0.5
2 39.7 2.1 2.6
3 239.7 25.4 28.0
4 118.6 -.- -.-
* RMS on smoothed data
line1C
Schlumberger Configuration
*RMS-error : 1.7
Appar. Resistivity [Ohmm]
10^3
10^2
10^1
10^0
10^0
10^1
10^2
10^3
Current Electrode Distance (AB/2) [m]

VES-4

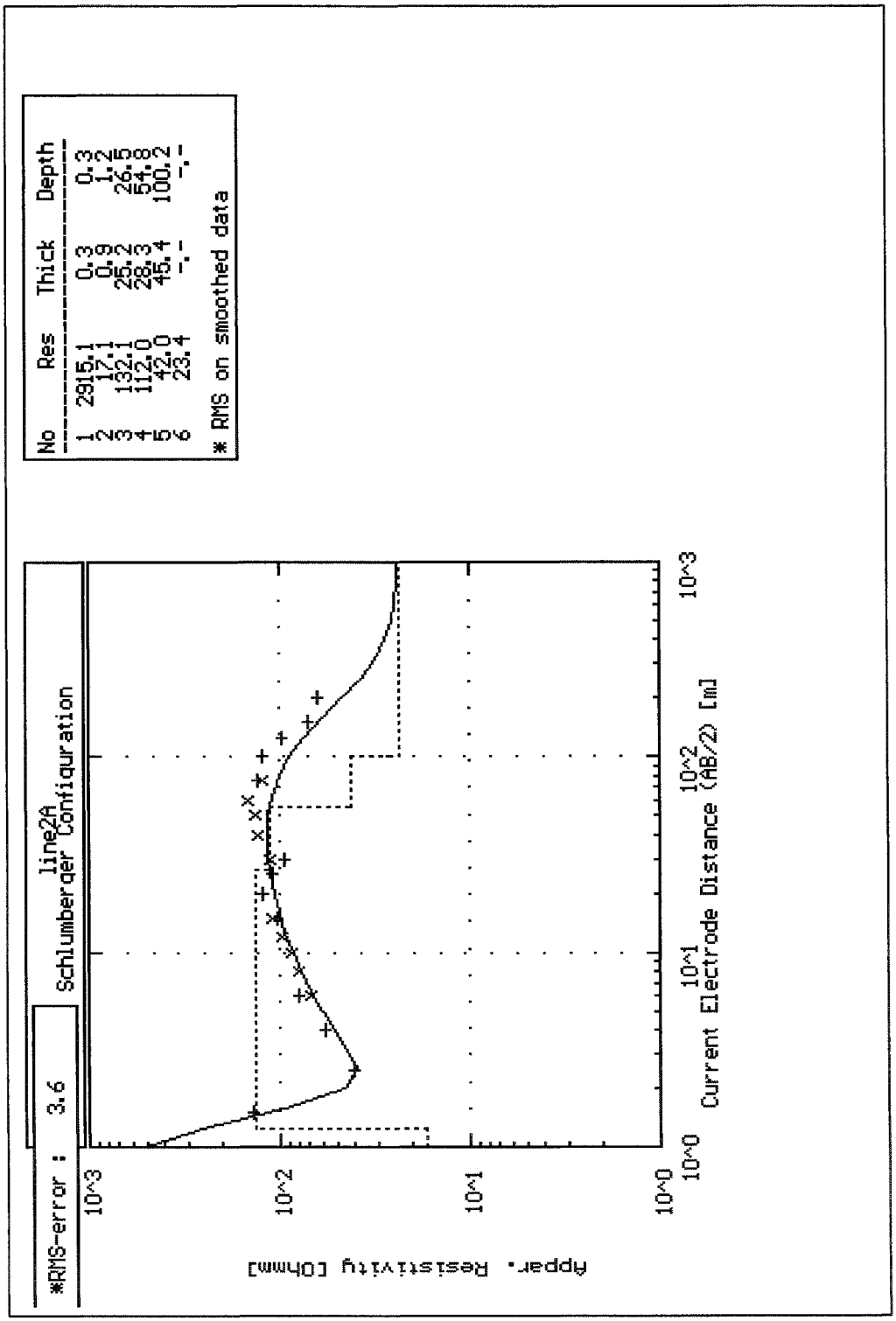
No Res Thick Depth
1 2815.1 0.3 0.3
2 17.1 0.9 1.2
3 132.1 25.2 26.5
4 112.0 28.3 54.8
5 42.0 45.4 100.2
6 23.4 -.- -.-
* RMS on smoothed data
line2A
Schlumberger Configuration
*RMS-error : 3.6
Appar. Resistivity [Ohmm]
10^3
10^2
10^1
10^0
10^0
10^1
10^2
10^3
Current Electrode Distance (AB/2) [m]

VES-5

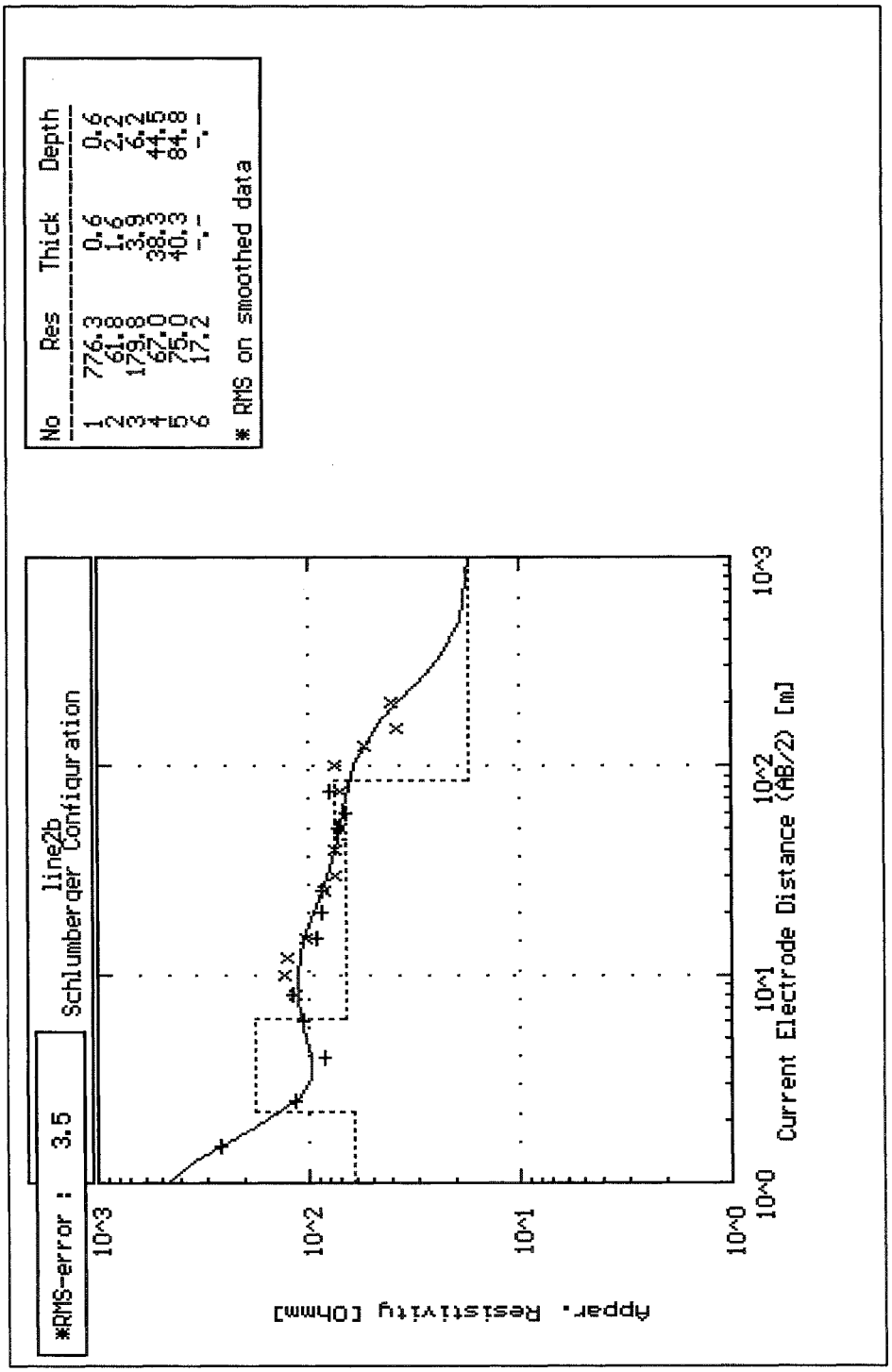
No Res Thick Depth
1 776.3 0.6 0.6
2 61.8 1.6 2.2
3 179.8 3.9 6.2
4 67.0 38.3 44.5
5 75.0 40.3 84.8
6 17.2 -.- -.-
* RMS on smoothed data
line2b
Schlumberger Configuration
*RMS-error : 3.5
Appar. Resistivity [Ohmm]
10^3
10^2
10^1
10^0
10^0
10^1
10^2
10^3
Current Electrode Distance (AB/2) [m]

VES-6

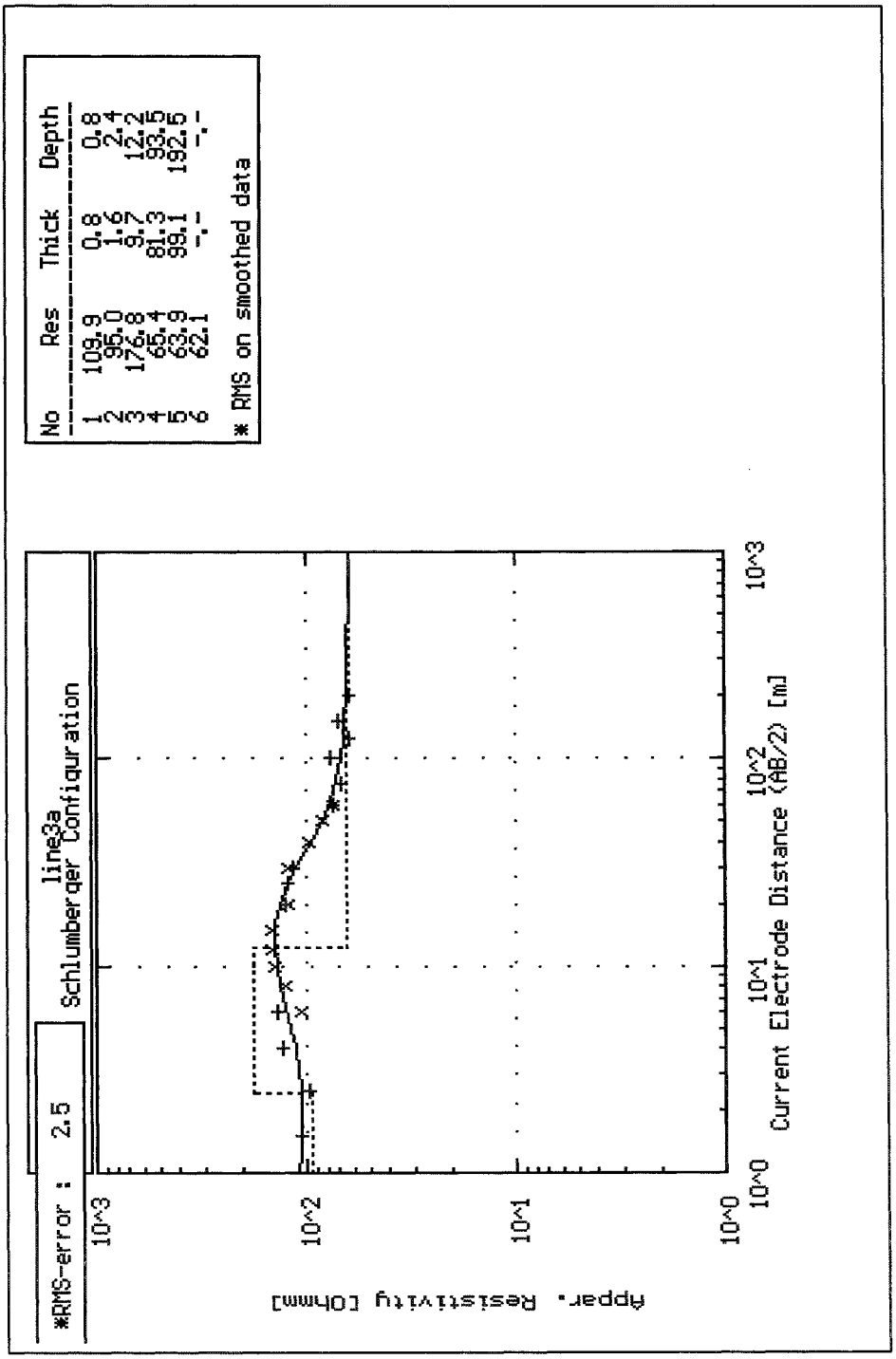
No Res Thick Depth
1 109.9 0.8 0.8
2 95.0 1.6 2.4
3 176.8 9.7 12.2
4 65.4 81.3 93.5
5 63.9 99.1 192.6
6 62.1 -.- -.-
* RMS on smoothed data
*RMS-error : 2.5
line3a
Schlumberger Configuration
Appar. Resistivity [Ohmm]
10^3
10^2
10^1
10^0
10^0
10^1
10^2
10^3
Current Electrode Distance (AB/2) [m]

VES-7

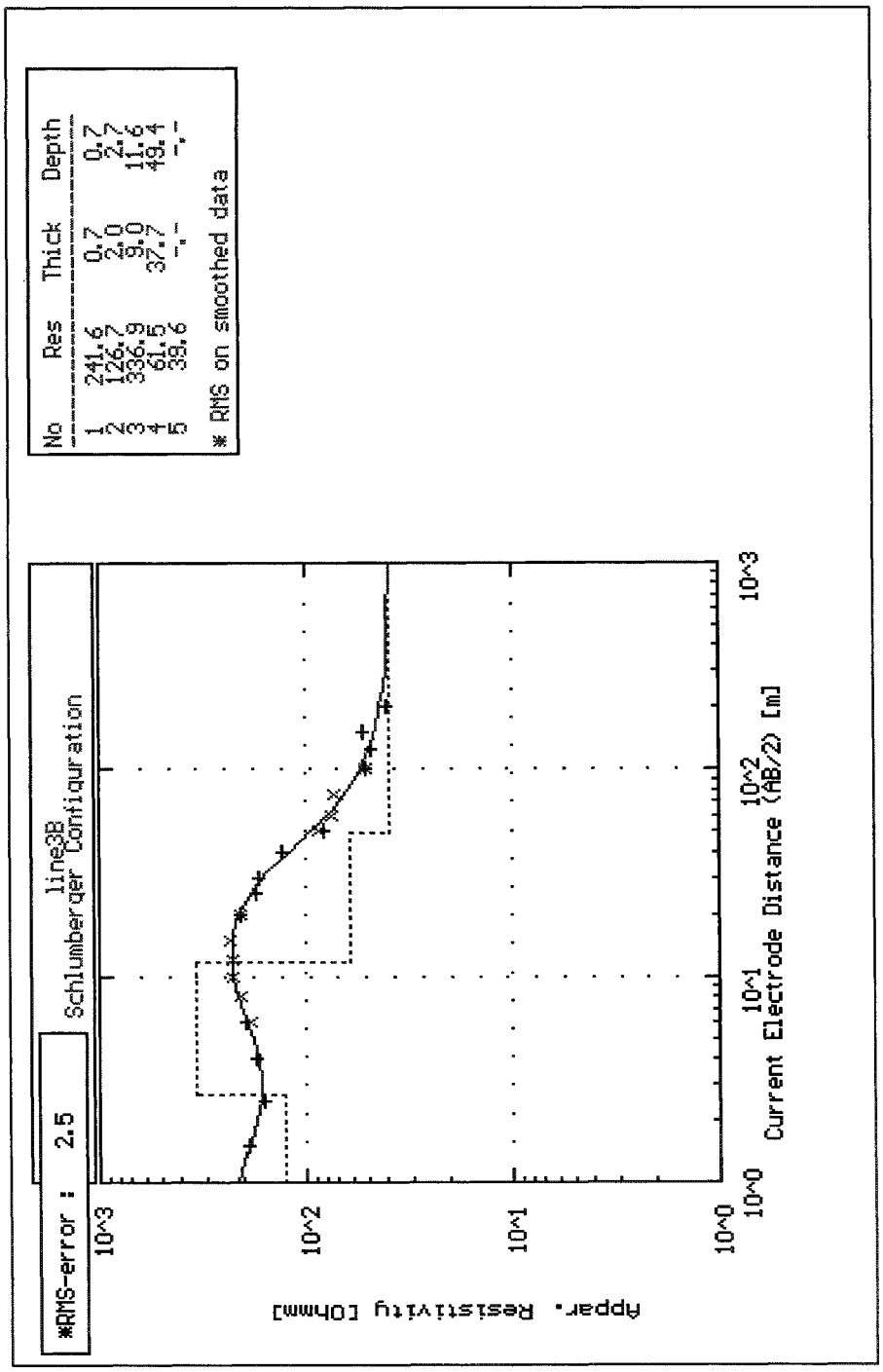
No Res Thick Depth
1 241.6 0.7 0.7
2 126.7 2.0 2.7
3 336.9 9.0 11.6
4 61.5 37.7 49.4
5 38.6 -.- -.-
* RMS on smoothed data
*RMS-error : 2.5
line3B
Schlumberger Configuration
Appar. Resistivity [Ohmm]
10^3
10^2
10^1
10^0
10^0
10^1
10^2
10^3
Current Electrode Distance (AB/2) [m]

VES-8

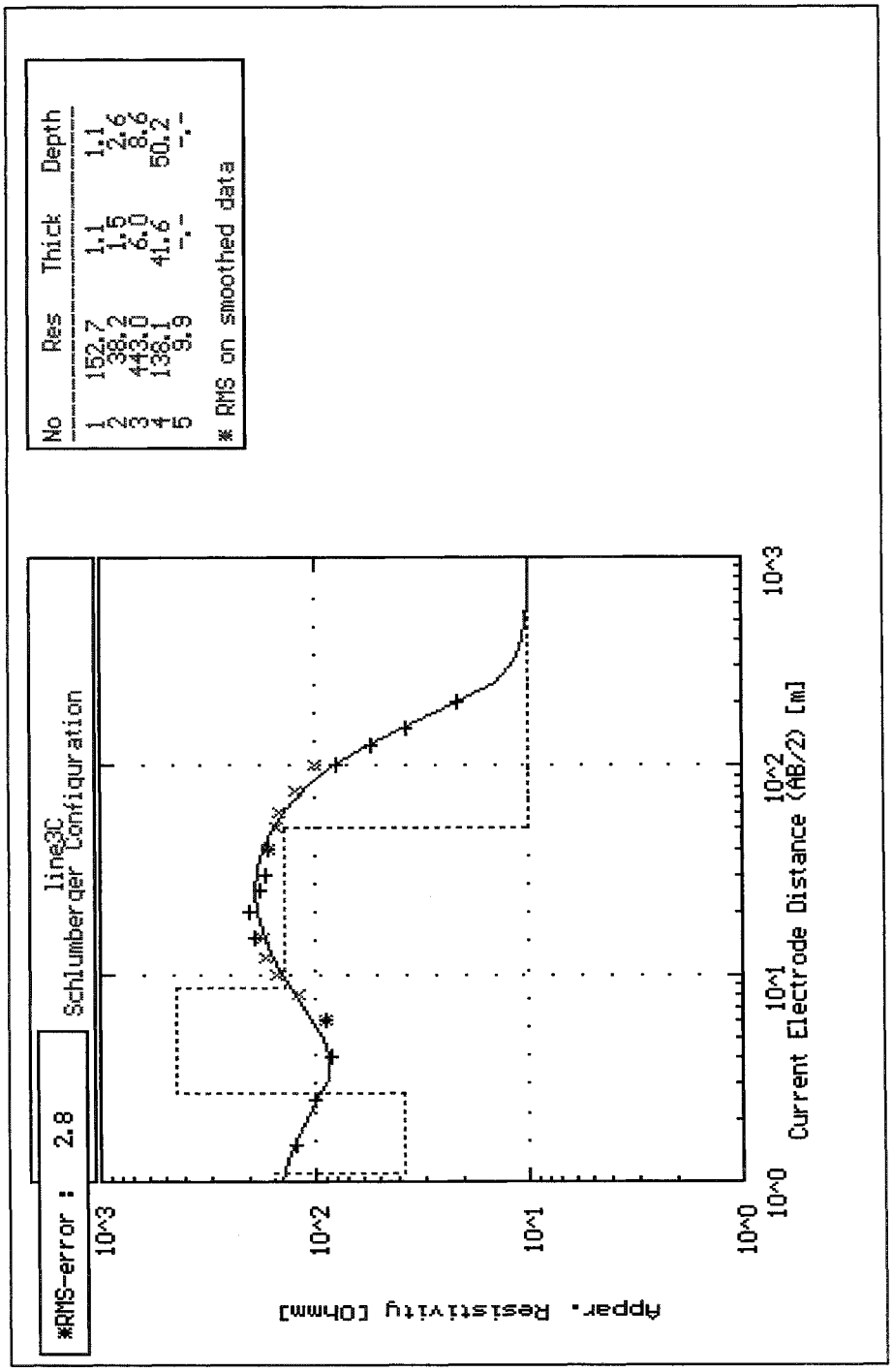
No Res Thick Depth
1 152.7 1.1 1.1
2 38.2 1.5 2.6
3 443.0 6.0 8.6
4 138.1 41.6 50.2
5 9.9 -.- -.-
* RMS on smoothed data
line3C
Schlumberger Configuration
*RMS-error : 2.8
Appar. Resistivity [Ohmm]
10^3
10^2
10^1
10^0
10^0
10^1
10^2
10^3
Current Electrode Distance (AB/2) [m]

VES-9

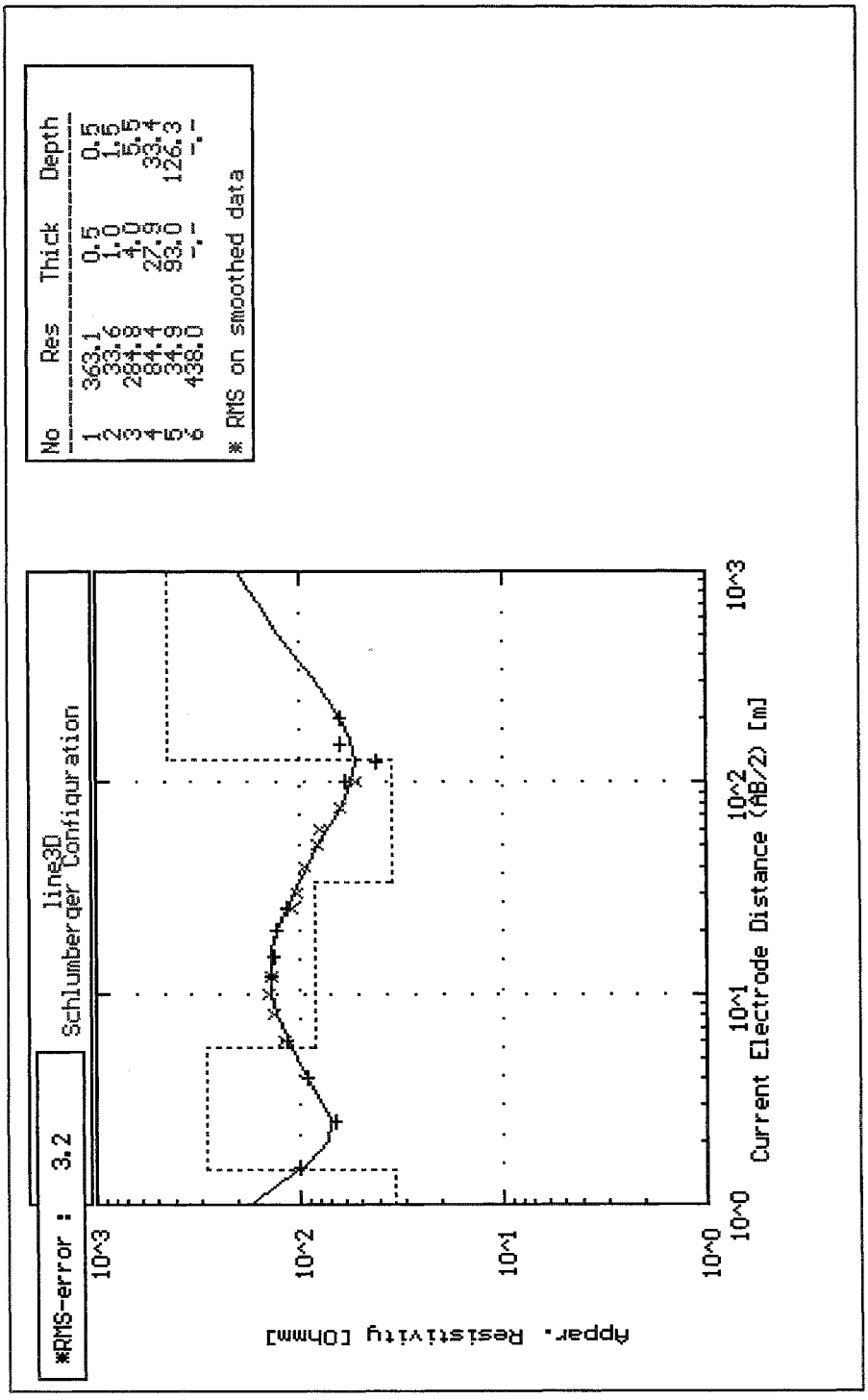
No Res Thick Depth
1 363.1 0.5 0.5
2 33.6 1.0 1.5
3 284.8 4.0 5.5
4 84.4 27.9 33.4
5 34.9 93.0 126.3
6 438.0 -.- -.-
* RMS on smoothed data
*RMS-error : 3.2
line3D
Schlumberger Configuration
Appar. Resistivity [Ohmm]
10^3
10^2
10^1
10^0
10^0
10^1
10^2
10^3
Current Electrode Distance (AB/2) [m]

VES-10

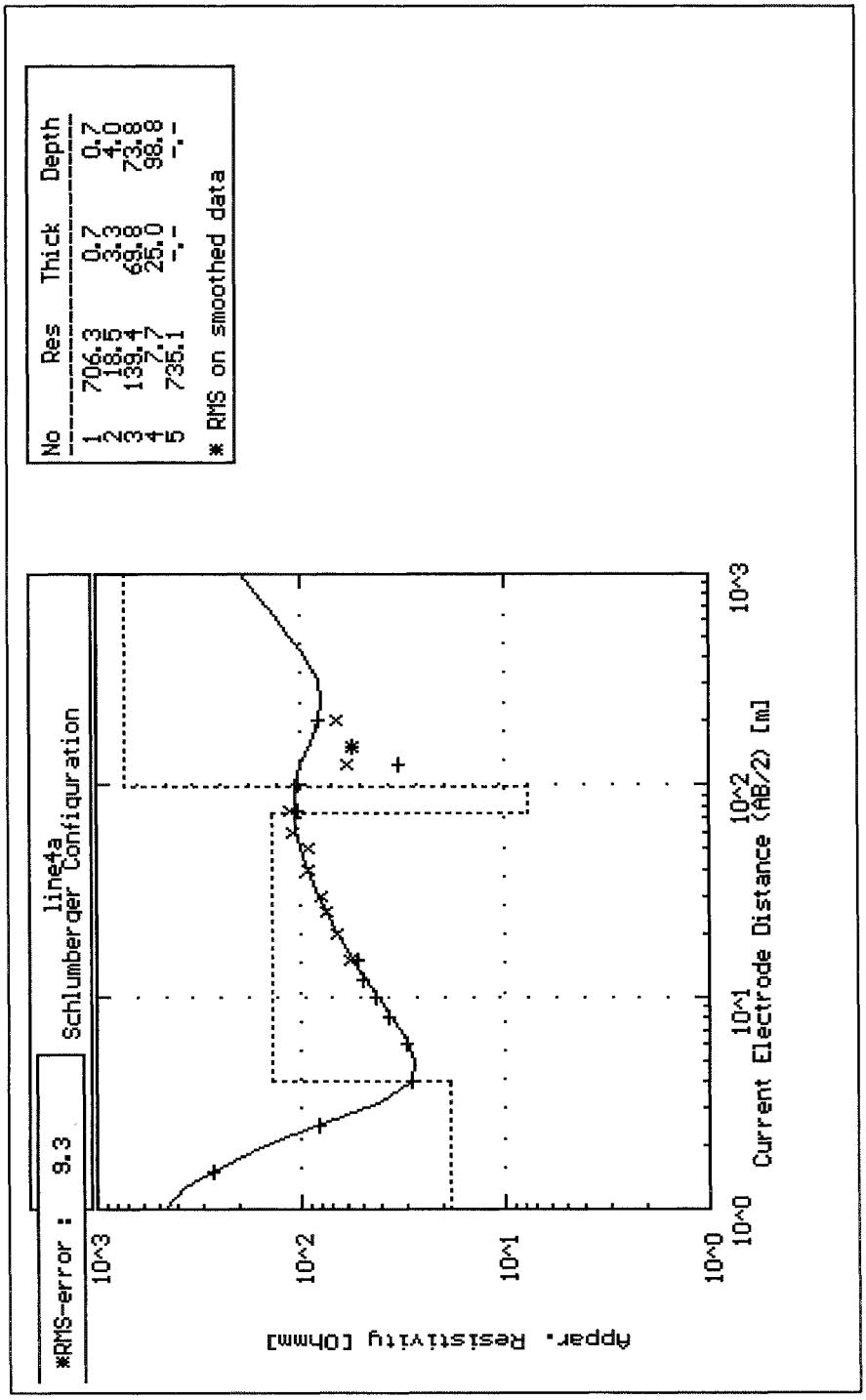
No Res Thick Depth
1 706.3 0.7 0.7
2 18.5 3.3 4.0
3 139.4 69.8 73.8
4 7.7 25.0 98.8
5 735.1 -.- -.-
* RMS on smoothed data
*RMS-error : 9.3
line4a
Schlumberger Configuration
Appar. Resistivity [Ohmm]
10^3
10^2
10^1
10^0
10^0
10^1
10^2
10^3
Current Electrode Distance (AB/2) [m]

VES-11

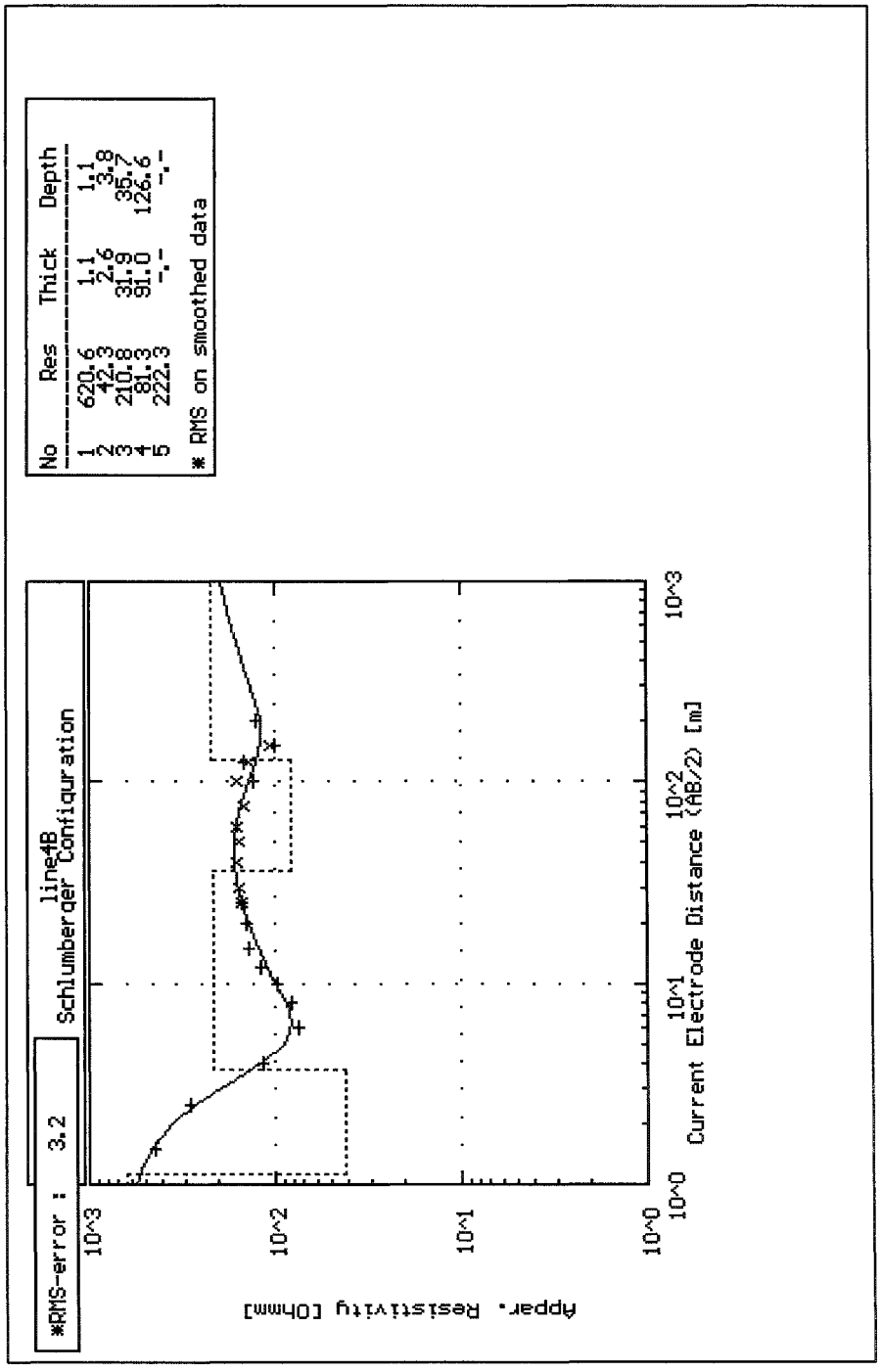
No Res Thick Depth
1 620.6 1.1 1.1
2 42.3 2.6 3.8
3 210.8 31.9 35.7
4 81.3 91.0 126.6
5 222.3 -.- -.-
* RMS on smoothed data
*RMS-error : 3.2
line4B
Schlumberger Configuration
Appar. Resistivity [Ohmm]
10^3
10^2
10^1
10^0
10^0 10^1 10^2 10^3
Current Electrode Distance (AB/2) [m]

VES-12

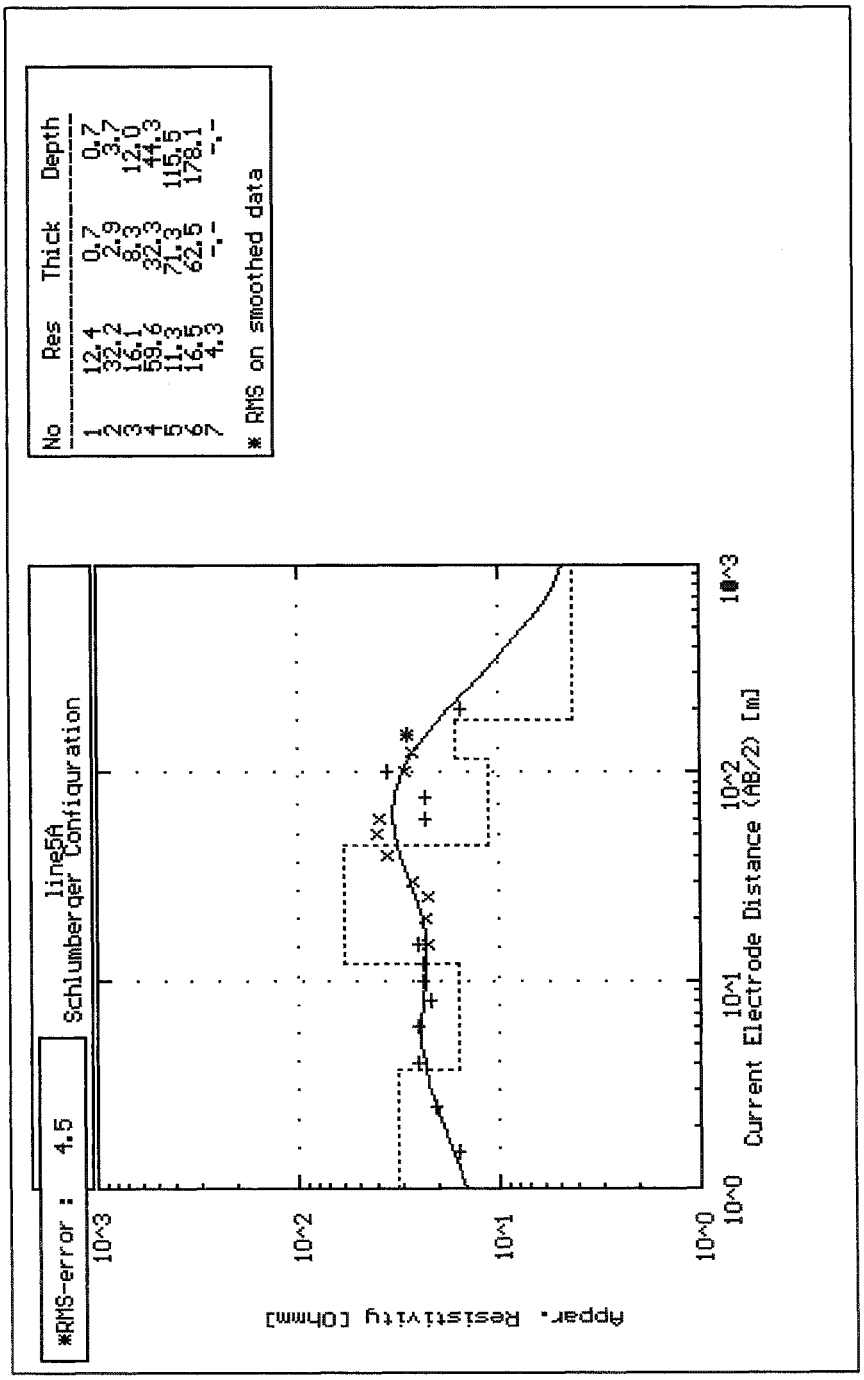
No Res Thick Depth
1 12.4 0.7 0.7
2 32.2 2.9 3.7
3 16.1 8.3 12.0
4 59.6 32.3 44.3
5 11.3 71.3 115.5
6 16.5 62.5 178.1
7 4.3 -.- -.-
* RMS on smoothed data
*RMS-error : 4.5
line5A
Schlumberger Configuration
Appar. Resistivity [Ohmm]
10^3
10^2
10^1
10^0
10^0
10^1
10^2
10^3
Current Electrode Distance (AB/2) [m]

VES-13

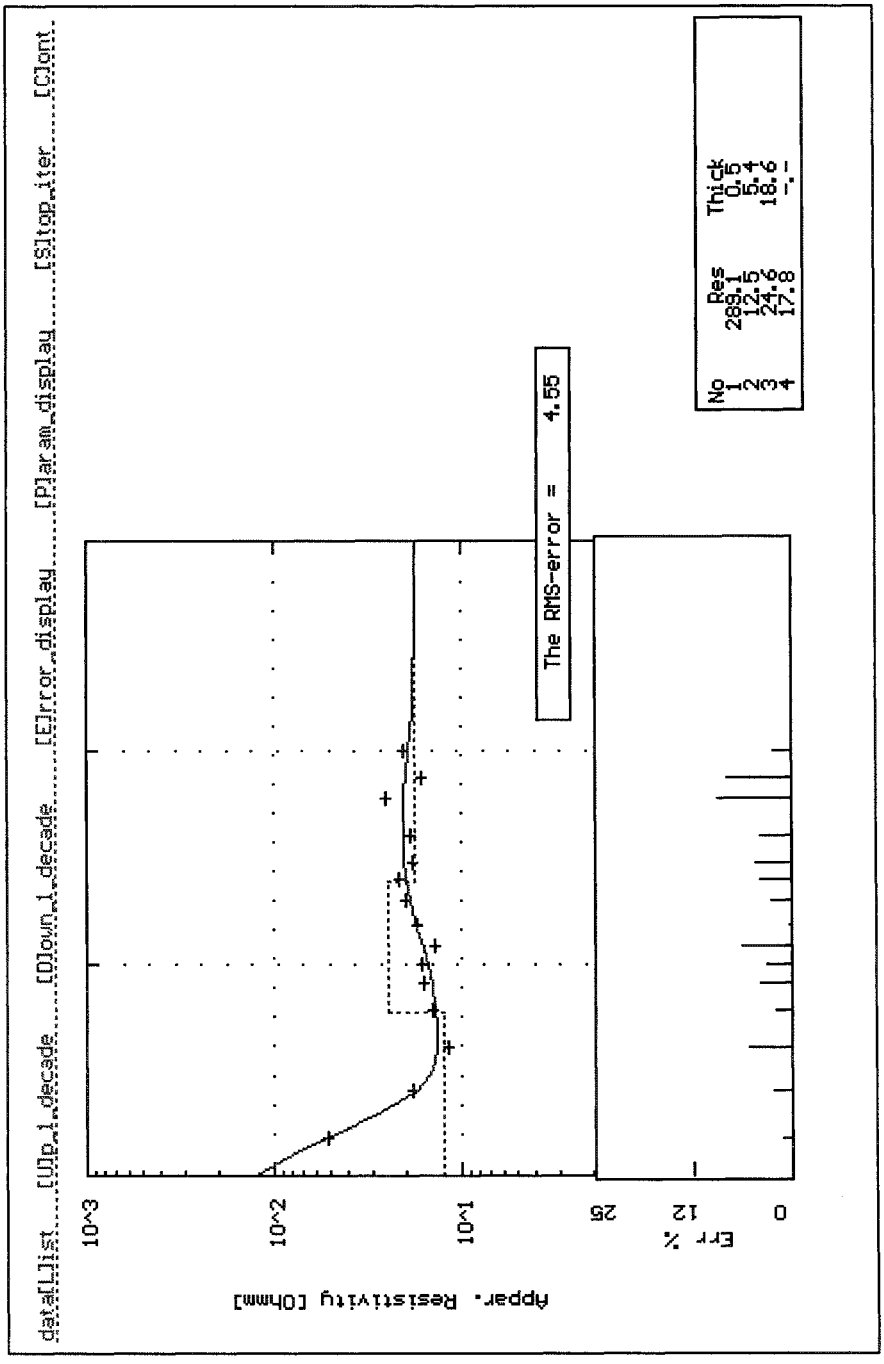
dataFlist [Up.1.decade [Down.1.decade [Error.display [Param.display [Stop.iter [Cont.
Appar. Resistivity [Ohmm]
10^3
10^2
10^1
Err %
25
12
0
The RMS-error = 4.55
No Res Thick
1 288.1 0.5
2 12.5 5.4
3 24.6 18.6
4 17.8 -.-

VES-14

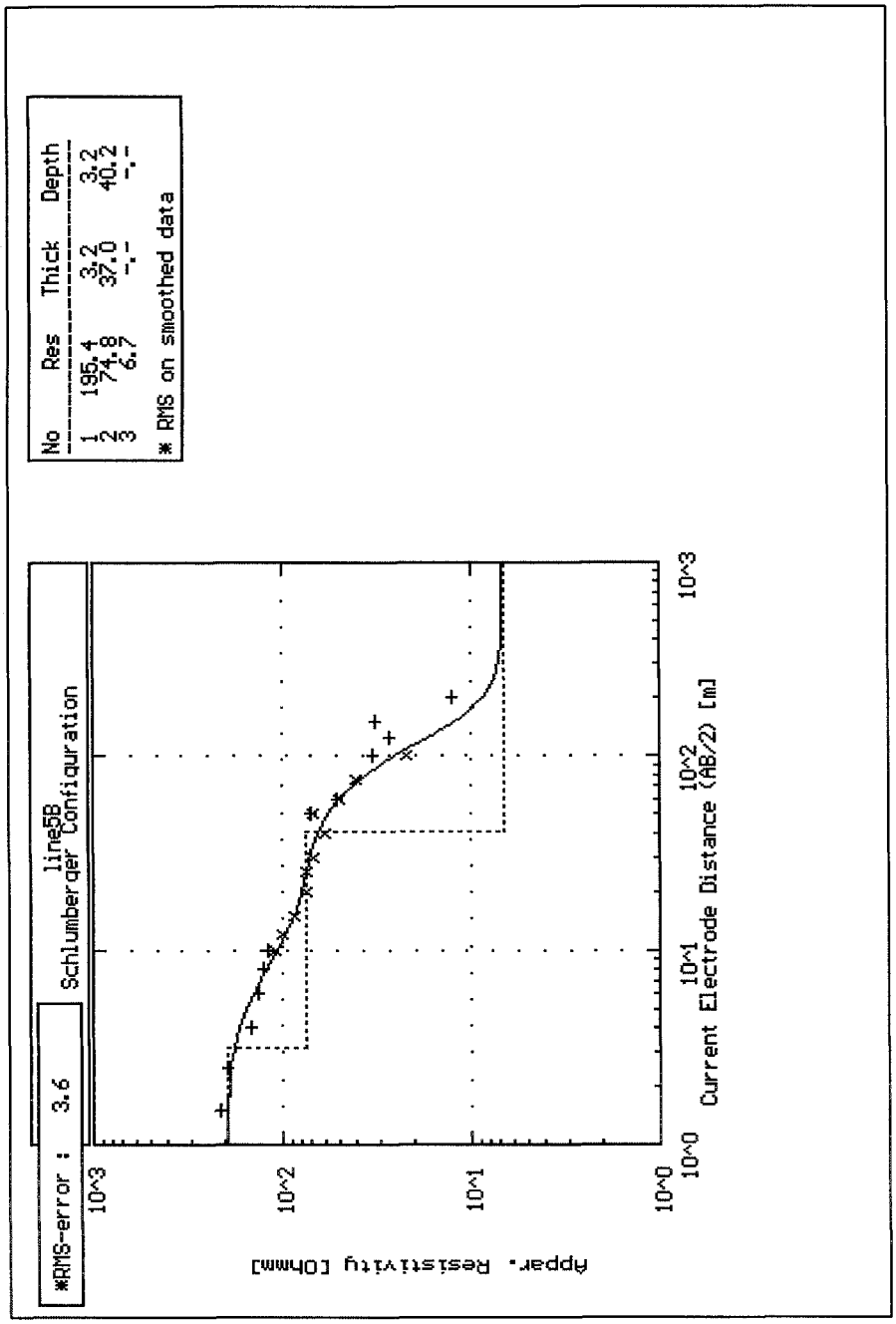
No Res Thick Depth
1 195.4 3.2 3.2
2 74.8 37.0 40.2
3 6.7 -.- -.-
* RMS on smoothed data
line5B
Schlumberger Configuration
*RMS-error : 3.6
Appar. Resistivity [Ohmm]
10^3
10^2
10^1
10^0
10^0
10^1
10^2
10^3
Current Electrode Distance (AB/2) [m]

VES-15

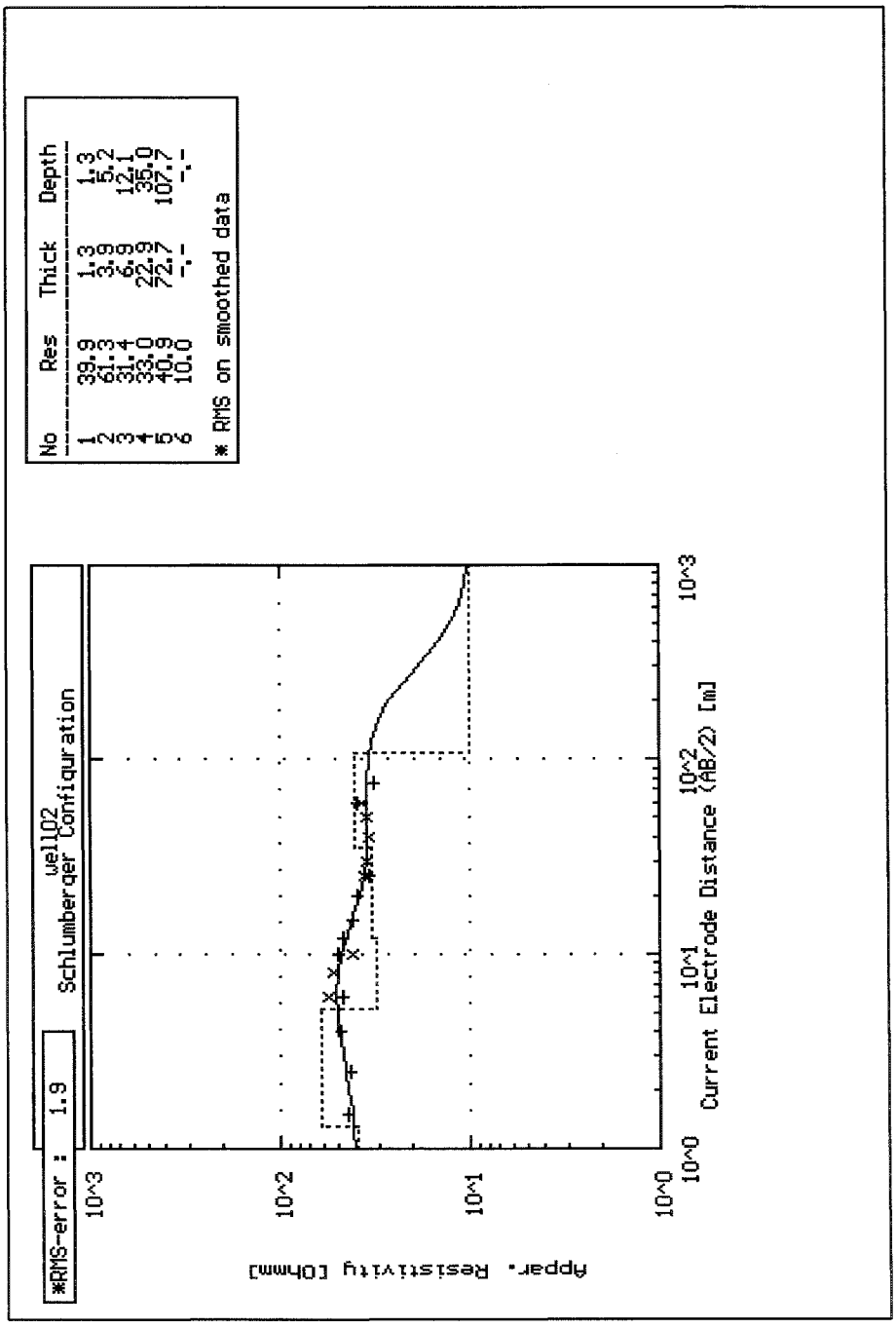
No Res Thick Depth
1 39.9 1.3 1.3
2 61.3 3.9 5.2
3 31.4 6.9 12.1
4 33.0 22.9 35.0
5 40.9 72.7 107.7
6 10.0 -.- -.-
* RMS on smoothed data
*RMS-error : 1.9
well02
Schlumberger Configuration
Appar. Resistivity [Ohmm]
10^3
10^2
10^1
10^0
10^0
10^1
10^2
10^3
Current Electrode Distance (AB/2) [m]

VES-16

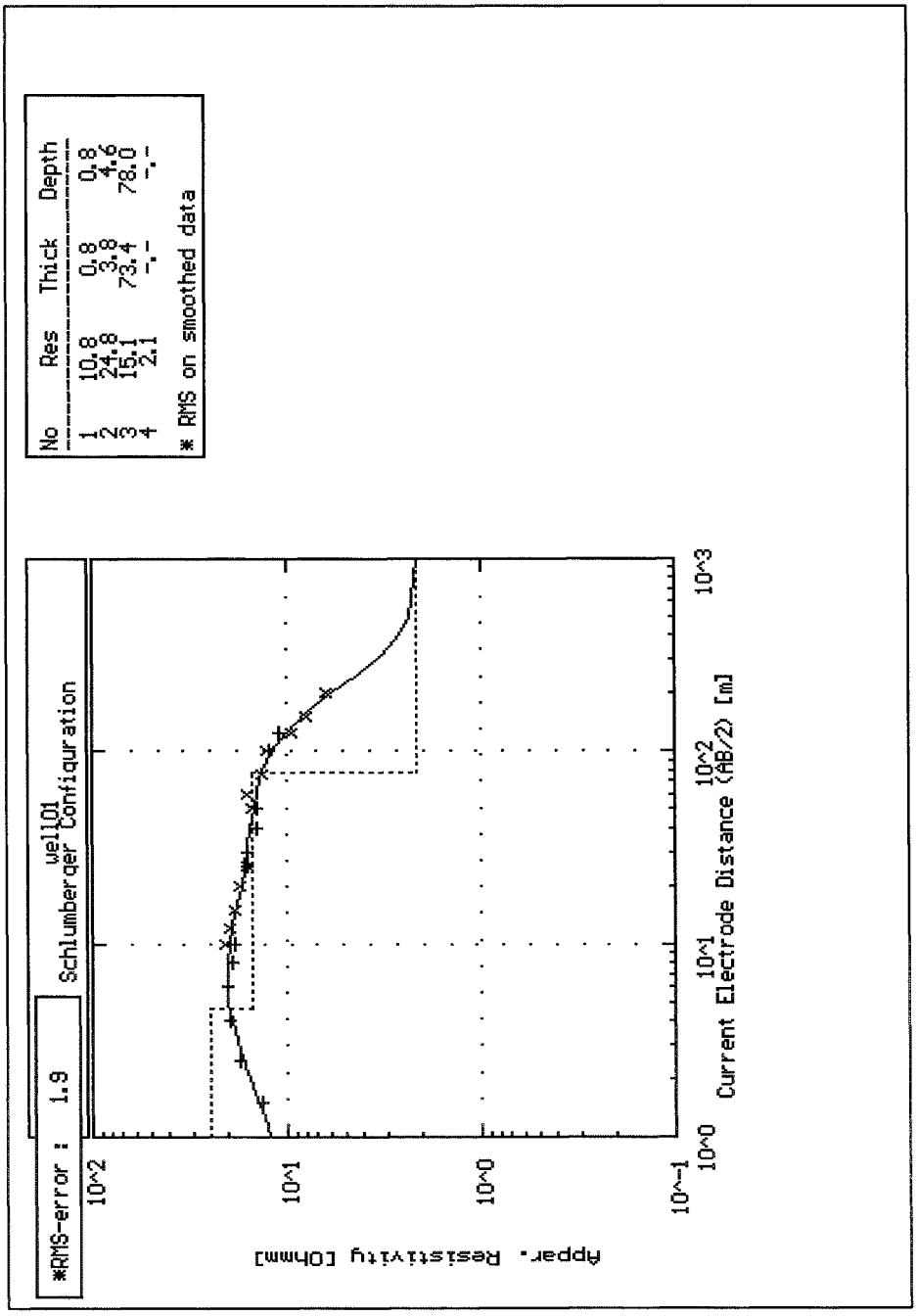
No Res Thick Depth
1 10.8 0.8 0.8
2 24.8 3.8 4.6
3 15.1 73.4 78.0
4 2.1 -.- -.-
* RMS on smoothed data
*RMS-error : 1.9
Schlumberger Configuration
well01
Appar. Resistivity [Ohmm]
10^2
10^1
10^0
10^-1
10^0
10^1
10^2
10^3
Current Electrode Distance (AB/2) [m]

VES-17

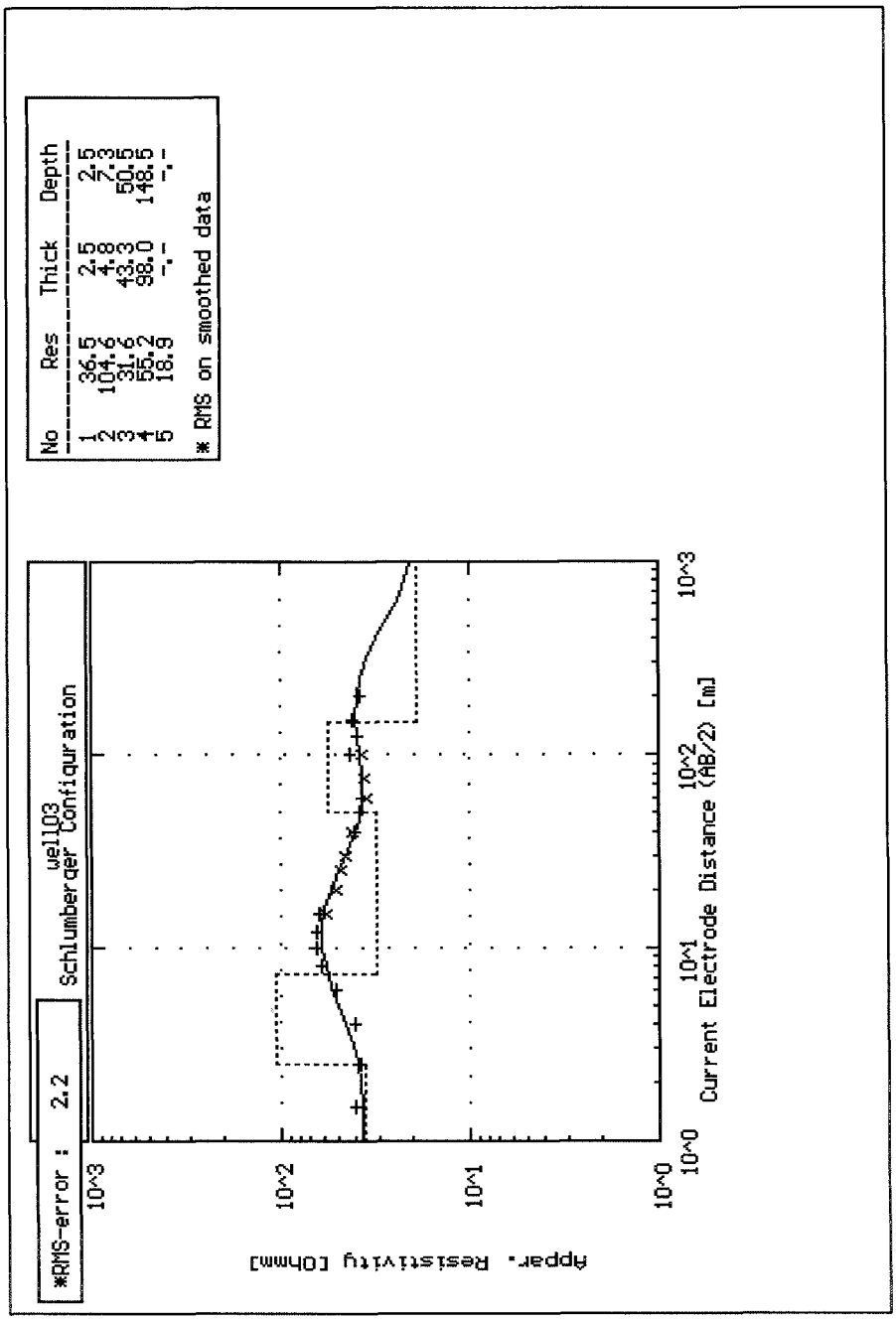
No Res Thick Depth
1 36.5 2.5 2.5
2 104.6 4.8 7.3
3 31.6 43.3 50.5
4 55.2 98.0 148.5
5 18.9 -.- -.-
* RMS on smoothed data
*RMS-error : 2.2
well03
Schlumberger Configuration
Appar. Resistivity [Ohmm]
10^3
10^2
10^1
10^0
10^0
10^1
10^2
10^3
Current Electrode Distance (AB/2) [m]

VES-18

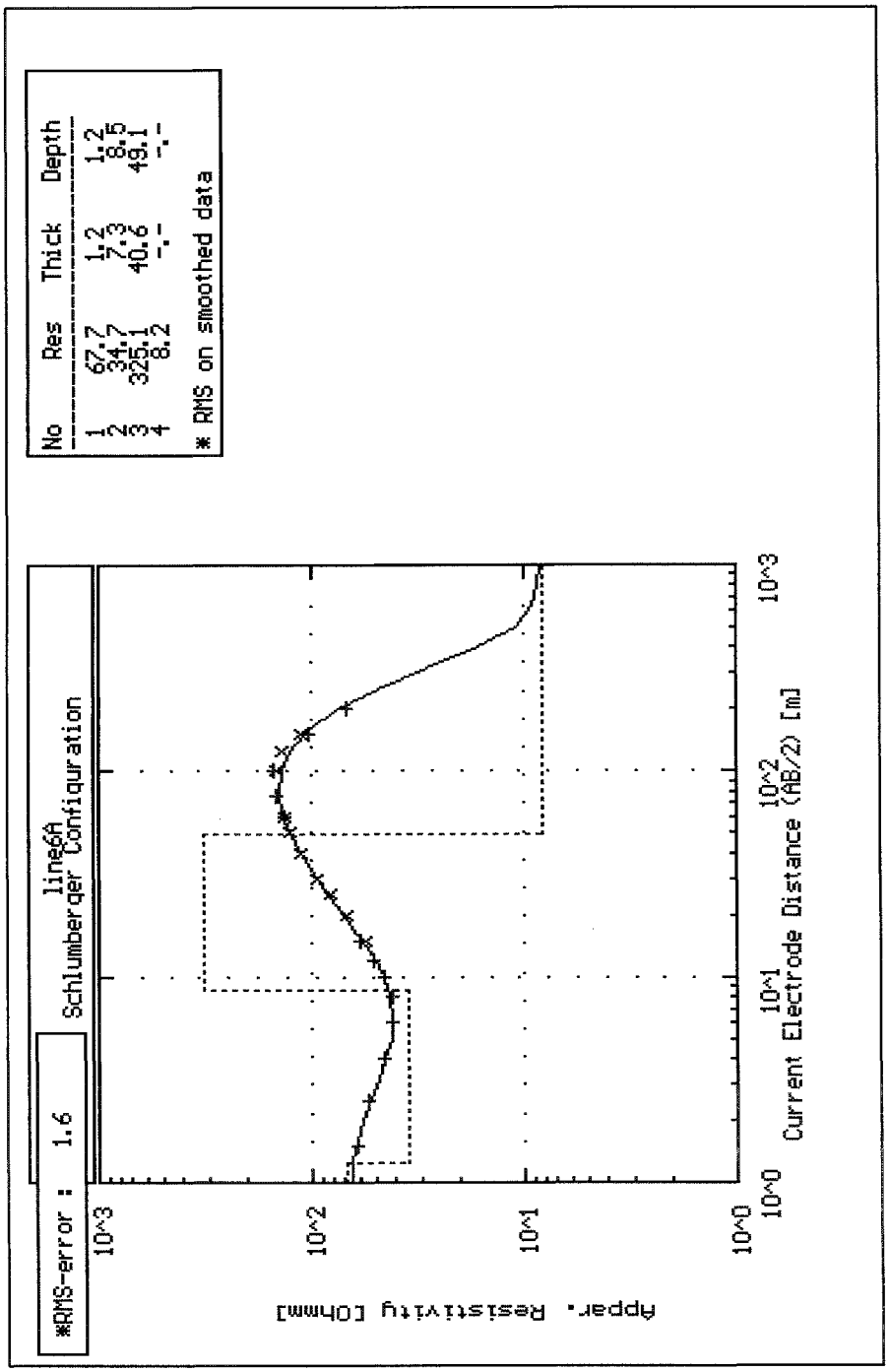
No Res Thick Depth
1 67.7 1.2 1.2
2 34.7 7.3 8.5
3 325.1 40.6 49.1
4 8.2 -.- -.-
* RMS on smoothed data
*RMS-error : 1.6
line6A
Schlumberger Configuration
Appar. Resistivity [Ohmm]
10^3
10^2
10^1
10^0
10^0
10^1
10^2
10^3
Current Electrode Distance (AB/2) [m]

VES-19

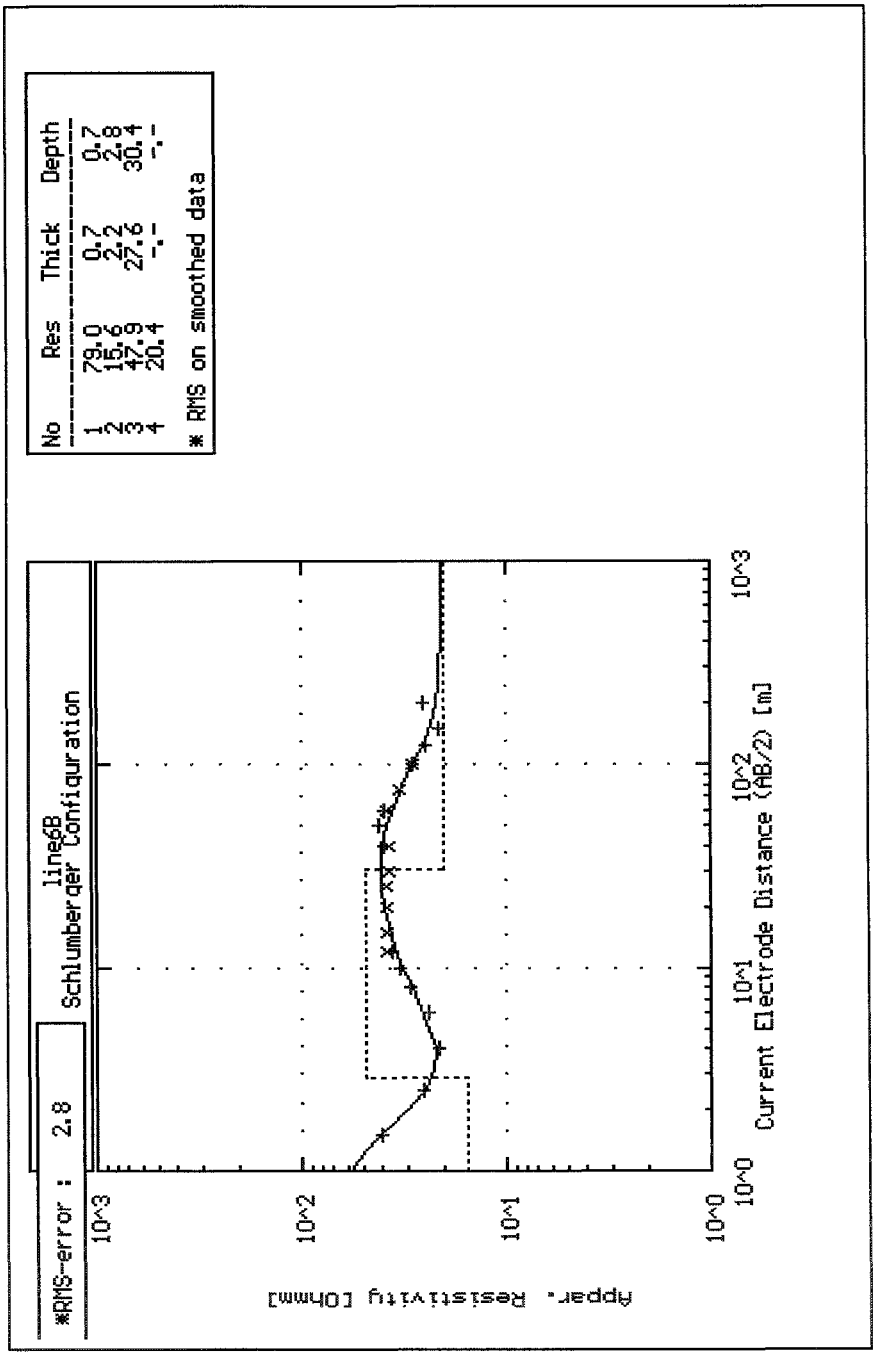
No Res Thick Depth
1 79.0 0.7 0.7
2 15.6 2.2 2.8
3 47.9 27.6 30.4
4 20.4 -.- -.-
* RMS on smoothed data
*RMS-error : 2.8
line6B
Schlumberger Configuration
Appar. Resistivity [Ohmm]
10^3
10^2
10^1
10^0
10^0
10^1
10^2
10^3
Current Electrode Distance (AB/2) [m]

VES-20

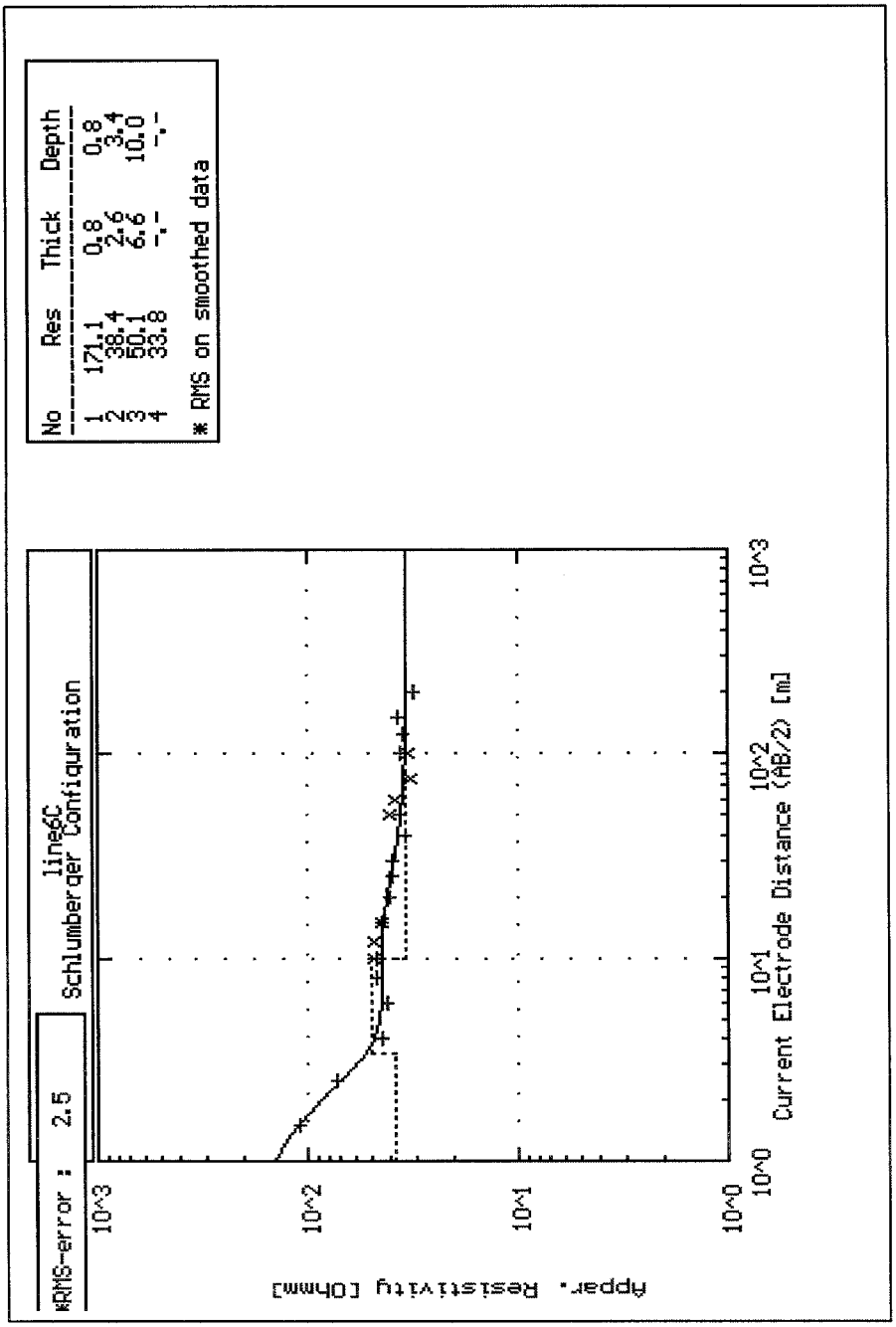
No Res Thick Depth
1 171.1 0.8 0.8
2 38.4 2.6 3.4
3 50.1 6.6 10.0
4 33.8 -.- -.-
* RMS on smoothed data
line6C
Schlumberger Configuration
*RMS-error : 2.5
Appar. Resistivity [Ohmm]
10^3
10^2
10^1
10^0
10^0 10^1 10^2 10^3
Current Electrode Distance (AB/2) [m]

VES-21

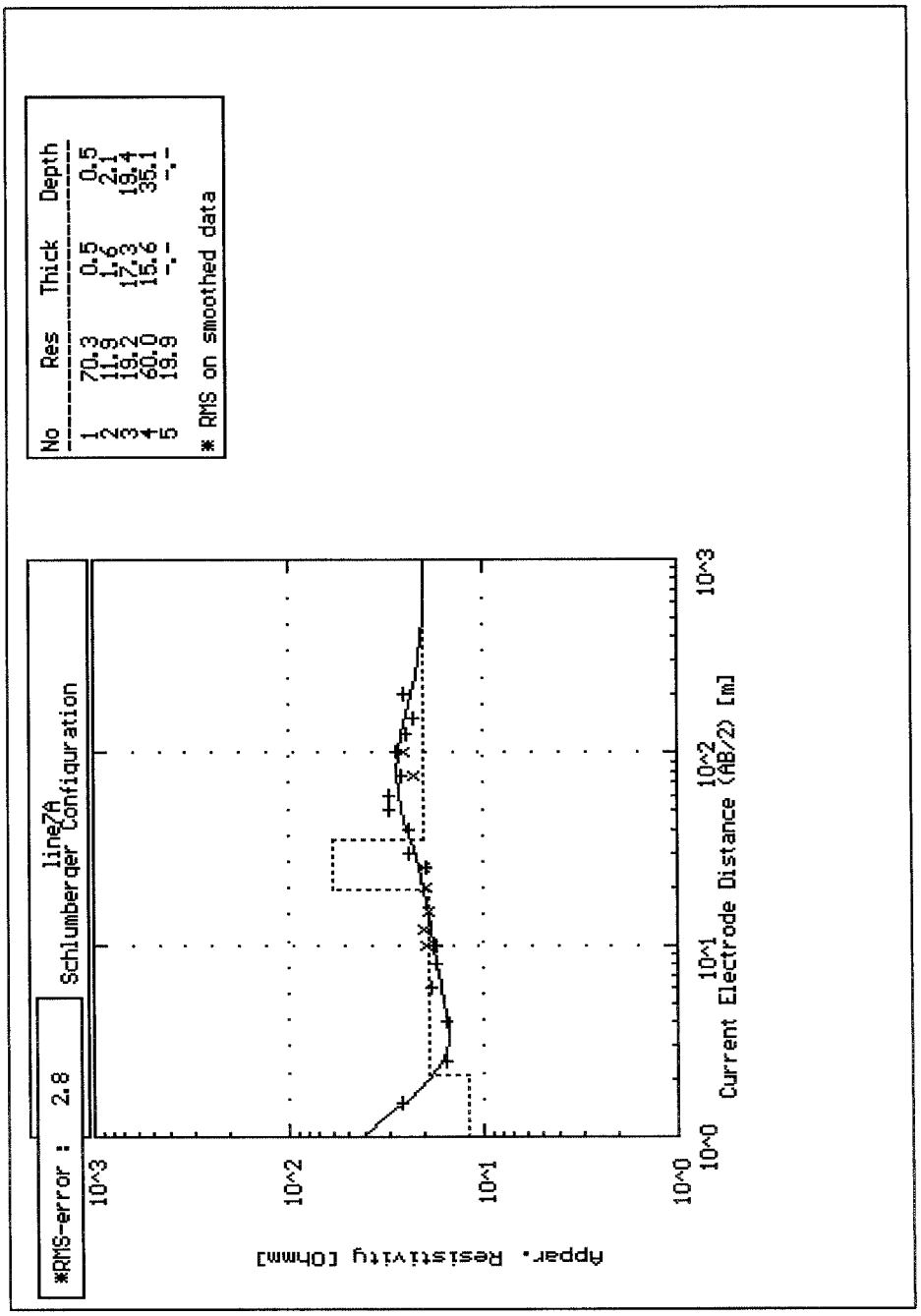
No Res Thick Depth
1 70.3 0.5 0.5
2 11.9 1.6 2.1
3 19.2 17.3 19.4
4 60.0 15.6 35.1
5 19.9 -.- -.-
* RMS on smoothed data
*RMS-error : 2.8
Schlumberger Configuration
line7A
Appar. Resistivity [Ohmm]
10^3
10^2
10^1
10^0
10^0 10^1 10^2 10^3
Current Electrode Distance (AB/2) [m]

VES-22

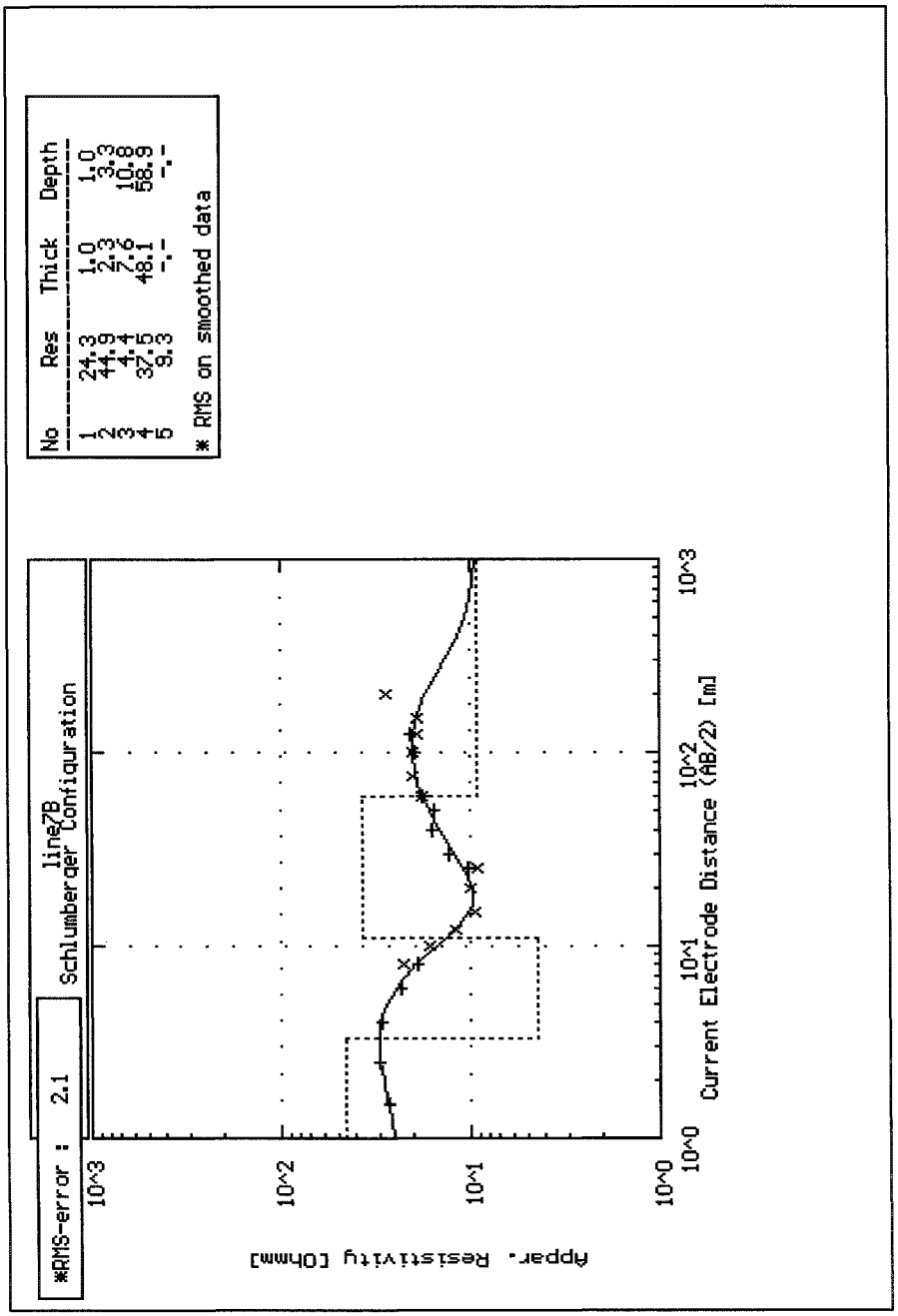
No Res Thick Depth
1 24.3 1.0 1.0
2 44.9 2.3 3.3
3 4.4 7.6 10.8
4 37.5 48.1 58.9
5 9.3 -.- -.-
* RMS on smoothed data
line7B
Schlumberger Configuration
*RMS-error : 2.1
Appar. Resistivity [Ohmm]
10^3
10^2
10^1
10^0
10^0
10^1
10^2
10^3
Current Electrode Distance (AB/2) [m]

VES-23

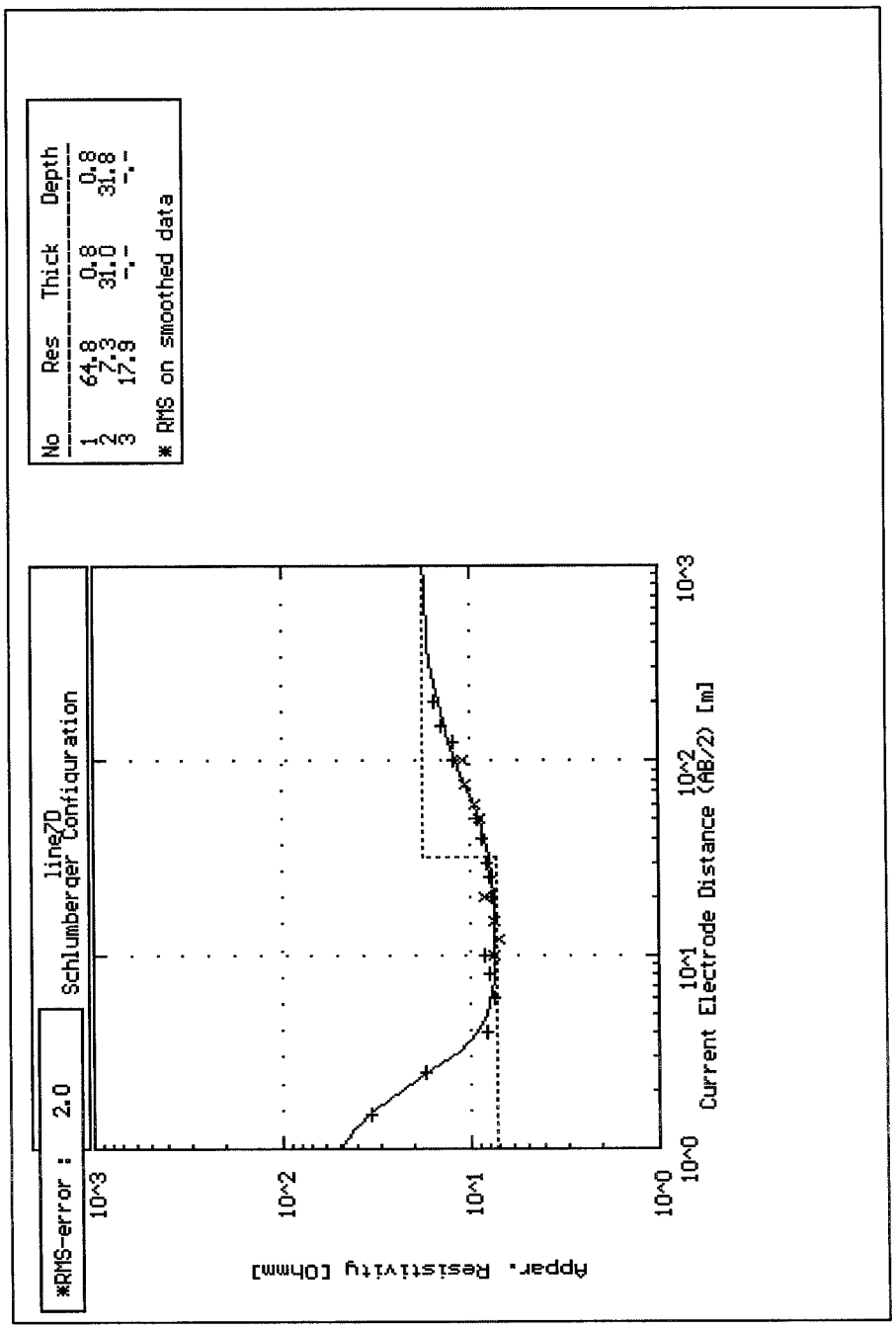
No Res Thick Depth
1 64.8 0.8 0.8
2 7.3 31.0 31.8
3 17.9 -.- -.-
* RMS on smoothed data
*RMS-error : 2.0
line7D
Schlumberger Configuration
Appar. Resistivity [Ohmm]
10^3
10^2
10^1
10^0
10^0 10^1 10^2 10^3
Current Electrode Distance (AB/2) [m]

VES-24

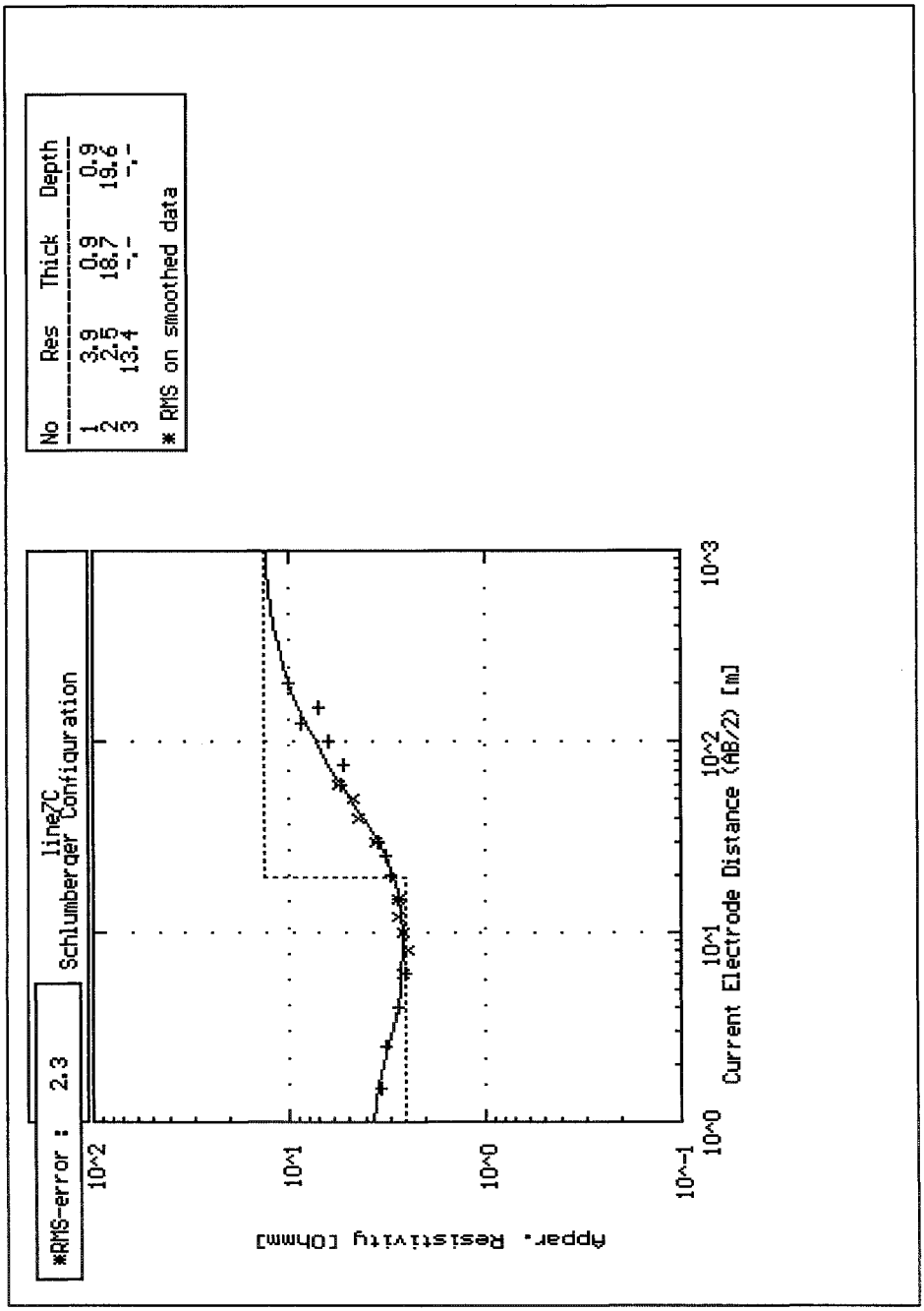
No Res Thick Depth
1 3.9 0.9 0.9
2 2.5 18.7 19.6
3 13.4 -.- -.-
* RMS on smoothed data
*RMS-error : 2.3
line7C
Schlumberger Configuration
Appar. Resistivity [Ohmm]
10^2
10^1
10^0
10^-1
10^0
10^1
10^2
10^3
Current Electrode Distance (AB/2) [m]

VES-30

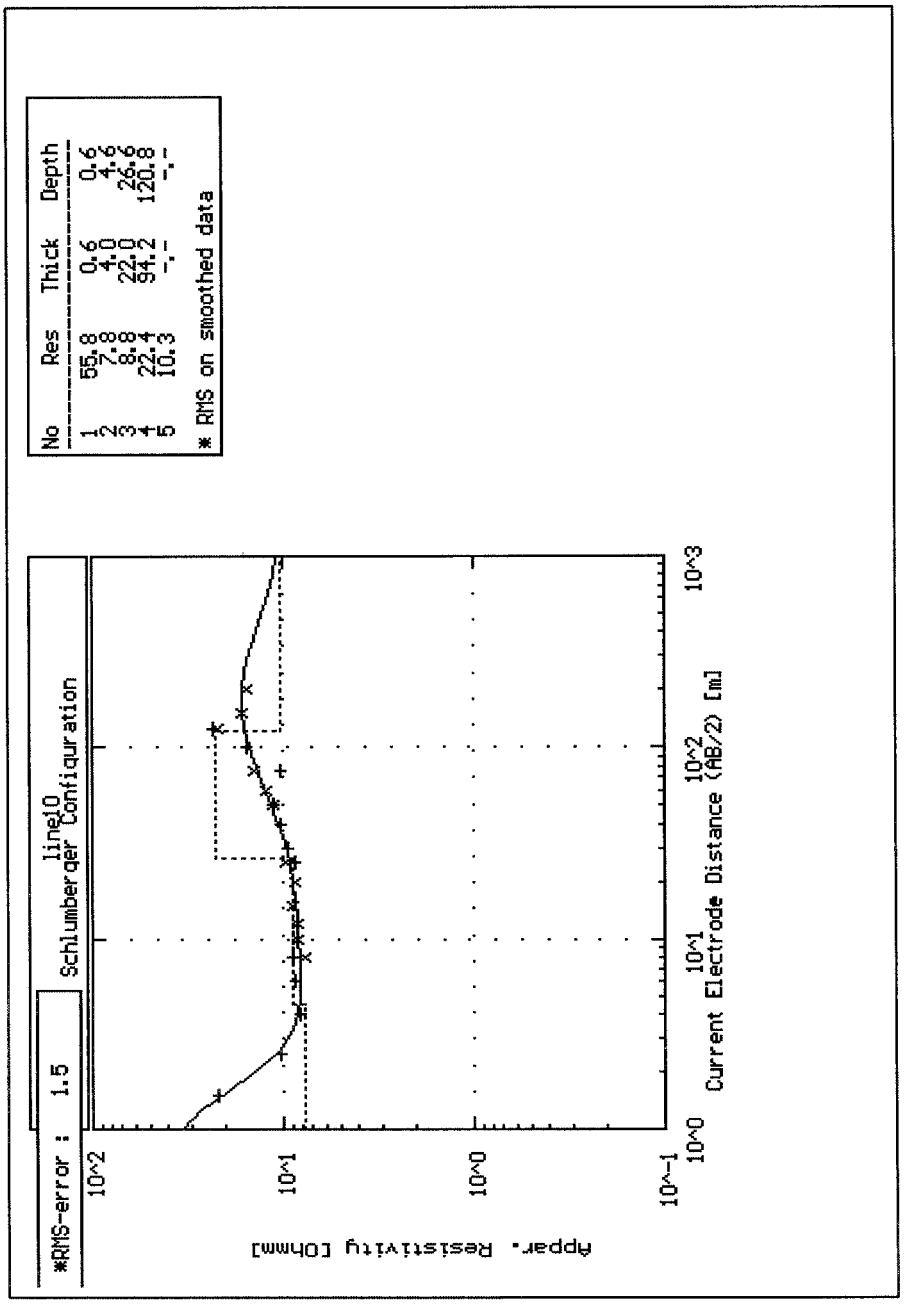
No Res Thick Depth
1 55.8 0.6 0.6
2 7.8 4.0 4.6
3 8.8 22.0 26.6
4 22.4 94.2 120.8
5 10.3 -.- -.-
* RMS on smoothed data
*RMS-error : 1.5
line10
Schlumberger Configuration
Appar. Resistivity [Ohmm]
10^2
10^1
10^0
10^-1
10^0
10^1
10^2
10^3
Current Electrode Distance (AB/2) [m]

INTERNATIONAL INSTITUTE FOR AEROSPACE SURVEY AND EARTH SCIENCES

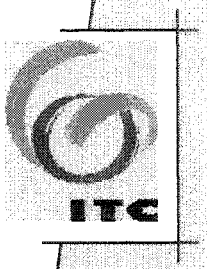

APPENDIX D

Geophysical Well Log Data

WELL LITHOLOGY, PERCUSION WELL.

Well: PV 3, BH 3 (after Ramirez, 1999)
Location: Three Austriche farms, near Delamere.
Coordinates: (0213712, 9925550)

Depth, m	Lithology
2	Sand ranging from fine to medium sized grains, angular and well rounded grains.
4	Sand ranging from fine to medium sized grains, angular and well-rounded grains, the amount of medium sized grains is lower than in two meters.
6	Siltstone, loose silt.
8	Medium sized grains of sand, coarse material formed by pebbles, which have been reworked, well rounded. Fewer amount of smaller angular pebbles.
10	Mixture of sand, siltstone and silt. Grains appear angular and well rounded. The grain size for the sand is variable, ranging from fine to coarse.
12	Sand ranging from fine to medium sized grains, well rounded, fine sand is predominant.
14	Mixture of fine sand and coarser material, angular and well-rounded grains. The composition is around 50 % fine to medium sized material and 50 % coarse material.
18	Mixture of fine sand and coarser material, angular and well-rounded grains. The composition is around 50 % fine to medium sized material and 50 % coarse material.
20	Fine sand, around 15 % medium sized grains, well rounded.
22	Fine sand.
24	Sand, fine to medium sized gains.
26	Sand fine to medium sized grains, angular and rounded, small quantities of silt.
28	Sand, fine to medium sized grains.
30	Pebbles ranging from medium sized to coarse, angular form.
32	Pebbles, a decrease in grain size is observed. Few amounts of sand and silt.
34	Coarse sand and pebbles, angular and rounded.
36	Pebbles, coarse material in angular form, few amount of sand with grains slightly rounded. Pebbles composed mainly by siltstone, calcite. In some pebbles the siltstone is the cement.
38	Medium to coarse sized grains of sand, few pebbles and silt, grains angular and sub-rounded. The composition is mainly silt and carbonaceous material.
40	Pebbles of limestone and sandstone, compact, no joints, hard, very angular and clean, no sand nor silt, some pebbles rounded
42	Reworked clasts of siltstone, others clasts of limestone and pumice, rounded and angular. A pebble shows thin interbedding of limestone and siltstone, reworked; clasts of pumice are present.
44	Coarse sand, mixture of rounded and angular grains. Main composition siltstone and limestone; clasts of pumice are present.
46	Coarse sand, mixture of rounded and angular grains. Composition siltstone and limestone. This sample has a larger amount of pumiceous material.
48	Fine to medium sized grains of sand, angular.
50	Medium sized grains of sand, angular.
52	Fine to medium sized grains of sand, angular.
54	Fine to medium sized grains of sand, angular.
56	Fine to medium sized grains of sand, angular to sub-rounded. Few pebbles are found.
58	Fine to medium sized grains of sand, angular to sub-rounded. Few pebbles are found.
60	Fine to coarse sand, pebbles of limestone, angular.

Geophysical well-log data in V17

No	Depth (m)	SNlog ohm-m	Lnlog ohm-m	Llat ohm-m	Res ohm-m	SP mV	T C	TDS ppm	EC micromhos/cm
1	-40	72.3	67.8	23	27	-26	25.2	237	152
2	-39	66.4	43.2	27.4	26.8	-5.28	25.2	239	153
3	-38	46.2	35.6	22.2	26.5	-2.91	25.2	242	155
4	-37	34.7	31.3	19.4	25.6	-28.1	25.2	250	160
5	-36	28.8	27.8	21.8	26.2	-3.56	25.2	244	157
6	-35	32.1	27.7	27.7	26	-3.31	25.1	246	158
7	-34	33.2	28.3	27	26.6	-4.69	25.1	241	154
8	-33	32.3	27.8	65	25.8	-1.64	25.1	248	159
9	-32	33.1	29.3	27.7	25.5	-2.07	25.1	251	161
10	-31	34	30.2	30.8	25.8	-1.91	25.1	248	159
11	-30	35	31.4	0	24.8	-2.22	25.1	258	165
12	-29	35.5	31.6	0	24.2	-2.11	25.1	264	170
13	-28	35.1	31.3	0	24	0.58	25.1	267	171
14	-27	32.4	33.3	0	23	-1.12	25.1	278	178
15	-26	24.1	42.5	0	15.85	-11.19	25.2	404	259
16	-25	24	0	0	15.41	-8.89	25.3	415	266
17	-24	0	0	0	0	-16.33	25.5	0	0
18	-23	0	0	0	0	-6.51	25.6	0	0

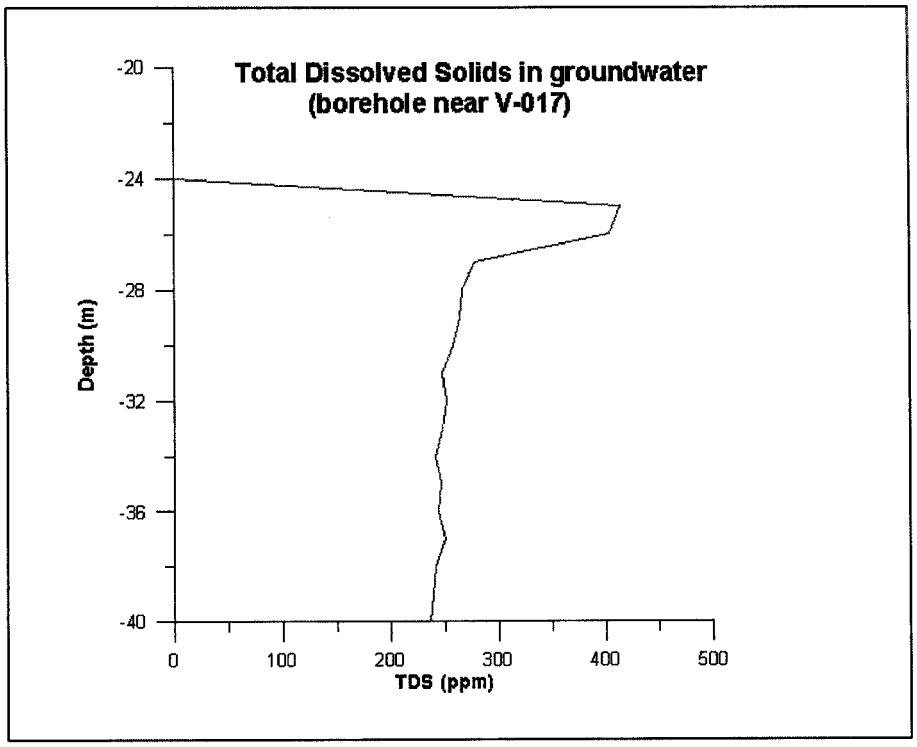
Total Dissolved Solids in groundwater
(borehole near V-017)
Depth (m)
-20
-24
-28
-32
-36
-40
0
100
200
300
400
500
TDS (ppm)

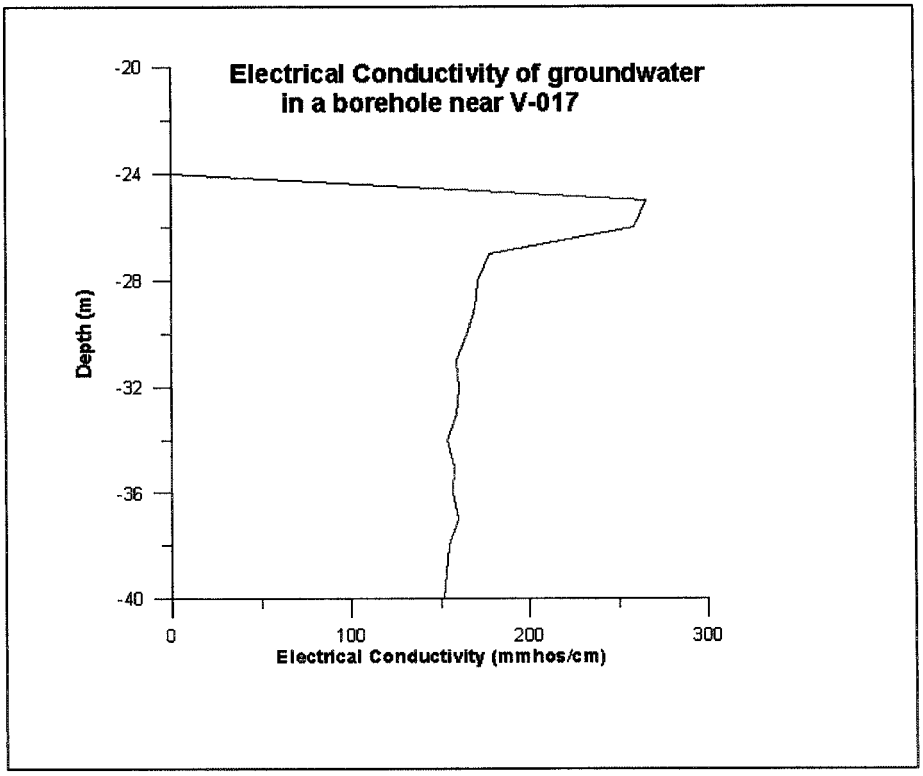
Electrical Conductivity of groundwater
in a borehole near V-017
Depth (m)
-20
-24
-28
-32
-36
-40
0
100
200
300
Electrical Conductivity (mmhos/cm)

La Belle Inn Well

The well is located at coordinates [214127, 9920848] (Universal Transverse Mercator / UTM coordinates, zone 37), at an elevation of approximately 1905 m above sea level (asl). The measured depth of the well is 46 and at the time of visit, the rest water level was t 19.97 m below ground level (bgl). Water was reportedly struck at 24 m depth.

A geophysical logging test was carried out down the well from a depth of 20-46 m, using a one-meter interval. The following parameters were measured: **longnormal, shortnormal and latero-log** electrical resistivity, **fluid resistance** and **self-potential.** Unfortunately the temperature probe was not working. Some results are shown in figure 1 and 2. Figure 1 shows the change in resistivity of the formation with depth. In sedimentary formations the higher the resistivity, the better the aquifer potential as a high resistivity indicates a lower percentage of clay, which is not good aquifer material. Based on the resistivity logs, the aquifer is thus located between 26-32 m depth. Figure 2 shows the change in water quality (EC – electrical conductivity/salt content) with depth. It appears as if the water quality is best at greater depths. The portion under the pumice layer has the best water quality and is well protected against contamination. However, overall, from a salinity point of view, the quality of water is acceptable.

It seems that under the pumice another 4 meters of lacustrine deposits occur. At a depth of 36-40 meters, the weathered zone of the underlying basalt starts, while at the bottom of the hole fresh basalt is encountered. The weathered basalt may constitute a reasonable aquifer, but it is not certain if it can support or sustain the desired yield.

At the timing of drilling, formation samples were taken at a 2 m interval. With the help of the driller, an attempt was made to reconstruct a detailed well log (see Fig.3). However, the samples had all been washed, so no definite information is available on the amounts of fine material (silt, clay) which is basically what determine the aquifer's hydraulic conductivity.

From the log it is evident that a hard basaltic layer at 20 – 22 m depth confines the aquifer. This is a favorable situation as this impervious basaltic layer function to seal off the aquifer, thus minimizing the potential of the aquifer to become polluted. The lateral extent of this basaltic layer is however unknown.

It is advised to maintain the current depth of the well as based on knowledge of other wells in the area, continued drilling is unlikely to tap another aquifer. It is further suggested that in order to realize an abstraction volume of 30 m^3/day, a pump with a capacity of 3 – 4 m^3/hour be installed in the well. A pump with a larger capacity is not necessary to obtain a yield of 30m^3/day and there is always the threat of pollution and pumping of silty water if the abstraction rates are too high. Another factor to

consider is electricity costs, which will be higher abstraction rates (due to drawdown).

The screened part of well (slotted casing) should not be higher than the layer of pumice (28 m). It must be ensured that the plain casing higher than the pumice is well grouted with a mixture of bentonite and cement or similar materials. Otherwise, the risk of contamination along the casing from the upper aquifer occurs.

It is common practice in Kenya to case the bottom 1 – 2 meters of the well with plain casing as a sediment trap, and to case the portion where the pump will be installed with plain casing also to prevent direct inflow next to the pump.

A water sample has been taken with the bailer of the rig. Since the well is not yet developed, the high nitrate levels detected may be due to water/agents used by the drillers during construction. Also it should be noted that a good bacteriological quality of the water during test pumping is not guarantee for the future as the well may with time draw contaminated water from the upper aquifer. It would be good practice to have a sample bacteriologically analyzed after one year.

In order to determine the optimum depth, at which the pump should be set, it is recommended that a pumping test be carried out on the well.

DESCRIPTION OF LITHOLOGY

Well: La Belle Inn
Location: La Belle Inn .
Coordinates: (214127, 9920848)

Depth, m	**Lithology**
0 - 2	Brown silty clay, little sand
2 - 4	Silt with clay
4 - 6	Fine to coarse-grained rounded sediments
6 - 8	Fine to coarse-grained rounded sediments, mod. clay
8 - 10	Med. to coarse-grained rounded sediments, mod. clay
10 - 12	Med. to coarse-grained rounded sediments, mod. clay (sediments derived from phonolites-nepheline crystals)
12 - 14	Fine to med.- grained sand. Some clay
14 - 16	Fine to med.- grained sand. Some clay
16 - 18	No sample available
18 - 20	Med. To coarse-grained sands with rounded pumice
20 - 22	Hard basalt layer (crushed – fine grained) (confining layer)
22 - 24	Mixture of sediments and crushed basalt (1^{st} water strike)
24 - 26	Coarse. Sub-angular sediments
28 - 30	Pumice layer (probably confining)
30 - 32	Rounded fine to med.-grained sand, little clay
32 - 34	Rounded fine to med.-grained sand, little clay
34 - 36	Rounded fine to med.-grained sand, some clay
36 - 38	Rounded to sub-angular fine to med-grained sand
38 - 40	Rounded to sub-angular fine to med-grained sand
40 - 42	Silt, well weathered basalt
42 - 44	Mod. weathered basalt, not very hard.
44 - 46	Weathered basalt (fine-grained)
46 - 48	Fresh basalt

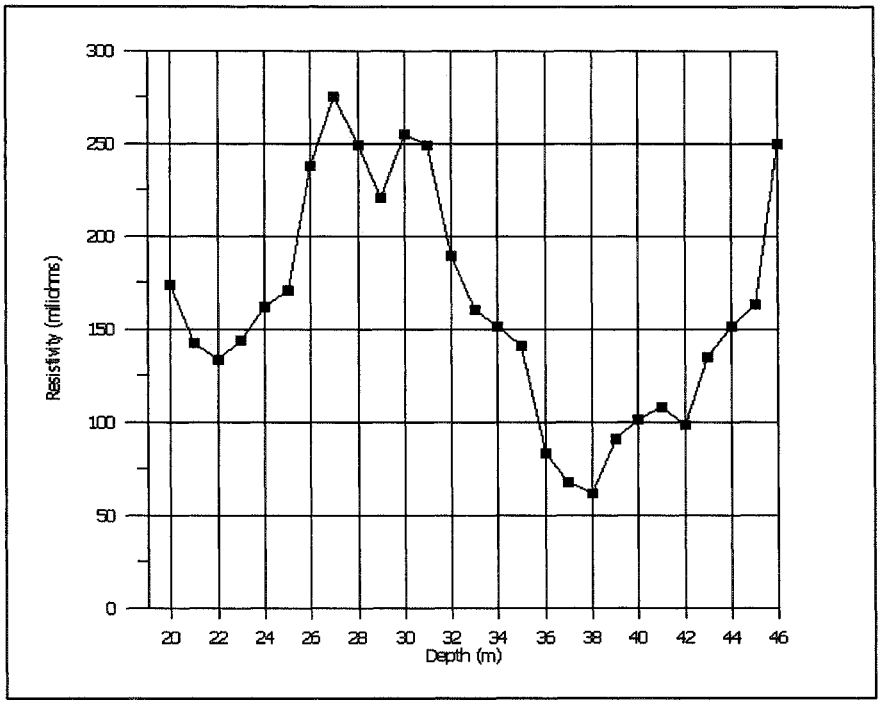

Figure 1. Resistivity Variation with Depth

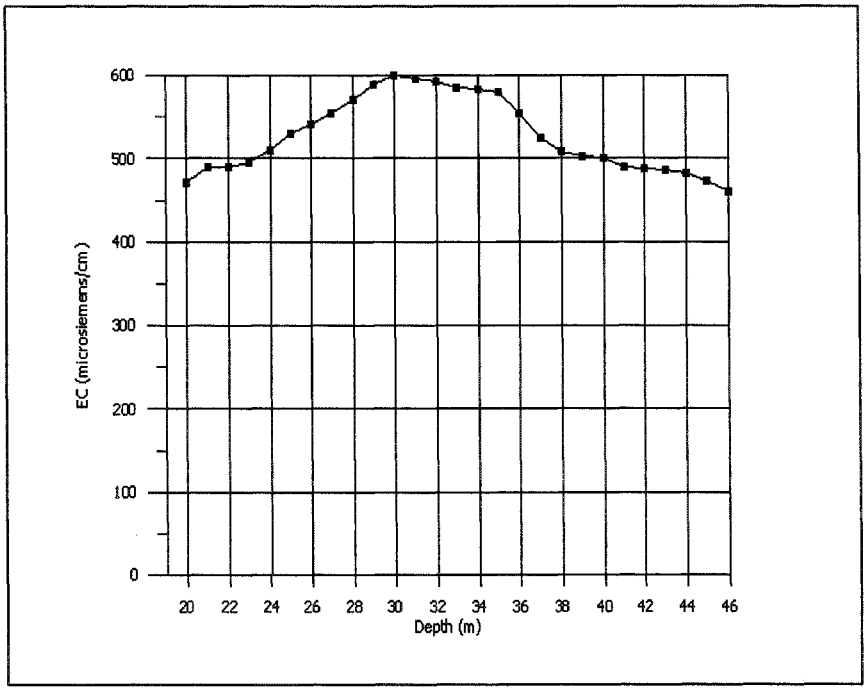

Figure 2. Electric Conductivity variation with depth

INTERNATIONAL INSTITUTE FOR AEROSPACE SURVEY AND EARTH SCIENCES

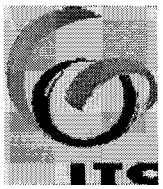

APPENDIX E

Borehole Data

INTERNATIONAAL INSTITUUT VOOR LUCHT – EN RUIMTEKAARTERING EN AARDKUNDE

INSTITUTO INTERNACIONAL PARA LEVANTAMIENTOS AEROESPACIALES Y CIENCIAS TERRESTRES

INSTITUT INTERNATIONAL DE LEVES AEROSPATIAUX ET SCIENCES DE LA TERRE

	Well	X	Y	Surface Elevation	Water level (masl)
2	Kongoni_2	195854	9908332	1899.12	1883.12
4	ADC Ndabibi	196964	9913088	1907.03	1882.10
5	Kongoni_1	194193	9908767	1911.80	1879.80
7	Mirera/Suswa	215784	9912357	1982.12	1886.12
8	C7829	206610	9908050	1889.55	1884.06
9	UW1	197450	9908750	1895.29	1882.08
10	C210	209200	9909350	1900.10	1884.40
11	C630-D	197700	9906200	1957.00	1856.80
12	C3675	212200	9922300	1889.50	1881.10
14	C10887	210850	9924300	1897.00	1881.50
15	Manera	211434	9921380	1890.30	1885.67
16	N-18	209054	9904649	1992.50	1979.60
17	N-23	213394	9921504	1896.00	1881.54
18	TOF_3	213854	9924903	1910.00	1885.50
19	Milk_Fact	211881	9924492	1902.70	1882.61
20	La Belle Inn	214151	9920906	1903.20	1884.98
22	C-465	208734	9937303	1963.53	1922.53
27	C-2522	193895	9918862	1932.94	1890.00
28	C-1404	190188	9915164	1949.87	1890.87
29	C-939	219883	9917030	2120.45	1994.00
30	C-1488	218031	9922560	2070.57	1994.00
31	C-6520	218030	9924407	2122.32	2010.00
35	N-54	219411	9926765	2190.94	2059.00
36	C-4600	193891	9926231	2297.22	2252.00